

4. Implementation aspects

The recursive data processing - estimation and quality control - has been dealt with in chapter 2, and some essential parts of the underlying theory were reviewed in chapter 1. In particular, attention was paid to the least squares estimation of integer parameters. The mathematical modelling of GPS surveying was discussed in chapter 3. The current chapter serves as the link between theory and practice.

estimation

The various components are implemented in one integrated (prototype) software package, which has been used for the processing of the campaigns to be discussed in chapter 5. The step from theory to algorithm calls for a tuning of the various components to the application at hand: kinematic surveying. We will briefly discuss some implementation aspects of the recursive estimation by means of the Square Root Information Filter (SRIF) and the integer ambiguity estimation with the Least-squares AMBiguity Decorrelation Adjustment method (LAMBDA). The first section concludes with a flow diagram of the data processing.

quality control

The second section is completely devoted to the quality control. First the importance of quality control is stressed. Estimation results should not be provided without a description of the quality of the estimators. The mathematical model, used in the estimation, is to be validated. The generalized likelihood ratio test statistic is used for hypothesis testing in linear models. We will be concerned with the specification of (relevant) alternative hypotheses, the strategy for testing on model errors, the setting of the parameters in the procedure for statistical testing and the implementation of the adaptation.

4.1 Estimation

Implementation aspects of the estimation have been dealt with already in chapter 3. In section 3.4.4 the rank deficiencies in the functional model were removed to allow for a proper estimation and in section 3.5 an equivalent model was given in terms of double differences. Remaining aspects on the implementation of the recursive estimation and the resolution of the ambiguities will be given here. We will thereby concentrate on the availability of the quantities of interest, rather than on their actual computation. In section 4.1.4 the flow diagram for processing the GPS data is given.

input

The software has been developed for the processing of GPS observations, that were collected with a kinematic measurement set up. The input is based on the RINEX standard [Gurtner et al, 1990] and [Gurtner, 1993]. The observations (code and phase)

are contained in the Rinex Observation file. The satellite clock and orbit parameters are provided by the Rinex Navigation file.

Dual frequency phase and code observations are supported (the observation equations in section 3.4.1):

$$\text{L1} \quad \underline{P}_r^s(t) \quad \text{phase observation on L1} \quad (4.1)$$

$$\text{L2} \quad \underline{P}_r^s(t) \quad \text{phase observation on L2} \quad (4.3)$$

$$\text{C1(P1)} \quad \underline{p}_r^s(t) \quad \text{code observation on L1} \quad (4.4)$$

$$\text{P2(C2)} \quad \underline{p}_r^s(t) \quad \text{code observation on L2} \quad (4.5)$$

It is assumed that all observations, all types to all satellites in view, are made simultaneously by/inside the receiver: only one receiver time tag t is assigned. The two receivers make in addition the observations (nearly) simultaneously. The sampling interval is usually small, 1, 5 or 10 seconds. Note that various measurement techniques exist to obtain (a subset of) the above list, see e.g. [Dierendonck, 1994].

The stochastic model for the observables was dealt with in section 3.4.3. The stochastic properties of the observables may be (slightly) different for a stationary receiver (the reference) and a moving one (the rover), but with kinematic surveying receiver (antenna) dynamics are usually (very) low.

output: baseline

Concerning the geometry, processing takes place in terms of Cartesian WGS84 coordinates. As discussed in section 3.3, GPS surveying provides coordinate differences. Based on the data, an estimator is computed for the coordinates of the antenna. In section 3.4.2 it is assumed that receivers of the same make and type are used together with identical antennas. The antennas have equal orientation and are put local level (on a smooth geoid). The baseline vector x_{12} is then defined from phase center to phase center and equals in this case the vector between the geometric centers of the antennas (mm-cm translation). Antenna phase center effects namely cancel in short distance relative positioning, [Schupler et al, 1994]. For the highest precision applications there may be a small additional antenna effect with kinematic surveying over static GPS surveying. The rover and reference antennas are in general not equally oriented and they may even be different antennas, e.g. for the reason of portability of the roving one. Phase center effects then need to be taken into account (mm-cm effects).

To connect the geometric information obtained with the measurement system again to reality, the antenna center needs to be related to a discrete point, the survey marker. In a static survey the baseline can be defined by the survey markers in/on the ground. The baseline is consequently transferred to these monuments by the antenna eccentricities. The antenna has to be centered above the marker (horizontal) and the antenna height has to be measured (vertical). The height of the tripod set up is measured with some special rod or an ordinary tape. In a kinematic survey, the centering is carried out by positioning the range pole with the antenna on top of it, above the marker, or feature, instead of using a (stable) tripod. It has to be realized that these processes are true potential error sources. When no marker is available, as with topographical surveying, in addition the idealization precision comes in: terrain features have to be reduced to geometric primitives. We will not further dwell upon this surveying practice, and refer to e.g. [Polman et al, 1996].

Beside monumentation, site selection and auxiliary doings by the surveyor, cf. [Hofmann-Wellenhof et al, 1997], it should be realized that in practice also several factors concerning the equipment have an impact on the overall quality of the geometric information finally obtained, cf. section 4.2. One may think of cabling and power supply and for real-time operation also the telemetry link. The (technical) equipment must operate as it is supposed to do.

For analysis and interpretation purposes in chapter 5, coordinate differences (estimated minus reference), expressed in Cartesian XYZ of the global WGS84, will be transformed into a local ellipsoidal or topocentric system, figure 1.1. This system has its origin at the reference coordinates of the point to be positioned, point P . The Cartesian coordinates $P(X,Y,Z)$ are expressed in ellipsoidal coordinates $P(\varphi,\lambda,h)$ latitude, longitude and height. East and North span the horizontal plane and the Height or Up-axis coincides with the ellipsoidal normal (and practically with the local vertical), see [Seeber, 1993]. Note that it is actually a East, North, Height system to be a right-handed triad.

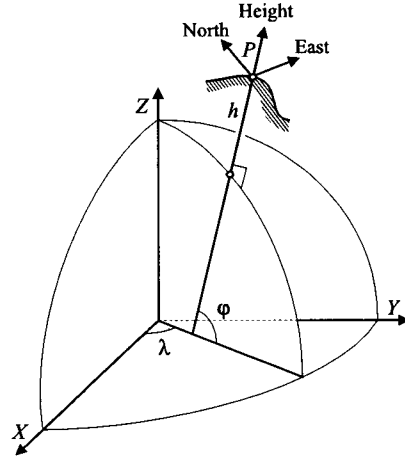


Figure 1.1: Local topocentric coordinate system

4.1.1 Recursive estimation

The recursive estimation by the Square Root Information Filter is a straightforward implementation of the theory in chapter 2. The observation equations for epoch k are given by (1.2) and (1.3), section 2.1.2. The recursion consists of alternatingly a time update, section 2.2.1, and a measurement update, section 2.2.2.

We aim at the computation of the filtered estimate $\hat{x}_{k|k}$ and the variance covariance matrix $Q_{\hat{x}_{k|k}}$. Vector $\hat{x}_{k|k}$ contains estimates for the unknown parameters one is interested in. As a result of the measurement update we have, see (2.10),

$$(1.1) \quad E\{\hat{z}_{k|k}\} = S_{k|k}^{-1} x_k$$

with $S_{k|k}^{-1}$ an $n \times n$ upper-triangular matrix. This set of equations can be solved for x_k by backward substitution. One can retrieve the estimate from the SRIF information array in this way any time, provided that it is in upper triangular shape. The transformation to realize this shape and its application are briefly reviewed in appendix A: the Householder transformation.

We concentrated on filtering, but also predicting and smoothing were mentioned in section 2.1.1. Prediction is made on a regular basis, one epoch ahead (the time-update). Smoothing with a SRIF is straightforward, but it is not implemented. For smoothing intermediate results have to be saved for each epoch: the matrices $S_{i,i}^{-1}$ and $S_{i,i+1}^{-1}$ together with z_i for $i=1, \dots, k-1$ in equation (2.5), section 2.2, are needed for the computation of smoothed estimators $\hat{x}_{i|k}$ with $i=1, \dots, k$, see also [Bierman, 1977].

An example of processing GPS data by means of a Square Root Information Filter for geodetic purposes can be found in [Blewitt, 1989] and for navigation (flight trajectory estimation) in [RAJPO, 1997].

partitioning of state vector

The model of observation equations for precise relative positioning (per epoch) was given in section 5 of chapter 3, equations (5.7) and (5.8). The state vector x is partitioned in time-varying parameters and bias parameters, that are constants. This corresponds to the partitioning in section 1.4, the real valued x_R and integer parameters x_I , equation (4.2). x_I is called the constant state space.

$$(1.2) \quad x = \begin{pmatrix} x_R \\ x_I \end{pmatrix}$$

The unknown parameters in the model are the double difference ambiguities x_I and the baseline coordinates x_R . If the second receiver is in motion, the ambiguities are constants (constant state space), but the baseline coordinates are time variant.

In a time-varying measurement system, one can have beside observations y_i , also pseudo-observations d_i , section 2.1.2. For the time update on x_R we have the following observation equation

$$(1.3) \quad E\{d_k\} = x_{Rk} - \Phi_{k,k-1} x_{Rk-1} \quad ; \quad D\{d_k\} = Q_{d_k}$$

If no knowledge about the motion of the rover is present (*full kinematic*), the time update can be skipped; new unknowns x_{Ri} are introduced epochwise $i=1, \dots, k$ (this corresponds to $Q_{d_k} = \infty$). The estimator for x_I at epoch $k-1$ can be directly used in the next measurement update as these parameters are constants, i.e. $x_{Ik-1} \doteq x_{Ik}$; there is actually only one vector of unknowns x_I (without time index).

If the roving receiver is stationary (*static*) with respect to the earth's surface, all parameters are constants, also the baseline coordinates x_{I2} ; differential geodynamic effects (earth tides, motions of tectonic plates) do not play a role in this small scale application. No time-update is needed; actually a sequential adjustment is made upon the unknown parameters (this corresponds to $Q_{d_k} = 0$).

Dynamic modelling of the time-varying parameters in the measurement system is beyond the scope of this research. We will restrict ourselves to the two limiting cases: stationary (coordinates constant) and full kinematic (receiver in permanent arbitrary motion). For model validation, section 4.2.1, misspecifications concerning the pseudo-observations (dynamic model) are not considered.

The partitioning of vector z and factor S^{-1} is according to (1.2). After the measurement update we have

$$(1.4) \quad E\left\{ \begin{pmatrix} \hat{z}_{k|k}^R \\ \hat{z}_{k|k}^I \end{pmatrix} \right\} = \begin{pmatrix} S_{Rk|k}^{-1} & S_{R,Ik|k}^{-1} \\ & S_{Ik|k}^{-1} \end{pmatrix} \begin{pmatrix} x_R \\ x_I \end{pmatrix}$$

4.1.2 Precision

The variance covariance matrix $Q_{\hat{x}}$ describes the random nature of the estimator \hat{x} under the null hypothesis H_0 , see also section 1.8.1. The diagonal elements give the variances of the individual estimators $\sigma_{\hat{x}_i}^2$, $i=1, \dots, n$. In the Square Root Information Filter, the variance covariance matrix of the filtered state estimator $Q_{\hat{x}_{k|k}}$ is found by inversion of $S_{k|k}^{-1}$: $Q_{\hat{x}_{k|k}} = S_{k|k} S_{k|k}^T$.

The variance covariance matrix will be used to evaluate the precision. In GPS surveying we are primarily interested in the geometric information, i.e. the baseline coordinates x_{12} . The 3 by 3 variance covariance matrix is $Q_{\hat{x}_{12}}$. In general x is an n -vector.

$$(1.5) \quad (\hat{x} - x)^T Q_{\hat{x}}^{-1} (\hat{x} - x) = \chi^2$$

The ellipsoid (1.5), centered at \hat{x} , represents locations of equal probability density for the expectation value x , see section 1.6, equation (6.5). χ^2 is some positive constant. The probability contained in the ellipsoid under the null hypothesis is easily found by the χ^2 -distribution as

$$(\hat{x} - x)^T Q_{\hat{x}}^{-1} (\hat{x} - x) \sim \chi^2(n, 0)$$

Matrix $Q_{\hat{x}}$ is symmetric and positive definite. The eigenvalue (singular value) decomposition allows further numerical interpretation of the precision. The n eigenvalues λ_i satisfy $|Q_{\hat{x}} - \lambda I| = 0$. Using the Rayleigh quotient, it can be shown that the variance of every (normalized) linear function of \hat{x} given by $v^T \hat{x}$, with norm equal 1, $v^T v = 1$, lies in between the smallest and largest eigenvalue:

$$\lambda_{\min} \leq \sigma_{v^T \hat{x}}^2 \leq \lambda_{\max}$$

with $\sigma_{v^T \hat{x}}^2 = v^T Q_{\hat{x}} v$ and v an n -vector. The lengths of the axes of the ellipsoid (1.5) equal $\chi \sqrt{\lambda_i}$. As such the eigenvalues describe the precision for n different normalized linear functions of the estimator. A rotation of the coordinate axes in R^n implies for the estimates $R\hat{x}$, where R is the $n \times n$ rotation matrix. As R is an orthogonal matrix, such a transformation does not alter the eigenvalues of the variance covariance matrix.

By considering the eigenvalue problem $|Q_{\hat{x}} - \lambda I| = 0$, the variance covariance matrix is actually analysed with respect to unit precision, represented by the matrix I , or in other words, precision is judged upon based on the unity criterion, see [Teunissen, 1997].

4.1.3 Ambiguity resolution

The implementation of the LAMBDA method for integer ambiguity estimation is discussed in full detail in [Jonge et al, 1996]. The input is basically \hat{x}_I and $Q_{\hat{x}_I}$, the vector of estimates for the ambiguities and the variance covariance matrix from the float solution. The consequence of resolving the ambiguities is that they are then treated as deterministically known quantities, see the discussion in section 1.6. The LAMBDA method is applied to short GPS baselines in [Teunissen et al, 1997a] and practical results are given in [Teunissen et al, 1997b].

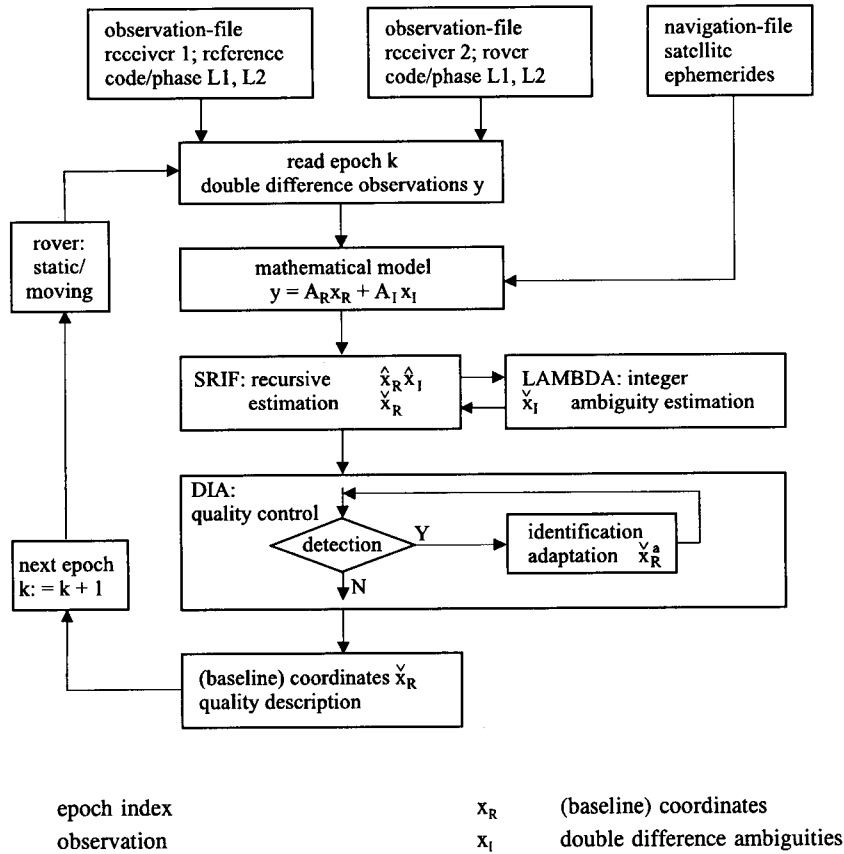


Figure 1.2: Flow diagram for GPS data processing

4.1.4 Flow diagram

The purpose of the research was to develop prototype software and to investigate the capabilities of the kinematic GPS surveying measurement technique in providing geometric information, in particular with respect to the (geodetic) quality of the data.

For the development of the software, several limiting assumptions were made in order to reduce the programming effort; not because of the mathematical modelling or the mechanization for the recursive data processing. It was tried to keep administrative overhead as small as possible; e.g. satellites once chosen for processing have then to be available for the whole session defined. The implementation was realized in a straightforward manner in Microsoft FORTRAN version 5.1 on an ordinary PC. Only little effort was made on the user-interface and on handling in- and output.

In figure 1.2 the flow diagram for processing the data for GPS surveying is given. The program reads the navigation file and then the observation files, epoch by epoch. The recursive estimation (filtering), together with the quality control is cycled through every epoch. The procedure basically provides filtered estimates for the coordinates of the rover receiver x_R with the ambiguities fixed, whenever possible, thus \hat{x}_R . Once the ambiguities are fixed (and lock is not lost from then on), the recursive estimation continues, but skips the integer estimation. The DIA-procedure for quality control is discussed in the next section.

4.2 Model validation

Data processing consists of estimation and quality control [Alberda, 1968]. The purpose of a geodetic measurement or survey system, like kinematic GPS, is to provide geometric information. This information usually concerns coordinates (the estimation part), but should comprise also the quality of the coordinate estimators (the quality control part). Quality as a measure, describes to what extent the estimation results will/can serve their use. The coordinates-file, together with the quality description can be further used or handled and for example be input in a Geographic Information System (GIS).

Quality assurance comprises three steps. They correspond to the stages before, during and after operation of the (time-varying) measurement system. The following general discussion is after [Salzmann, 1993].

In the design phase of the system, optimization with respect to quality takes place, by using measures on precision and reliability. These measures can be computed prior to operation of the system. In these computations, the null hypothesis usually is the default mathematical model. In order to meet the specifications on quality in terms of precision and reliability, the measurement system can be (re-) designed and/or the statistical testing procedure can be tuned.

In the second step, the operational phase, the statistical testing procedure is carried out parallel with the estimation. The null hypothesis is opposed to alternative hypotheses. After carrying out the testing procedure, one can be sure, to a certain degree, about the validity of the model used. This degree is described by reliability. In a time-varying measurement system, such as for kinematic GPS surveying, we strive for quality control in real time. The DIA testing procedure can be executed directly in real time when the data are actually being processed.

In the design phase, quality was described a-priori, based on the assumed modelling. The a-posteriori quality description (realization) can be given only after the operational phase. Specifically it can be checked whether the specifications on quality have been met. Under the null hypothesis the estimate obtained is a sample from the estimator with the stated (design) quality (conformance); the quality measures have been computed using the null hypothesis. The check should be carried out when the null hypothesis has been rejected in favour of some alternative hypothesis. Besides, an additional validation can be carried out in this step. This implies comparison of the estimates and accompanying quality description with some ground-truth. This validation (inspection) is made only incidently as a geodetic ground-truth is usually not available.

Real time kinematic GPS surveying in its measurement scenario and data processing, quite much resembles a (precise) positioning/navigation system. Therefore three more aspects of quality may be involved in a high survey production environment. They are availability, continuity and integrity. Availability describes for what percentage of time, the system can be used, and for what period it is scheduled out. Availability concerns a single epoch in time. Continuity concerns an interval in time and describes for what period the system will be operational without interruption. Integrity deals with the information of the user by either external report or autonomous detection, that the system does not meet the operational specifications. Integrity has to do with aspects of precision and reliability [Salzmann, 1993].

Requirements on all these aspects of quality of GPS positioning likely depend on the application, which may range from precise geodesy through surveying to navigation. In this research, the attention is restricted to geodetic quality. Measures for the quality are presented, rather than requirements upon these measures. In our case such requirements will depend on the purpose that is to be served by the geometric information obtained by kinematic GPS surveying. Moreover, for a particular application, specifications on precision may be available, but specifications on reliability are still very rare in practice.

4.2.1 Alternative hypothesis

The null hypothesis, the mathematical model used in the estimation, therefore also called the working model, may not be (completely) adequate. We have to assess the validity of this model and detect possible misspecifications, if there are any. The null hypothesis has to be confronted with alternative hypotheses.

The specification of alternative hypotheses is usually not a trivial task. One has to predict the signature of possible model error types. It is however, of vital importance and must therefore be done very carefully. The specification will directly determine the value of the reliability description.

slippage tests

In this research we will limit ourselves to one-dimensional misspecifications in the functional model. They are directly related to one specific (sequence of) observation(s). As compared with the null hypothesis, the alternative hypothesis is extended by one unknown parameter, $q=1$. The matrix C , reduces to a vector. The misspecifications are additive. This type of model errors is classified as slips. The identification tests are also referred to as slippage tests. Examples of slips are outliers and (cycle) slips in observations.

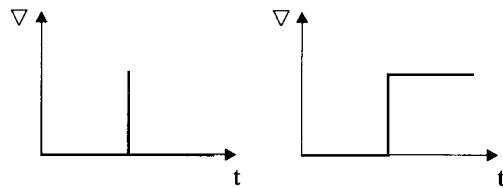


Figure 2.1: Outlier/spike (left) and slip/jump (right)

An outlier is one erroneous observation in a sequence (in time) of observations. The error occurs only once. When a slip occurs, the observations get biased by a constant error. The error starts and continues to occur. In figure 2.1 we represent both error types. The error is given as function of time. The outlier is a spike function, the slip a jump function.

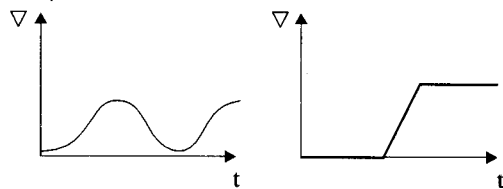


Figure 2.2: Periodic error (left) and ramp error (right)

For a sequence from epoch 1 to k of phase or code observations $p_{r,i}^s$, made by receiver r to satellite s , the functional model of the null hypothesis is symbolically given by (2.1). The alternative hypotheses for an outlier and a slip at epoch l then become respectively (2.2).

Specifying an outlier hypothesis for each observation available and testing the null hypothesis against them, is called data-snooping, [Baarda, 1968].

$$(2.1) \quad H_0 : E \left\{ \begin{pmatrix} p_{r1}^s \\ \vdots \\ p_{r,l-1}^s \\ p_{r,l}^s \\ p_{r,l+1}^s \\ \vdots \\ p_{r,k}^s \end{pmatrix} \right\} = Ax$$

$$(2.2) \quad H_a : E \left\{ \begin{pmatrix} p_{r1}^s \\ \vdots \\ p_{r,l-1}^s \\ p_{r,l}^s \\ p_{r,l+1}^s \\ \vdots \\ p_{r,k}^s \end{pmatrix} \right\} = Ax + \begin{pmatrix} 0 \\ \vdots \\ 0 \\ 1 \\ 0 \\ \vdots \\ 0 \end{pmatrix} \nabla \quad \text{and} \quad H_a : E \left\{ \begin{pmatrix} p_{r1}^s \\ \vdots \\ p_{r,l-1}^s \\ p_{r,l}^s \\ p_{r,l+1}^s \\ \vdots \\ p_{r,k}^s \end{pmatrix} \right\} = Ax + \begin{pmatrix} 0 \\ \vdots \\ 0 \\ 1 \\ 1 \\ \vdots \\ 1 \end{pmatrix} \nabla$$

Slip and outlier as discussed above, are limiting cases of each other. A slip ∇ at epoch l , followed by a slip $-\nabla$ at epoch $l+1$ (thus same magnitude, opposite sign), is identical to an outlier ∇ at epoch l . An outlier ∇ that occurs at epoch l and keeps on occurring until epoch k (with same size) can be interpreted as a slip ∇ that starts at epoch l .

Slip and outlier are two elementary error types in observations. More complex error types can be thought of: a periodic error (periodic function) and an error which size ∇ increases as time proceeds (ramp function), see figure 2.2.

In GPS surveying we have code and phase observations. As alternative hypotheses we will consider outliers and slips. In particular, the slip in the phase observation (cycle slip) and the outlier in the code observation (blunder) are well known error types in GPS positioning. A slip in the code observation may be less realistic. The errors are assumed to have their cause typically at or inside the receiver where the measurements are made, not at the satellite.

Note that currently the phase observations will be tested for cycle slips that can be of any size, $\nabla \in R$. The error is estimated as a real number, see also section 7.3 of chapter 1, whereas it is known a-priori to amount to an integer number of cycles.

As an example the alternative hypothesis for an outlier at epoch l , and the alternative hypothesis for a slip at epoch l , were specified in (2.1) and (2.2) for one observation p_r^s . In principle, the outlier hypothesis has to be specified for each of the code observations at epoch l , from m satellites and 2 receivers (possibly at two frequencies): p_1^1, \dots, p_1^m , p_2^1, \dots, p_2^m and $\bar{p}_1^1, \dots, \bar{p}_1^m$, $\bar{p}_2^1, \dots, \bar{p}_2^m$ and the slip hypothesis for each of the phase observa-

$$E \begin{pmatrix} \Delta p_{12}^1 \\ \Delta p_{12}^{12} \\ \vdots \\ \Delta p_{12}^{1m} \end{pmatrix} = \begin{pmatrix} -(e_2^1)^T & 1 \\ -(e_2^2 - e_2^1)^T & 0 \\ \vdots & \vdots \\ -(e_2^m - e_2^1)^T & 0 \end{pmatrix} \begin{pmatrix} \Delta x_2 \\ c \Delta \partial_2 t \end{pmatrix} + \begin{pmatrix} 1 & & & \\ -1 & 1 & & \\ \vdots & & \ddots & \\ -1 & & & 1 \end{pmatrix} \begin{pmatrix} \nabla^1 \\ \vdots \\ \nabla^m \end{pmatrix}$$

Leaving out the single difference p_{12}^1 yields the model with $(m-1)$ double differences:

$$(2.7) \quad E \begin{pmatrix} \Delta p_{12}^{12} \\ \vdots \\ \Delta p_{12}^{1m} \end{pmatrix} = \begin{pmatrix} -(e_2^2 - e_2^1)^T \\ \vdots \\ -(e_2^m - e_2^1)^T \end{pmatrix} (\Delta x_2) + \begin{pmatrix} -1 & 1 & & \\ \vdots & & \ddots & \\ -1 & & & 1 \end{pmatrix} \begin{pmatrix} \nabla^1 \\ \vdots \\ \nabla^m \end{pmatrix}$$

In terms of double differences, we have to test for an outlier in each of the $(m-1)$ observations p_{12}^{1i} $i=2, \dots, m$ (caused by an outlier in the single difference p_{12}^i) and also for one simultaneous outlier in all of the $(m-1)$ double differences; the first column with -1 's. The latter is caused by an outlier in the observation p_{12}^1 to the pivot satellite. With $(m-1)$ double differences, we have to test thus for m (*single difference*) outlier hypotheses.

From the above model it can also be seen that with only one double difference, $m=2$, one can never distinguish between the two single difference outlier hypotheses; at least two double differences are needed, $m=3$.

Considering the above model as a whole, there must be at least $m \geq 6$ satellites. Statistical testing is based on (sufficient) redundancy. When only $m=4$ satellites are observed, there is no redundancy at all. With $m=5$ satellites, detection is possible, but identification - separation between different alternative hypotheses - is not.

4.2.2 Testing strategy

In this section on testing strategy we will elaborate on the implementation of the DIA-procedure, cf. appendix 2.B. The computations for this testing can be easily embedded in the Square Root Information Filter, section 3 of chapter 2. Testing is based on the normalized predicted residuals \underline{w}_k . These residuals have a unit variance covariance matrix. The DIA-procedure can be run in the operational phase at every epoch in close parallel with the recursive estimation. Examples of statistical testing applied to GPS positioning can be found in [Cross et al, 1994], [Abusaleem et al, 1994], [Nikiforov, 1996], [Elema, 1997] and [Powe et al, 1997].

In a time-varying measurement system we have to deal with time-series of observations. An observation from a certain combination of a satellite and a receiver is available for every epoch from 1 to k . Such a combination is also referred to as channel. The measurement system consists of a set of channels.

In a time-varying measurement system, we must specify a series (in time) of alternative hypotheses per channel and per observation type. Not only the channel is not known, but also the time of occurrence is unknown. In practice, the number of epochs considered in the testing procedure at a certain epoch, will be limited by a window. In this respect we will discuss the detection and identification step of the DIA testing procedure. The adaptation is deferred to the next section.

In the detection and identification step we use statistical tests that have different degrees of freedom. A possible link between the overall model tests and the slippage tests is discussed and some considerations in choosing the parameters of the testing procedure are given.

detection

In the detection step, the overall model test is carried out. At epoch k in the recursion, this test should concern all data from epoch 1 to epoch k . The dimension of the C -matrix equals $\sum_{i=1}^k m_i - n$. In practice, taking into account all normalized predicted residuals may not be feasible, especially when k gets large, [Teunissen et al, 1989]. The test is rigidly restricted to the epochs l to k . A window is set for the test. The window length equals $N=k-l+1$ epochs. The window length is kept fixed and as the recursion proceeds, k increases and l is incremented as well. The dimension of the C -matrix equals $\sum_{i=l}^k m_i$ (for $l > 1$). The overall model teststatistic is denoted by \underline{I}^{lk} (cf. (B.21) of appendix 2.B).

identification

In the identification step, slippage tests are carried out. We limit ourselves to one-dimensional model errors ($q=1$). The slippage teststatistic is denoted by \underline{t}^{lk} (cf. (B.22) appendix 2.B). In some observation, a slip or an outlier may occur. But as we are concerned with a time-varying system, the epoch of occurrence can vary from 1 to k . For the code observation p_r^s for instance, we should test for all of the following hypotheses in case of an outlier:

$$E\left\{ \begin{pmatrix} p_{r1}^s \\ p_{r2}^s \\ \vdots \\ p_{r,l-1}^s \\ p_{rl}^s \\ p_{r,l+1}^s \\ \vdots \\ p_{rk}^s \end{pmatrix} \right\} = Ax + \begin{pmatrix} 1 \\ 0 \\ \vdots \\ 0 \\ 0 \\ \vdots \\ 0 \end{pmatrix} \nabla ; + \begin{pmatrix} 0 \\ 1 \\ \vdots \\ 0 \\ 0 \\ \vdots \\ 0 \end{pmatrix} \nabla ; \dots ; + \begin{pmatrix} 0 \\ \vdots \\ 1 \\ 0 \\ 0 \\ \vdots \\ 0 \end{pmatrix} \nabla ; + \begin{pmatrix} 0 \\ \vdots \\ 0 \\ 1 \\ 0 \\ \vdots \\ 0 \end{pmatrix} \nabla ; + \begin{pmatrix} 0 \\ \vdots \\ 0 \\ 0 \\ 1 \\ \vdots \\ 0 \end{pmatrix} \nabla ; \dots ; + \begin{pmatrix} 0 \\ \vdots \\ 0 \\ 0 \\ 0 \\ \vdots \\ 1 \end{pmatrix} \nabla$$

Only the last few hypotheses will be tested for in practice. This yields then the window from epoch l to k . The considerations for using a window are given in [Teunissen et al, 1989] and [Salzmann, 1993]. In chapter 5 model validation will be limited to local

testing, $l=k$; the windowlength is $N=1$. If errors are encountered and identified, they are put out immediately at the same instant.

procedure for data processing

The data processing starts with the estimation under the null hypothesis and the set up of a collection of relevant alternative hypotheses. The estimation is directly followed by the DIA procedure. In the detection step, the overall validity of the null hypothesis is checked.

Rejection of the overall model test $T^{l,k}$ at epoch k makes us decide that the null hypothesis, concerning the epochs l to k , is not valid. A systematic consideration of the slippage tests $t^{l,k}, t^{l+1,k}, \dots, t^{k,k}$ for all channels and for all types of errors is needed to localize the model error. The identification is carried out. The null hypothesis is tested against the alternative hypotheses, one at a time. As all slippage tests have $q=1$ degree of freedom, they can be mutually compared. The alternative hypothesis that corresponds to the teststatistic with the largest value is most likely, thus time of occurrence, type of observation and which satellite (channel) are determined. If this slippage test is rejected indeed, the model error can be considered sufficiently more likely than the null hypothesis and this alternative hypothesis becomes the new null hypothesis.

The adaptation concludes the model validation. In this step we switch to estimation under the alternative hypothesis. If after adaptation the overall model test is still rejected however, yet another identification needs to be carried out. Several model errors can occur simultaneously at some epoch. The procedure is repeated in order to handle multiple model errors. In this way the original null hypothesis is stepwise extended. The number of unknowns thereby increases. The number of observations is fixed and the redundancy therefore decreases.

The iteration goes on in principle, until detection is not positive anymore. The limit of this process is the case of zero redundancy. Nor the overall model test, nor the identification tests will then be rejected. This does not necessarily imply however, that there are absolutely no errors left in the observations. The only correct conclusion is that the observations do fit now the (adapted) model exactly.

Discrepancies between detection and identification may occur in practice. This can be due to the specification of alternative hypotheses. The correct hypothesis is not included in the specified set. The overall model test will then be rejected without one of the slippage tests being rejected. Another cause is of statistic nature and has to do with the linking of statistical tests with different degrees of freedom.

B-method of testing

The overall model teststatistic and the slippage teststatistic will have different degrees of freedom. A possible linking of these teststatistics is provided by the B-method of testing [Baarda, 1968]. This method is briefly reviewed.

The overall model teststatistic $I^{l,k}$ has $\sum_{i=l}^k m_i$ degrees of freedom, whereas the slippage teststatistic $t^{l,k}$ has only $q=1$ degree of freedom. Tests with different degrees of freedom can be linked by requiring equal non-centrality parameter for all dimensions. The inverse power function gives the non-centrality parameter λ for the generalized likelihood ratio

teststatistic as function of the level of significance α , the degrees of freedom q and the power γ .

$$(2.8) \quad \lambda(\alpha_q, q, \gamma_o) = \lambda_o$$

Power γ is fixed to some reference value, usually $\gamma_o=0.80$. The power γ , the probability of correct detection, should be as large as possible; $\beta=1-\gamma$ is the probability of missed detection. Together with the level of significance for the one-dimensional test $\alpha_{q=1}$ this determines the reference value λ_o for the non-centrality parameter (section 8, chapter 1). The non-centrality parameter equals the squared norm of the model error in terms of misclosures (8.1).

The levels of significance for other dimensions α_q , $q > 1$, now directly follow from the inverse power function (1.8). In figure 2.3 after [Kösters, 1992], the levels of significance α_q are given as function of q for five values of power γ ($\gamma_o=0.5, 0.6, 0.7, 0.8$ and 0.9). A common choice is $\alpha_{q=1}=0.001$ (in geodetic networks). The level of significance α , the probability of false alarm, should be small. The default values yield $\lambda_o=17.075$. In navigation applications, with safety as a prior condition, a larger γ may be preferred and a larger α is put up with.

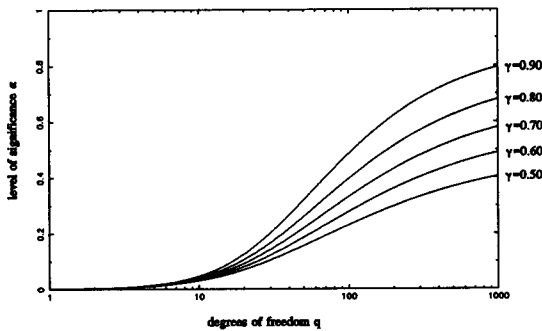


Figure 2.3: B-method of testing, α versus q , $\alpha_{q=1} = 0.001$

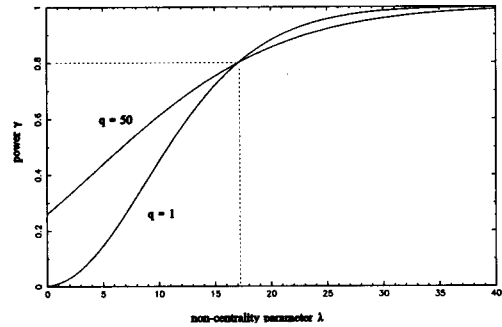


Figure 2.4: B-method of testing, γ versus λ , $\gamma_o = 0.80$, $\alpha_{q=1} = 0.001$ and $\alpha_{q=50} = 0.260$

The Minimal Detectable Bias gives the size of a model error that can be detected with a probability of γ_o by the appropriate slippage test ($q=1$), see section 8 of chapter 1. The idea behind the B-method of testing with slippage tests and more dimensional tests is that such a model error should be detected by the more dimensional tests with a probability of γ_o as well, when these tests also encompass this particular error.

In figure 2.4 power γ is given as function of the non-centrality parameter λ for $q=1$ and $q=50$. Both lines pass through $(\lambda_o, \gamma_o=0.80)$. Figure 2.4 shows that if the size of the model error does not equal the MDB ($\lambda \neq \lambda_o$), the power of the slippage test ($q=1$) will differ from the power of the overall model test ($q > 1$), as the tests have different degrees of freedom. This may cause discrepancies between detection and identification.

Returning to figure 2.3, we see that α as function of q is a monotone increasing function: $\alpha_{q=1} < \alpha_{q>1}$ for some fixed power γ_o . This means that the overall model test will be more conservative than a slippage test, see also [Heus et al, 1994]. The probability of rejecting

the null hypothesis when in fact it holds true, is larger for the overall model test than for a slippage test.

A serious handicap of the B-method of testing is that when the redundancy increases, the level of significance α_q for the overall model test may become unacceptable large, e.g. larger than 50%, see [ibid]. Using a window in the testing procedure will bound the redundancy.

The B-method can be used to provide a link between detection and identification. In the reference [ibid] also a strategy is proposed for simultaneous handling alternative hypotheses of different dimensions in the identification step. It is suggested to divide the value for the teststatistic by the corresponding critical value. As such test-ratios are obtained, that can be mutually compared.

4.2.3 Adaptation

The estimate \hat{x}^o and the accompanying variance covariance matrix $Q_{\hat{x}^o}$ have been computed using the null hypothesis, the working model. In the detection step, this model was found to be invalid. The identification was carried out to spot the model error. Based on the data available, a certain alternative hypothesis turns out to be sufficiently more likely than the null hypothesis. It is decided to use this alternative hypothesis as the new null hypothesis.

The estimation results have to be re-computed, now using the new null hypothesis: \hat{x}^a and $Q_{\hat{x}^a}$, i.e. we have to account for the model error. In practice, this estimation is not started over from scratch. The results under the previous null hypothesis are used. This is the adaptation step.

$$H_0 : \begin{matrix} \hat{x}^o \\ Q_{\hat{x}^o} \end{matrix} \quad \text{-- adaptation --} \quad H_a : \begin{matrix} \hat{x}^a \\ \hat{\nabla} \\ Q_{\hat{x}^a} \end{matrix}$$

The adaptation in the Square Root Information Filter mechanization has been treated in section 3 of chapter 2. By additional orthogonal transformations both the estimator $\hat{x}_{k|k}^o$ and the normalized predicted residuals \underline{w}_k were updated. Adaptation strategies for the standard Kalman filter are discussed in [Salzmann, 1995]. In this section we will outline the strategy for adaptation for the model errors previously considered: outliers and slips. We are primarily interested in filtered state estimates $\hat{x}_{k|k}$. Adaptation of smoothed estimates is not considered.

outlier

Adaptation for an outlier in an observation is straightforward. The estimators $\hat{x}_{k|k}^a$ and $\hat{\nabla}$ are computed and the normalized predicted residuals are updated. As an outlier is a model error that occurs only once, no future observations will be related to the model error ∇ . The estimator $\hat{\nabla}$ can therefore be left out from the state vector. After adaptation for an outlier, one can revert to estimation under the null hypothesis immediately [ibid].

slip

Adaptation for a slip in general is more complicated. The estimators $\hat{x}_{k|k}^a$ and $\hat{\nabla}$ are computed and the normalized predicted residuals are updated. A slip is a model error that

starts and continues to occur in principle for ever. Future observations will still be related to the model error ∇ . This has to be accomodated in the mathematical model.

By adaptation for the slip, the state vector is enlarged by ∇ . After that, this model error parameter should remain in the state vector for ever (and be propagated along with the other constant parameters). In practice one may decide to make an approximation, and leave the estimator $\hat{\nabla}$ out from the state vector after a certain number of epochs. The incoming observations need then to be corrected a-priori with the most recent estimate $\hat{\nabla}$. The stochasticity of $\hat{\nabla}$ is neglected, see also [ibid].

slip in constant state space

Adaptation for a slip in an observation that is already related to a constant parameter, as is the GPS phase observation (the ambiguity), is straightforward. This type of slip is also referred to as slip in the partially constant state space [Teunissen, 1992], see [Salzmann, 1993]. The adaptation is discussed by means of a simple example.

Observable y is, among other parameters in x , related, via coefficient b , to some constant parameter denoted by c (not to be confused with the speed of light).

$$(2.9) \quad H_o: \quad E\{y\} = a^T x + bc$$

A slip ∇ occurs. The adaptation is carried out. The estimators $\hat{x}_{k|k}^a$ and $\hat{\nabla}$ are computed and the normalized predicted residuals are updated.

The state vector now contains two biases both related to the observable y : c and ∇ . As the slip continues to occur, future observations are still related to both c and ∇ .

$$(2.10) \quad H_a: \quad E\{y\} = a^T x + bc + b\nabla$$

Note that the bias and the slip have identical coefficients; the slip ∇ can be directly absorbed by the constant parameter c . We apply the following reparametrization of unknowns:

$$\begin{pmatrix} \bar{c} \\ c \end{pmatrix} = \begin{pmatrix} 1 & 1 \\ 0 & 1 \end{pmatrix} \begin{pmatrix} \nabla \\ c \end{pmatrix}$$

where $\bar{c} = \nabla + c$ denotes the new constant parameter for observable y . Future observations are related to \bar{c} only and not to c anymore. As the estimator for this quantity is of no interest, the old constant parameter c can be left out. After this adaptation, one can revert to estimation under the null hypothesis, now with the new constant parameter \bar{c} instead of c . The slip in the observation is actually absorbed by the constant parameter c . The size of this bias is changed.

$$(2.11) \quad H_a: \quad E\{y\} = a^T x + b\bar{c}$$

In section 2.3, the adaptation was carried out for a local model error. As it was stated, the adaptation for a global model error can be carried out similarly in a straightforward

manner. When many epochs are in between occurrence, epoch l , and detection, epoch k , of the model error however, such a rigorous adaptation may become computationally very demanding.

Detection, identification and adaptation for global model errors inevitably leads to temporarily biased estimates. The filtered estimates $\hat{x}_{l|l}, \dots, \hat{x}_{k-1|k-1}$ are computed still using the null hypothesis. The model error is taken into account not until epoch k . The reader is referred again to the considerations in [Salzmann, 1993].

We have discussed the adaptation for an outlier, a slip in general and a slip in the constant state space. For GPS observations, the outlier in a code observation and the (cycle) slip in a phase observation are of importance. The adaptation for these model errors is exact and straightforward. After adaptation one can again use the null hypothesis. As stated in section 2.3 the adaptation can be repeated, if multiple model errors are present. In this way it is possible to finally have adapted for a composite model error ($q > 1$).

4.2.4 Reliability

Reliability describes the nominal performance of the model validation. The theoretical background of reliability was discussed in section 1.8.2. In particular we will consider the Minimal Detectable Bias ∇ and the bias to noise ratio λ_x . The formulae for their computation in the Square Root Information Filter in chapter 2, are (3.13) and (3.16) respectively.

The Minimal Detectable Bias is a measure for internal reliability. The MDB gives for a one-dimensional alternative hypothesis, the size of a model error that can be detected with probability γ by the corresponding slippage test. As we consider outliers and slips in observations, the MDB can be directly interpreted. The MDB for an outlier in the code is expressed in meters, for a slip in the phase in cycles. In the design phase of the system one should also check the separability of the one-dimensional alternative hypotheses, see equation (8.4) in chapter 1.

For external reliability we consider the effect on the state estimate of a model error of the size of the MDB, when it is left undetected. The significance of the effects is given by the bias to noise ratio $\lambda_{\hat{x}_{k|k}}$; the bias is weighted against the precision. Below equation (B.32) of chapter 2, the following interpretation was given. $\sqrt{\lambda_{\hat{x}_{k|k}}}$ provides an upperbound for the bias in an individual element of the estimate $\hat{x}_{k|k}$. Also a part of the state vector can be considered, e.g. the coordinates x_{12} .

The reliability measures are computed for every epoch simultaneously with the DIA-procedure. As in the adaptation, the matrices C_w are updated, the reliability measures automatically refer to the working hypothesis; i.e. the null hypothesis or after adaptation - possibly for multiple model errors - the alternative hypothesis.

4.3 Summary

In the chapters 1 through 3, we have discussed the concepts and principles of estimation and testing, the recursive data processing and the mathematical modelling. In this chapter, it is briefly shown how these components synergize in the recursive data processing for

kinematic GPS surveying. A flow diagram was given and several practical aspects of the implementation were described. The implementation is the basis for the computations and analyses discussed in chapter 5.

In section 4.2 we were concerned with the DIA-procedure, the statistical testing procedure that is carried out along with the recursive estimation. The purpose of the procedure is to find actual model errors. The elementary error types outlier and (cycle) slip are relevant alternative hypotheses in kinematic GPS surveying. Considerations on setting the parameters of the statistical testing procedure were given. When a model error occurs, it must be accounted for. The adaptation for the outlier and slip error type was outlined.

It must be noted that the occurrence of a (large) model error in itself need not to be severe. The model error will be detected with high probability, properly identified and adapted for. The 'repaired' measurement system can then still be of sufficient quality. The DIA-procedure is the tool to effectively bring the data and mathematical model in mutual correspondence during the data processing.

Measures for quality refer to precision and reliability. Measures on precision are based on the variance covariance matrix of the estimator. Precision describes the quality of the estimator under the original mathematical model, the null hypothesis. Reliability describes the performance of the statistical testing procedure and concerns 'what if' scenarios. Can it be detected, when a certain model error occurs and if not, what is the effect on the desired positioning results. Measures on reliability are primarily the Minimal Detectable Bias for internal reliability and the bias to noise ratio which expresses the significance concerning the external reliability.

Appendix 4.A Householder transformation

In the Square Root Information Filter, the Householder transformation is the major tool to get the data processing done; the orthogonal transformation was applied in appendix 2.A. It was introduced by [Householder, 1958]. The use of this transformation for solving linear least-squares problems via QR-factorization was discussed in [Golub, 1965] and the implementation was given in [Businger et al, 1965]. Further references include [Lawson et al, 1969] and with respect to recursive estimation [Dyer et al, 1969] and [Bierman, 1977]. A comprehensive treatment can be found in [Golub et al, 1989] and [Björck, 1996].

In this appendix we will briefly discuss how the orthogonal Householder transformation is used to bring the design matrix into upper-triangular shape.

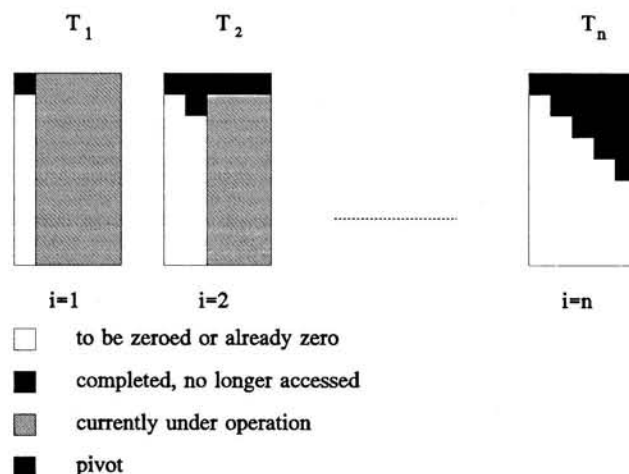


Figure A.1: Triangularization of matrix A

triangularization of the design matrix

The computation, the properties and the geometric interpretation of the Householder transformation are discussed in [Bierman, 1977]. The idea is that by means of an orthogonal transformation, an arbitrary (non-zero) vector has been reflected such that all elements equal zero except for the first. The vector has been reflected such that it has only one non-zero component and this non-zero component lies in the e_j -direction $(1,0,\dots,0)^T$.

This vector can be a column of the $m \times n$ design matrix A (we have assumed that $m \geq n$). This column is the pivot column. For example the first column is then zeroed, except for the first element, by the Householder transformation. The first column completely determines the matrix T_1 . The observations y and the remaining columns of A are then transformed using the same T_1 : $T_1 y = T_1 A x$, see section 2.A.1. An $m \times n$ -matrix A can now be triangularized by a sequence of n elementary Householder transformations:

$$(A.1) \quad T = \begin{bmatrix} I_{n-1} & & \\ & \ddots & \\ & & T_n \end{bmatrix} \cdots \begin{bmatrix} I_1 & \\ & T_2 \end{bmatrix} [T_1]$$

where T_1 has dimension m , T_2 dimension $m-1$ and T_n dimension $m-n+1$. The triangularization process of the design matrix is illustrated in figure A.1. Matrix T_1 operates on the full $m \times n$ -matrix and zeroes the first column of A below element $(1,1)$. Matrix T_2 operates only on the $(m-1) \times (n-1)$ -lower part of A . It zeroes the second column of A below element $(2,2)$. This process is continued and finally matrix T_n operates only on the $(m-n+1) \times 1$ -lower part of A . It zeroes the n^{th} column of A below element (n,n) . Note that all n $m \times m$ -matrices in (A.1) are orthogonal.

As a result of the sequence of transformations, we have the desired upper triangular shape. The transformation matrix T is not explicitly computed. As indicated in appendix 2.A, prior to the QR-factorization of designmatrix A , the observables are normalized, equations (A.7) and (A.8). The Cholesky factors of both Q_{d_k} and Q_{y_k} are thus to be computed first.

SRIF

The Square Root Information Filter is implemented using the concept of the information-array [Bierman, 1977]. The term 'information' is explained in section 6.8 of [Grewal et al, 1993]. The information matrix is the inverse of the variance covariance matrix, thus the normal matrix. All information is contained in two arrays (for the measurement update; equations (2.9) and (2.10) of chapter 2):

- a two-dimensional array (matrix), basically containing design matrix A on the input and upper-triangular factor S^{-1} on the output
- a one-dimensional array (vector), containing the vector of observations y on the input and the transformed state vector z on the output

References

[Abousalem et al, 1994] Abousalem, M.A., M.A. Forkheim and J.F. McLellan (1994). Quality GPS post processing with JUPITER. Proceedings of KIS94. Banff, Canada. August 30 - September 2. pp. 197-206.

- [Alberda, 1968] Alberda, J.E. (1968). Decision-making and surveying. The 12th International Congress of Surveyors. September 2-12. London, England. 7 pp.
- [Baarda, 1968] Baarda, W. (1968). A testing procedure for use in geodetic networks. Publications on Geodesy, Vol. 2, No. 5. Netherlands Geodetic Commission. Delft.
- [Bierman, 1977] Bierman, G.J. (1977). Factorization methods for discrete sequential estimation. Volume 128 in Mathematics in science and engineering. Academic Press, Inc. New York.
- [Björck, 1996] Björck, Å. (1996). Numerical methods for least squares problems. SIAM. Philadelphia.
- [Blewitt, 1989] Blewitt, G. (1989). Carrier phase ambiguity resolution for the Global Positioning System applied to geodetic baselines up to 2000 km. Journal of Geophysical Research. Vol. 94, No. B8 August. pp. 10-187-10.203.
- [Businger et al, 1965] Businger, P. and G.H. Golub (1965). Linear least squares solutions by Householder transformations. Numerische Mathematik. Vol. 7. Handbook series linear algebra. Springer Verlag, Berlin. pp. 269-276.
- [Cross et al, 1994] Cross, P.A., D.J. Hawksbee and R. Nicolai (1994). Quality measures for differential GPS positioning. The Hydrographic Journal. No. 72. April. pp. 17-22.
- [Dierendonck, 1994] Dierendonck, A.J. van (1994). Understanding GPS receiver terminology: a tutorial on what those words mean. Proceedings KIS94. Banff, Canada. August 30 - September 2. pp. 15-24.
- [Dyer et al, 1969] Dyer, P. and S. McReynolds (1969). Extension of square-root filtering to include process noise. Journal of optimization theory and applications. Vol. 3. No. 6. pp. 444-458.
- [Elema, 1997] Elema, I.A. (1997). Integrating raw Loran-C and GPS observations with integrity monitoring for marine and land applications. Publication on Bridge 2000. Royal Netherlands Naval College. December. 8 pp. Internet URL <http://www.tno.nl/instituut/fel/brug2000>
- [Golub, 1965] Golub, G.H. (1965). Numerical methods for solving linear least squares problems. Numerische Mathematik. Vol. 7. Handbook series linear algebra. Springer Verlag, Berlin. pp. 206-216.
- [Golub et al, 1989] Golub, G.H. and C.F. van Loan (1989). Matrix computations. The Johns Hopkins University Press. Baltimore, Maryland. Second edition.
- [Grewal et al, 1993] Grewal, M.S. and A.P. Andrews (1993). Kalman filtering; theory and practice. Prentice-Hall, Inc. Englewood Cliffs.
- [Gurtner et al, 1990] Gurtner W. and G.L Mader (1990). The RINEX format: current status, future developments. Proceedings of the 2nd International Symposium on Precise Positioning with the GPS. Ottawa, Canada. September 3-7. pp. 977-992.
- [Gurtner, 1993] Gurtner, W. (1993). RINEX: the Receiver Independent Exchange Format version 2. Astronomical Institute, University of Berne. April, last rev. Feb 95.
- [Heus et al, 1994] Heus, H.M. de, P. Joosten, M.H.F. Martens en H.M.E. Verhoef (1994). Geodetische deformatie analyse. 1-D deformatieanalyse uit waterpasnetwerken. LGR rapport No. 5. Faculteit der Geodesie. Technische Universiteit Delft.
- [Hofmann-Wellenhof et al, 1997] Hofmann-Wellenhof, B., H. Lichtenegger and J. Collins (1997). GPS Theory and Practice. Springer-Verlag. Wien, New York. Fourth revised edition.

- [Householder, 1958] Householder, A.S. (1958). Unitary triangularization of a nonsymmetric matrix. *Journal of Association for Computing Machinery (ACM)*. Vol. 5. New York. pp. 339-342.
- [Jonge et al, 1996] Jonge, P.J. de and C.C.J.M. Tiberius (1996). The LAMBDA method for integer ambiguity estimation: implementation aspects. LGR-series No. 12. Delft Geodetic Computing Centre. August. 49 pp. Internet URL <http://www.geo.tudelft.nl/mgp/>
- [Kösters, 1992] Kösters, A.J.M. (1992). Some aspects of a 3-dimensional reference system for surveying in the Netherlands. Quality analysis of GPS phase observations. Report No. 92.1. Mathematical and Physical Geodesy. Department of Geodetic Engineering, Delft University of Technology.
- [Lawson et al, 1969] Lawson C.L. and R.J. Hanson (1969). Extensions and applications of the Householder algorithm for solving linear least squares problems. *Mathematics of Computation*. No. 108, Vol. 23. pp. 787-812.
- [Nikiforov, 1996] Nikiforov, I.V. (1996). New optimal approach to Global Positioning System/Differential Global Positioning System Integrity Monitoring. *Journal of Guidance, Control and Dynamics*. Vol. 19. No. 5. September-October. pp. 1023-1033.
- [Polman et al, 1996] Polman J. and M.A. Salzmann (Eds) (1996). Handleiding voor de Technische Werkzaamheden van het Kadaster. Kadaster, Apeldoorn.
- [Powe et al, 1997] Powe, M. and J. Owen (1997). A flexible RAIM algorithm. *Proceedings of ION GPS-97*. Kansas City, USA. September 16-19. pp. 439-448.
- [RAJPO, 1997] Range Application Joint Program Office (RAJPO). Air Force Flight Test Center (AFFTC), Edwards Air Force Base, California. March 26. Internet URL <http://tspiserv1.elan.af.mil/>
- [Salzmann, 1993] Salzmann, M.A. (1993). Least-squares filtering and testing for geodetic navigation applications. Ph.D. thesis. Department of Geodetic Engineering, Delft University of Technology.
- [Salzmann, 1995] Salzmann, M.A. (1995). Real-time adaptation for model errors in dynamic systems. *Bulletin Géodésique*. Vol. 69. pp. 81-91.
- [Schupler et al, 1994] Schupler, B.R., R.L. Allshouse and T.A. Clark (1994). Signal characteristics of GPS user antennas. *Navigation*. Vol. 41. No. 3, Fall. pp. 277-295.
- [Seeber, 1993] Seeber, G. (1993). *Satellite Geodesy*. de Gruyter Berlin, New York.
- [Teunissen et al, 1989] Teunissen, P.J.G. and M.A. Salzmann (1989). A recursive slippage test for use in state space filtering. *Manuscripta-Geodaetica*. Vol. 14. pp. 383-390.
- [Teunissen, 1992] Teunissen, P.J.G. (1992). Een voorbeeld van de DIA-procedure toegepast op het partially constant state space model. Intern memo. Faculteit der Geodesie, Technische Universiteit Delft. Januari.
- [Teunissen, 1997] Teunissen, P.J.G. (1997). Quality control and GPS. Chapter 7 in *GPS for Geodesy*. P.J.G. Teunissen and A. Kleusberg (Eds). Lecture notes in Earth Sciences. Springer Verlag, 1998. 2nd edition.
- [Teunissen et al, 1997a] Teunissen, P.J.G., P.J. de Jonge and C.C.J.M. Tiberius (1997). The least-squares ambiguity decorrelation adjustment: its performance on short GPS baselines and short observation spans. *Journal of Geodesy*. Vol. 71. No. 10. pp. 589-602.
- [Teunissen et al, 1997b] Teunissen, P.J.G., P.J. de Jonge and C.C.J.M. Tiberius (1997). Performance of the LAMBDA method for fast GPS ambiguity resolution. *Navigation*. Vol. 44. No. 3, Fall. pp. 373-383.

5. GPS surveying: experiments and results

The results of the processing of various data sets enables a deeper insight in the quality of the geometric information, as obtained by kinematic GPS surveying or, in just the quality of positioning of a moving receiver.

quality: design (Ypenburg 94)

Knowledge of the measurement configuration and scenario allows to examine the quality of the system in terms of precision and reliability beforehand, thus prior to actual field operation. The quality is analysed in detail for the benchmark data set, a 2.2 km baseline.

analysis GPS code and phase observables (UNAVCO 95)

In the second section of this chapter, a closer analysis is made on the code and phase observables to check whether the assumed mathematical modelling is adequate and if not, to explore the shortcomings. Data from zero baselines and a short baseline are used for this special purpose. We will see that the stochastic model needs refinements.

kinematic GPS surveying: practice (Flevo 96)

The results will be analysed that are obtained by the measurement set up typical for kinematic GPS surveying, thus one stationary reference receiver and a roving one that visits the points to be surveyed, or is even in permanent motion. The distance from the rover to the reference ranges to over 10 kilometers. We will focus on performance concerning positioning and ambiguity resolution.

The three campaigns, description, results and analysis, are independent and can be read separately. For each, a summary and conclusions are given at the end of the respective sections.

5.1 Quality of kinematic GPS surveying

The Ypenburg 94 data set was originally used for testing purposes during the software development. Extensive design computations were made for this benchmark data set. The measurement configuration was analysed on quality. An attempt was made to identify a workable set of parameters that can be used to represent the quality and examples are given of the DIA procedure for quality control at work.

5.1.1 Experiment description

The Ypenburg 94 campaign was measured by the Department in May 1994 on the former air force base Ypenburg, near The Hague in the Netherlands. The early-evening session is used for the analysis. The characteristics of the experiment are listed on the next page.

```

number of satellites: 7 (all Block II and IIA)
PRNs: 17 19 21 22 23 31 28
pivot: 28 (double differencing)
number of receivers: 2 (stationary)
receiver type: Trimble 4000 SSE (cross-correlation)
observation types: C1,P2,L1,L2 (AS on)
date: May 5th, 1994 (GPS week 747)

observation session: 1 hour (3596 seconds)
start: 16:45:04 GPS ; 405904 seconds in GPS week
end: 17:44:59 GPS ; 409499 seconds
sampling interval: 1 second

processing session: ~ 1 hour (359 epochs)
start: 16:45:10 GPS ; 405910 seconds
end: 17:44:50 GPS ; 409490 seconds
sampling interval: 10 seconds * GPS = UTC + n [s] with n=9

station: YP01
coordinates marker: X= 3920397.2498 m
in WGS84 Y= 298788.2909 m (reference coordinates)
Z= 5005349.5126 m

station: YP09
coordinates marker: X= 3918981.3860 m at cm-level, relative)
in WGS84 Y= 300212.4750 m
Z= 5006364.9701 m

baseline-length: 2250.361 m

```

5.1.2 Results and analysis

For the Ypenburg 94 campaign we concentrate on analysis of the quality of precise relative positioning on a local scale. We will consider both the static and the (full) kinematic case. There can be one set of coordinates for the roving receiver for the whole session, model 00, or new coordinate unknowns are introduced epochwise, model 02, see section 4.1.1.

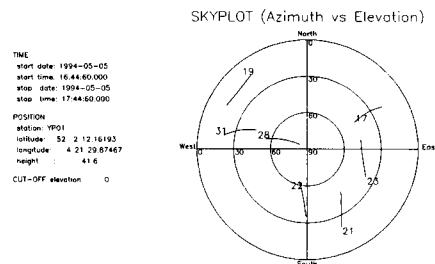


Figure 1.1: Skyplot at YP01 for Ypenburg 94

The analysis on quality is made for a variety of measurement scenarios. For three of them, also an example of the DIA procedure for quality control will be shown. As a side step, we start with single point positioning.

5.1.2.1 Single point positioning

The single point positioning case is analysed first, as, due to the same geometry, the mathematical model has the same structure as for relative positioning. This may help in explaining the analysis of quality for relative positioning. We consider the reference receiver.

Single point positioning with CA-code observations was carried out; $m=7$ satellites were available. The standard deviation was taken $\sigma_p=20.6$ meter (all satellites), see [Parkinson et al, 1996]. The SA δ -dither in the satellite clocks actually hinders the normal distribution assumption for the CA-code observations in practice. The effective satellite clock stability is about 10^{-9} s/s and the broadcast satellite clock error coefficients do not account for the short term (several minutes) varying effects. The mathematical model for one epoch of data was given in section 3.3, equation (3.2). For single point positioning, as a limiting case, also model C1 is considered: a stationary receiver, model 00, but with the coordinates already initially constrained, so that there is only one unknown parameter per epoch.

In table 1.1, the quality of the measurement system is analysed for 4 epochs (out of the 359 epochs processed): $k=1$, $k=100$, $k=200$ and $k=300$. Given are the standard deviations of the coordinates North, East and Height (or Up) and of the receiver clock error (also in meters), and the Minimal Detectable Biases for outliers in the code-observations (local model validation); per epoch the minimum and maximum values are given together with the PRN-numbers of the corresponding satellites.

epoch	02 kinematic				precision (σ)		MDB outliers		
	North [m]	East [m]	Height [m]	Clock [m]	min [m]	PRN	max [m]	PRN	
1	17.5	15.0	34.3	21.2	109.3	23	172.9	21	
100	18.1	14.5	41.5	26.1	107.4	23	166.3	21	
200	18.8	14.0	45.4	29.1	107.5	23	183.3	28	
300	18.6	13.5	40.7	26.5	108.1	23	171.5	19	
00 static									
1	17.5	15.0	34.3	21.2	109.3	23	172.9	21	
100	1.8	1.5	3.8	8.1	92.1	23	92.2	17	
200	1.3	1.0	2.9	8.0	92.0	23	92.1	17	
300	1.0	0.8	2.4	7.9	92.0	21	92.1	17	
C1 constrained									
1	0.0	0.0	0.0	7.8	91.9	all			
100	0.0	0.0	0.0	7.8	91.9	all			
200	0.0	0.0	0.0	7.8	91.9	all			
300	0.0	0.0	0.0	7.8	91.9	all			

Table 1.1: Precision and reliability for single point positioning

precision

For model 02 (in fact single epoch solutions), the precision figures are about the same for all epochs. The slight variation is caused by the changing satellites-receiver geometry (long term effect). The PDOP ranges from 2.0 at the start, to 2.5 in the middle and back to 2.1 at the end. It can also be seen that the precision for the height is about twice as poor as for the horizontal coordinates.

With model 00, a sequential adjustment upon the coordinates is made. The more epochs of data are processed, the more precise the coordinate estimators get. From epoch $k=1$ to epoch $k=300$, the precision improves by approximately a factor $\sqrt{300}$, $Q_{\hat{x},k=300} \approx \frac{1}{\sqrt{300}} Q_{\hat{x},k=1}$. As compared with model 02, there are less unknowns and therefore also the estimator for the clock error gets more precise. It almost reaches the level of model C1 ($\sigma=7.8\text{m}$).

In model C1, we actually have one unknown per epoch, namely the receiver clock error. The receiver clock error (expressed in meters) is involved in each observation equation with same coefficient, namely 1.0, and therefore the precision of the estimator as well as the MDBs are constant over the whole session. The precision of the receiver clock error estimator could have been easily predicted: $\sigma_{\text{clock}} = \sigma_p / \sqrt{7} \approx 7.8 \text{ m}$ (averaging).

PRN	MDB [m]	$\sqrt{\lambda_e}$	$\sqrt{\lambda_{NEH}}$	$\sqrt{\lambda_{NE}}$	$\sqrt{\lambda_H}$
17	145.7	5.7	5.1	4.8	1.3
19	149.2	5.9	5.3	3.6	3.0
21	172.9	7.3	6.6	5.9	4.1
22	123.4	4.3	3.7	2.1	3.0
23	109.3	3.3	2.7	2.6	0.4
31	120.6	4.1	3.5	2.9	1.3
28	119.1	4.0	3.4	2.4	2.9

Table 1.2: Internal and external reliability for model 02

reliability

The Minimal Detectable Biases were given in table 1.1 (minimum and maximum value). We will consider reliability in more detail for model 02 (full kinematic), at the first observation epoch $k=1$. Table 1.2 concerns internal reliability (MDBs) and external

reliability. For external reliability, the propagation is considered of (undetected) model errors, outliers, on the estimator for the vector of unknown parameters.

reliability: external

The $\sqrt{\lambda_{\hat{x}}}$ significance measures are represented also graphically in figure 1.2. $\sqrt{\lambda_{\hat{x}}}$ (white; third column of table 1.2), is a general significance measure for the effect of an undetected outlier (of size MDB) on the full vector of unknown parameters (coordinates and receiver clock error). For the remaining three columns, only a part of the unknowns is considered. $\sqrt{\lambda_{\hat{x}_{NEH}}}$ (black) concerns the coordinates in three dimensions, expressed in either XYZ or North, East, Height, as $\lambda_{\hat{x}_{XYZ}} = \lambda_{\hat{x}_{NEH}}$. For the horizontal coordinates and the vertical coordinate we have respectively $\sqrt{\lambda_{\hat{x}_{NE}}}$ (hatched) and $\sqrt{\lambda_{\hat{x}_H}}$ (gray).

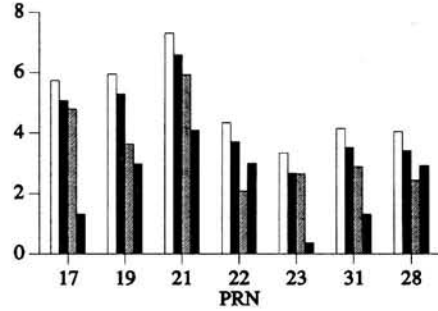


Figure 1.2: External reliability: significance of outlier $\sqrt{\lambda_{\hat{x}}}$, $\sqrt{\lambda_{NEH}}$, $\sqrt{\lambda_{NE}}$ and $\sqrt{\lambda_H}$

The propagation of outliers ∇ on the estimates is given by $\nabla\hat{x} = X\nabla$, where X is an n -vector, see equation (8.5) in section 1.8.2. In figure 1.3 the bias in the horizontal position $\sqrt{\nabla N^2 + \nabla E^2}$ (North and East; the length of the 2-vector $\nabla\hat{x}$ in standard metric) is plotted versus the size of the outlier ∇ , for all seven satellites. An outlier of 150 meter in satellite 28 causes the horizontal position to be off by 40 meters. The asterisk represents the value of the MDB. From the figures 1.2 and 1.3, it can be concluded that outliers in the satellites 17, 19 and 21, when left undetected, have largest impact on the estimator.

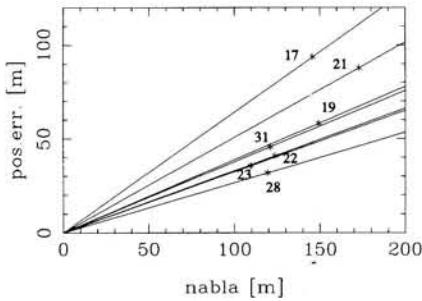


Figure 1.3: External reliability: propagation of outlier ∇ into horizontal position

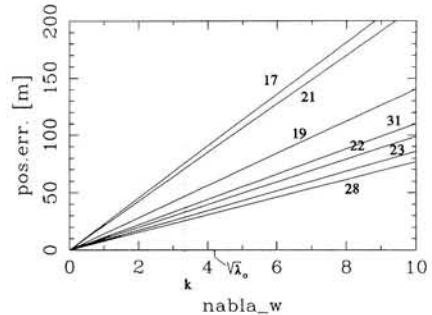


Figure 1.4: External reliability: horizontal position error versus bias in teststatistic ∇t

Testing for outliers is carried out with the slippage teststatistic, see (7.12) in section 1.7.2. Under the null hypothesis H_0 , the slippage teststatistic \underline{t} has expectation value zero: $E\{\underline{t}\} = 0$. When the model error occurs with size ∇ , the teststatistic gets affected. Under H_a we have $E\{\underline{t}\} = \nabla t = \sqrt{c_t^T Q_t^{-1} c_t} \nabla$, with the model error expressed in terms of misclosures: $c_t \nabla$. As we have seen in figure 1.3, the outlier will cause a bias in the horizontal position.

In figure 1.4, the horizontal position error is given as function of the bias in the teststatistic $|\nabla t|$, again for all seven satellites. When the model error has the size of the MDB, equation (8.2): $|\nabla t| = \sqrt{\lambda_o} \approx 4.13$. In practice, the slippage test, for an outlier in a code observation, is rejected when the (sample) value t for the teststatistic exceeds the critical

value: $|t| > k$. In this case, the critical value is $k=3.29$ and it is indicated by the dotted line. Also figure 1.4 shows that outliers in the satellites 17, 19 and 21 have large impact on the horizontal position.

Figure 1.5 shows the direct effect on the horizontal position of an outlier of size MDB (vectors $\nabla \hat{x} = X \nabla$, with the coordinates expressed in North, East and Height). The formal precision ellipse, $\alpha=0.05$, has been provided for reference. The contour line of the ellipse corresponds to the value $\sqrt{\lambda_{\hat{x}, NE}} = \chi = 2.4$ for the external reliability (vector). An outlier of $\nabla=145.7$ meter (MDB) in satellite 17, when left undetected, shifts the receiver position over 93.7 meters towards the (local) South-West.

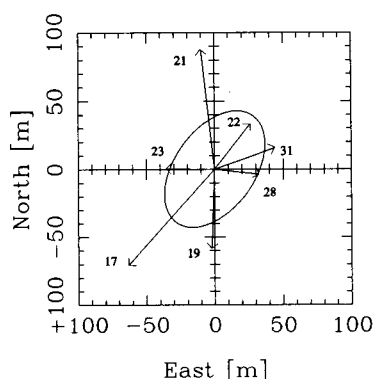


Figure 1.5: External reliability: bias in horizontal position

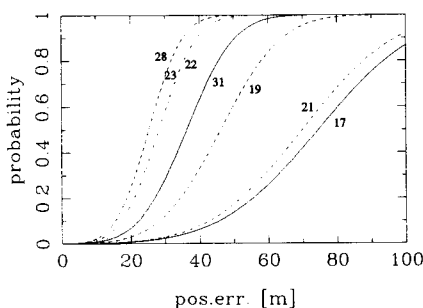


Figure 1.6: External reliability: probability of outlier detection by slippage test versus horizontal position error

An outlier ∇ in one of the seven range observations, will bias the (horizontal) position. By means of the slippage test, it can be detected with a certain probability γ . Under $H_a: t^2 \sim \chi^2(q=1, \lambda)$ with $\lambda = \nabla^T Q_{\hat{v}}^{-1} \nabla$, cf. formula (7.10) in chapter 1. The non-centrality parameter λ can then be related to probability γ . Figure 1.6 gives γ versus the horizontal position error; there are 7 curves, one per outlier hypothesis H_{ai} with $i=1, \dots, 7$. The MDBs are related to $\gamma=0.8$.

reliability: internal

Model 02 (full kinematic) is considered at epoch $k=1$ for the cases with 7, 6, 5 and 4 satellites (realized by successively leaving out PRN 21, 31, and 17). With 4 unknown parameters, the redundancy then equals 3, 2, 1, and 0 respectively. The MDBs, in meters, are given for these cases in table 1.3.

Leaving out PRN 21, causes the MDB for PRN 23 to switch from being the smallest MDB to being the largest one. Next, leaving out PRN 31 has a major effect on the MDBs of PRNs 17 and 19, see table 1.3. The table clearly shows that as the redundancy gets less, the internal reliability gets worse: the MDB values increase. With 4 satellites there is no redundancy left at all, and model validation is not possible anymore; the ** denote infinite MDB values.

PRN	7 svcs	6 svcs	5 svcs	4 svcs
17	145.7	162.9	376.9	--
19	149.2	149.8	478.3	**
21	172.9	--	--	--
22	123.4	128.0	138.2	**
23	109.3	189.0	205.7	**
31	120.6	138.4	--	--
28	119.1	138.0	140.5	**

Table 1.3: MDBs [m] for model 02

With formula (8.4) in section 1.8.2, the separability between two one-dimensional alternative hypotheses can be analysed. We will find out how well one can distinguish between an outlier in satellite i and one in satellite j . In table 1.4, we give the values for $\cos^2 \phi$, where ϕ is the angle between the two alternative c_i -vectors. If ϕ equals 0 or π , the vectors are parallel and can not be distinguished ($\cos^2 \phi = 1$). If ϕ equals $\pi/2$ or $-\pi/2$, they are perpendicular and separability is optimal ($\cos^2 \phi = 0$).

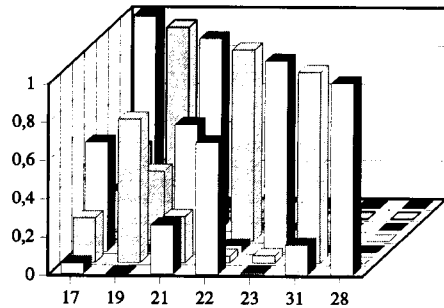
PRN	17	19	21	22	23	31	28
17	1.000	.364	.200	.005	.571	.233	.055
19		1.000	.008	.361	.000	.752	.004
21			1.000	.069	.665	.242	.255
22				1.000	.031	.036	.689
23					1.000	.040	.006
31						1.000	.153
28							1.000

PRN	17	19	22	23	31	28
17	1.000	.519	.004	.568	.812	.356
19		1.000	.422	.008	.902	.016
22			1.000	.492	.143	.700
23				1.000	.156	.955
31					1.000	.036
28						1.000

PRN	17	19	22	23	28
17	1.000	1.000	1.000	1.000	1.000
19		1.000	1.000	1.000	1.000
22			1.000	1.000	1.000
23				1.000	1.000
28					1.000

Table 1.4: Correlation-matrices $\cos^2\phi$, model 02, 7,6 and 5 satellites

The correlation matrices show whether outliers in different observations interfere or not (they are symmetric; only the upper-triangle is given). The value for $\cos^2\phi$ can range from 0 to 1. The diagonal elements (satellite i with itself) are equal to 1.0 by definition. The trend is that with decreasing redundancy, the correlation increases and identification becomes more difficult. With 7 satellites, the correlations are small to moderate, see also figure 1.7. With 6 satellites, in particular an outlier in satellite 23 and one in satellite 28, strongly interfere, $\cos^2\phi=0.955$. And as we have seen with the MDBs, satellite 31 interferes with 17 and 19. With 5 satellites, the redundancy equals 1. Detection is possible, but identification is not. As shown in the table, one can not distinguish between the 5 alternative hypotheses. It is possible to notice that the model and the data do not correspond (something wrong), but not to point out what.

Figure 1.7: Correlation-coefficients ($\cos^2\phi$) with 7 satellites

cases with four satellites: precision

For single point (single epoch) positioning, based on the linearized model of observation equations, two types of rankdeficient receiver-satellites geometries are identified in [Teunissen, 1990]. We will, as examples, consider four cases A through D, figure 1.9.

(1) When all satellites are on a cone, that has its top at the receiver, the receiver position can not be determined in the direction of the center-axis of this cone (caused by the fact that also the receiver clock error has to be estimated; the observables are pseudo-ranges, not ranges). Case C is a clear example of this configuration and also case A is close to it. Note that all satellites at equal elevation, is just a special case of this deficiency; the axis then points towards the local zenith and the height is undetermined.

(2) When all satellites are in a plane, that also passes through the receiver, the receiver position is not determined in the direction perpendicular to this plane. The configuration of case B is quite close to this situation.

The type (2) rankdeficiency is actually a limiting case of type (1), i.e. the top-angle of the cone is 90°. When the receiver clock error is not to be estimated, the rankdeficiency of type (2) remains; the deficiency of type (1) disappears.

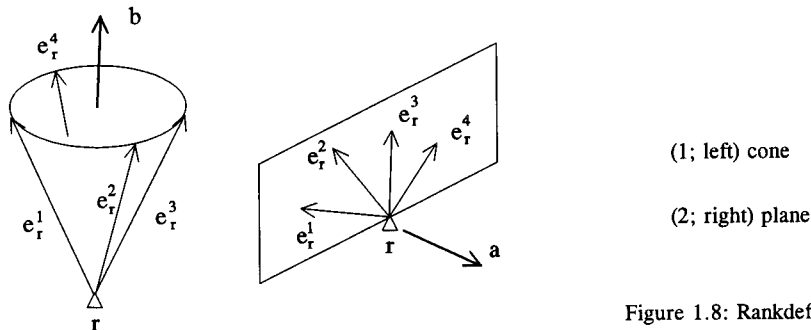


Figure 1.8: Rankdeficient geometries

The above rankdeficient geometries are mathematically described by

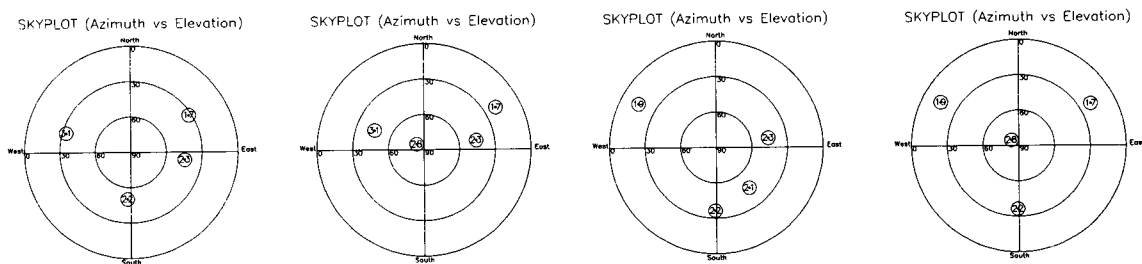
(1) $e_r^{iT} b = 1$ for $i=1,2,3,4$ where b is the 3x1 vector along the axis of the cone

(2) $e_r^{iT} a = 0$ for $i=1,2,3,4$ where a is the 3x1 normal vector of the plane

The rankdeficient geometries are sketched in figure 1.8 with four satellites, but they may occur with more than four as well. The vectors e_r^i have unit length and point to the satellites. Case D finally, is quite close to the perfect receiver-satellites geometry for the case with four satellites.

case	precision (σ)				PDOP [m/m]
	North [m]	East [m]	Height [m]	clock [m]	
A	177.7	37.0	785.8	490.8	39.2
B	244.3	27.3	191.9	189.8	15.1
C	92.7	357.1	1248.6	670.2	63.2
D	21.3	17.6	39.6	24.4	2.3

Table 1.5: Precision of 4-satellites-cases



case A: 17:15:00 YP01 case B: 17:44:00 YP01 case C: 17:44:00 YP01 case D: 17:44:00 YP01

A PRN	17	22	23	31	B PRN	17	23	28	31
azim	58.2	184.5	99.5	285.8	azim	60.0	80.9	300.4	290.6
elev	32.8	49.2	44.4	33.0	elev	20.6	45.9	82.5	45.3
C PRN	19	21	22	23	D PRN	17	19	22	28
azim	298.9	142.0	181.3	80.9	azim	60.0	298.9	181.3	300.4
elev	15.3	45.4	35.6	45.9	elev	20.6	15.3	35.6	82.5

Figure 1.9: Skyplots for 4-sv cases

For the cases A through D in figure 1.9, a single point solution was computed, based on one epoch of data (instantaneous receiver-satellites geometry). Receiver coordinates and clock error were estimated from four CA-code observations. There is no redundancy.

In case A, the satellites are all quite close to a cone, with the top at the receiver. The axis of the cone points mainly towards the zenith-direction. Therefore the Height of the receiver has poor precision.

In case C, the satellites are close (more than in case A) to a cone. The axis points up to North-West-West (azimuth 284.3°, elevation 73.6°). The angles between the unit-direction vectors to the satellites and the axis (of the best fitting cone) are 58.9°, 58.2°, 59.5° and 59.4°. The Height has very poor precision and also the East is poorly determined.

In case B, all satellites are almost in the receiver-zenith-West-East plane. This causes that the North-coordinate of the receiver is poorly determined. Case B is an exaggeration of the typical mid-latitudes situation, see figure 1.10 middle. Most satellites are in the South (possibly only one or two at low elevation in the Northern part), and only satellites above a certain cut-off elevation-angle are used. This causes that they all more or less tend to be in the aforementioned West-East plane. The East-coordinate has better precision than the North-coordinate.

In addition we can state that around the equator, the satellites pass over South-North and the whole sky is covered; North and East coordinate will have (about) equal precision, figure 1.10 left. As no satellites are available below the horizon (we miss the elevations 0° to -90°), the height will have poorer precision as compared with the horizontal coordinates. With four satellites, three at zero degree elevation (azimuths 0°, 120° and 240°) and one in the local zenith, thus the limiting configuration of case D, the precision of the horizontal coordinates is factor $\sqrt{2}$ better than the precision of the height: $\sigma_N = \sigma_E$ and $\sigma_H = \sqrt{2} \sigma_N$ (PDOP=1.6). The satellite in zenith is needed to determine the height. The correlation between the height and the clock error is $\rho=0.5$. In practice, an elevation cut-off is used and zero degree elevation satellites are thus not observed, which makes this factor increase to typically 2, see also case D: $\sigma_N \approx \sigma_E$ and $\sigma_H \approx 2\sigma_N$. At the higher latitudes, as the satellites do not reach the local zenith, the precision of the height will be even poorer, figure 1.10 right. At the poles, the North and East coordinate will again have (about) equal precision.

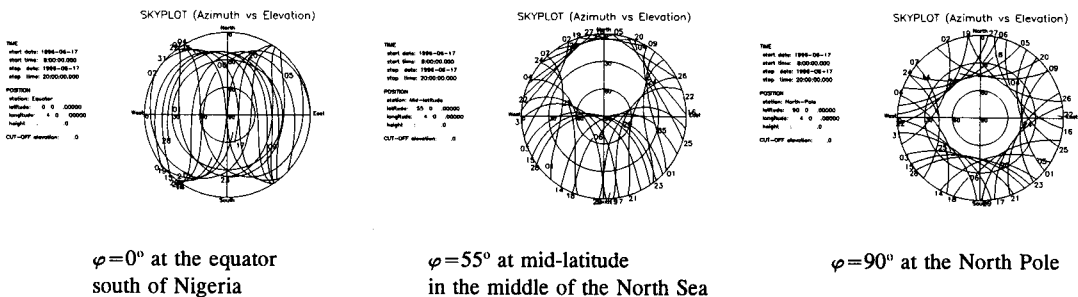


Figure 1.10: Skyplots for 12 hour period (08:00-20:00 GPS), based on almanac data of June 17th, 1996. The constellation consists of 25 satellites, all block II and IIA. Three locations were considered, along the $\lambda=4^\circ$ (East) meridian on the WGS84 ellipsoid. The inclination of the satellite orbit is $i=55^\circ$, which implies that at $\varphi=55^\circ$ (plot in middle), they just can reach the local zenith. By South in the plot at right is meant, the direction down to the equator along the $\lambda=4^\circ$ meridian.

Case D represents the almost perfect geometry. According to chapter 11, table 1 in [Parkinson et al, 1996] the best precision is found with three satellites equally spaced on the horizon, at minimum elevation angle (e.g. 5°) and one satellite directly overhead. In case D the total spread of elevation angles is almost at maximum.

known receiver clock error: precision

It was pointed out, that one of the two rankdeficient geometries has its origin in the presence of the receiver clock error as an unknown in the observation equations. In this section we will show what happens when an (almost) perfect clock is available at the receiver. One can think of an atomic clock. It has to be synchronized at the 10^{-10} s level with the GPS time.

We will discuss again the cases A through D with 4 satellites. For the purpose of reference, we also give the precision of model 02, with 7 satellites. The precision of the coordinate estimators is listed in table 1.6.

The receiver clock error has been constrained (it is known or even physically zero). There is one less unknown; the redundancy increases by one. Less unknowns yields more precise estimators for the remaining unknowns. As shown in the previous two sections, the height is usually less precise than the horizontal coordinates. As is the case for model 02, the gain in precision by introducing a perfect receiver clock, is in general largest for the height. A similar conclusion is drawn in [Kuang et al, 1996]. For model 02, the standard deviation for the height is reduced by more than a factor 2. The improvement in precision of the horizontal coordinates is marginal.

case	precision (σ)			clock [m]
	North [m]	East [m]	Height [m]	
A	25.6	16.6	16.9	0.0
B	53.3	18.4	18.2	0.0
C	22.8	20.0	20.6	0.0
D	19.7	17.5	16.8	0.0
02	17.5	14.7	12.8	0.0

Table 1.6: Precision with perfect receiver clock

Removing the receiver clock error from the vector of unknowns, solves the rankdeficiency for the cases A and C (all satellites on a cone). The precision largely improves. The standard deviation of the height is reduced by about a factor 45 and 60, for case A and case C respectively. The axis of the cone pointed mainly towards the zenith-direction. With a perfect receiver clock, case C in particular, yields a good and homogeneous precision for the coordinates.

The precision of the coordinates is improved also for case B. But note, that although the receiver clock error has been removed, the North-coordinate is still poorly determined. The rankdeficient geometry remains; the satellites are all close to the West-East plane.

The optimal configuration of case D, shows only a minor improvement in the precision of the horizontal coordinates and a slightly-over-factor 2 improvement in the height.

Without receiver clock error, the situation concerning precision, seems to be reversed as compared with the previous sections: the height tends to be more precise than the horizontal coordinates. This can be explained by the fact that a satellite can be in the local zenith (optimal for height determination), but not, as a consequence of the cut-off elevation, on the local horizon (optimal for the horizontal coordinates). Each satellite (elevation $>0^\circ$) aids the estimation of the height.

5.1.2.2 Single frequency code

Relative positioning with C1-code observations was carried out. With $m=7$ satellites, there are $(m-1)=6$ double difference observations per epoch. There are no ambiguities, only three (baseline) coordinates. The standard deviation of the undifferenced code observable was taken $\sigma_p=0.3$ meter (all satellites). The mathematical model for one epoch of data in terms of (single frequency phase) single differences was given by equation (5.5) in section 3.5; the ambiguities can be just left out. The standard deviation of the single difference observable is $\sigma=\sqrt{2}*0.3\approx 0.4$ m. Note that this model for relative positioning in its structure, is identical to the model for single point positioning. The design matrix is identical (apart from the fact that the unit-direction vectors e_i now concern receiver 2 instead of receiver 1, a very small effect) and the variance covariance matrix is again a scaled unit matrix; only the scale factor differs. Instead of $\sigma=20.6$ m, $\sigma=\sqrt{2}*0.3$ m is used. In a qualitative sense, the conclusions concerning precision and reliability for single point positioning, will also apply here. The factor $(\sqrt{2}*0.3)/20.6\approx 1/50$ will be frequently encountered. In table 1.7, the quality of the measurement system is analysed for the 4 epochs.

precision

The behaviour of the precision of the models 02 and 00 is identical to single point positioning. Only a scale factor of $(\sqrt{2}*0.3)/20.6\approx 1/50$ has been applied.

epoch	precision (σ)			min [m]	MDB outliers		PRN
	North [m]	East [m]	Height [m]		PRN	max [m]	
02 kinematic							
1	0.36	0.31	0.71	2.25	23	3.56	21
100	0.37	0.30	0.85	2.21	23	3.42	21
200	0.39	0.29	0.93	2.22	23	3.78	28
300	0.38	0.28	0.84	2.23	23	3.53	19
00 static							
1	0.36	0.31	0.71	2.25	23	3.56	21
100	0.04	0.03	0.08	1.90	23	1.90	17
200	0.03	0.02	0.06	1.90	23	1.90	17
300	0.02	0.02	0.05	1.89	21	1.90	17

Table 1.7: Precision and reliability for single frequency code

The precision (standard deviation North, East, Height) of the single epoch solution, model 02, over the full one hour session is given in figure 1.11 (left). The σ_N and σ_E are almost constants. There is some variation in σ_H as function of time (by slightly changing receiver-satellite geometry). In figure 1.11 (right) the precision of the coordinate estimators for model 00 is given as function of the number of epochs. The sampling interval is 10 seconds. The more observations are used in the solution, the better the precision. Apart from a small effect of the changing receiver-satellites geometry, the standard deviations σ_N , σ_E and σ_H behave as a $1/\sqrt{k}$ function, with k the number of epochs.

The rankdeficient receiver-satellites geometries discussed for single point positioning, also hold for relative positioning. The design matrices are similar. For relative positioning the geometry concerns the second receiver r2.

PRN	MDB [m]	$\sqrt{\lambda_{NEH}}$	$\sqrt{\lambda_{NE}}$	$\sqrt{\lambda_H}$
17	3.00	5.1	4.8	1.3
19	3.07	5.3	3.6	3.0
21	3.56	6.6	5.9	4.1
22	2.54	3.7	2.1	3.0
23	2.25	2.7	2.6	0.4
31	2.48	3.5	2.9	1.3
28	2.45	3.4	2.4	2.9

Table 1.8: Internal and external reliability model 02 single frequency code

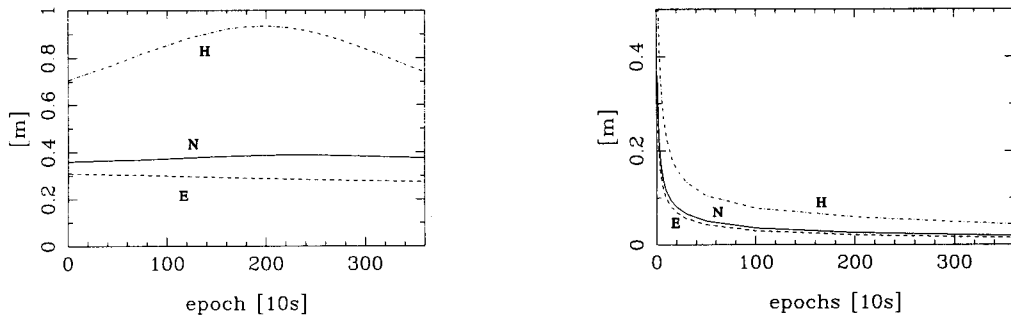


Figure 1.11: Precision (standard deviation) of coordinates as function of time for model 02 (kinematic, left) and model 00 (static, right); single frequency code

reliability

Also the MDB-values can be derived from the single point positioning results (factor $\sim 1/50$). With model 00 (static), a sequential adjustment is made on the coordinates. When k becomes large, the coordinate estimators get very precise. In terms of single differences, there is only one (new) unknown per epoch: the (differential) receiver clock error $c\Delta\delta_2 t$. It is common to all observations of that epoch, via (the same) coefficient 1.0. When k gets large, the MDBs all tend towards the value of 1.89 m, see table 1.7. From this we can trace back that the standard deviation of the clock error, when estimated with the single difference model, tends to $\sigma_{c\delta_2 t} = 0.16$ m, or $\sigma_{\delta_2 t} = 0.54 \times 10^{-9}$ s (cf. single point positioning, model 00; $\sigma_{c\delta_2 t}$ tends towards 7.8 m of model C1). Table 1.8 concerns reliability for model 02, at the first observation epoch $k=1$.

reliability: external

Note that $\sqrt{\lambda_{\hat{x}}} = \sqrt{\lambda_{\hat{x}_{NEH}}}$ as there are only three coordinate unknowns (in the double difference implementation). $\sqrt{\lambda_{\hat{x}_{NE}}}$ and $\sqrt{\lambda_{\hat{x}_H}}$ are significance measures for the effect of an undetected outlier (of size MDB) on the horizontal coordinates and the vertical coordinate respectively. The above scalar measures for external reliability ($\lambda_{\hat{x}}$) are identical to the single point positioning case, cf. figure 1.2; the scale factor cancels.

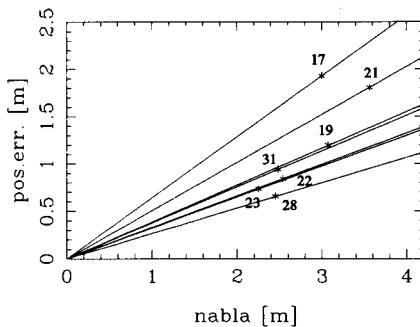


Figure 1.12: External reliability: propagation of outlier ∇ into horizontal position

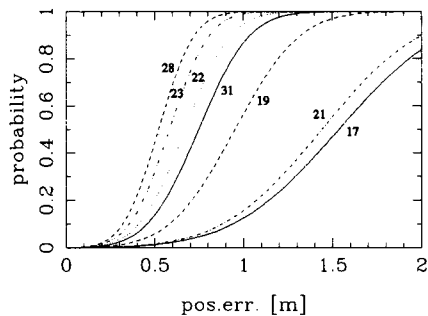


Figure 1.14: External reliability: probability of outlier detection by slippage test versus horizontal position error

In figure 1.12, we consider the propagation of outliers ∇ on the estimated horizontal position. Note that vector X is identical as to single point positioning. The bias in the horizontal position $\sqrt{\nabla N^2 + \nabla E^2}$ (North and East) is plotted versus the size of the outlier ∇ , for all seven satellites. An outlier of 2 meter in satellite 21 causes the horizontal

position to be off by 1 meter. The asterisk represents the value of the MDB. The graph is similar to the single point positioning case, figure 1.3; we have actually zoomed in on the lower left part. The MDB values were scaled by the factor $\sim 1/50$.

Figure 1.13 shows the direct effect on the horizontal position of an outlier of size MDB (vectors $\nabla\hat{x} = X\nabla$, with the coordinates expressed in North, East and Height). The formal precision ellipse, $\alpha=0.05$, has been provided for reference. An outlier of $\nabla=3.00$ meter (MDB) in satellite 17, when left undetected, shifts the receiver position over 1.93 meters towards the (local) South-West.

Figure 1.14 gives the size of the horizontal position bias, caused by an outlier in one of the seven C1-code observations, versus the probability γ that the outlier can be detected by the slippage test. The MDB-values are related to $\gamma=0.8$.

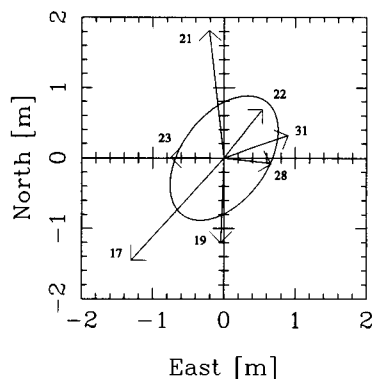


Figure 1.13: External reliability: bias in horizontal position; single frequency code

reliability: internal

Model 02 is not further considered on internal reliability (cases with 7, 6, 5 and 4 satellites for epoch $k=1$) as the outcome can be predicted from the single point positioning case. The MDB-values are scaled by the factor $\sim 1/50$. The correlation matrices will be identical (the scale factor cancels in the ratio for $\cos^2\phi$).

estimation and model validation

The coordinates of receiver r2 are estimated and differenced with the reference values and expressed in a local North, East, Height. Model 02 was used; although the receivers were stationary, single epoch (kinematic) solutions were computed. The horizontal coordinate differences, North versus East, are plotted in figure 1.15.

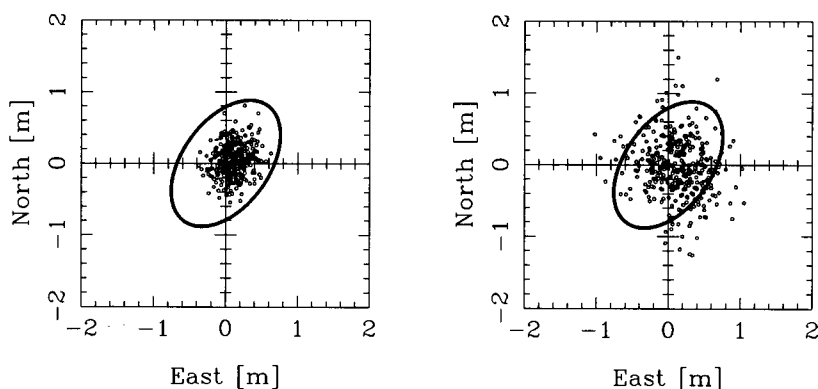


Figure 1.15: Coordinate differences, North vs East, C1-code at left and P2-code at right

Based on the variance covariance matrix $Q_{\hat{x}}$ of model 02, the two-dimensional formal precision ellipse is also plotted, with $\chi^2=5.99$, $\alpha=0.05$ (thus 5 out of 100), see section 4.1.2. It describes the precision for epoch $k=1$ (and is approximately valid for the whole one hour session). The shape and orientation are determined by the receiver-satellites

geometry. The correlation coefficient is $\rho_{EN}=0.44$. The ellipse is centered at the origin (reference coordinates).

Each of the 359 little dots represents one single epoch solution and they all lie inside the ellipse; $0.05 \cdot 359 \approx 18$ samples are formally allowed to lie outside the confidence ellipse. It seems that for the C1-code the current stochastic model is a too pessimistic description of the data; for the P2-code on the contrary, too many dots lie outside the ellipse.

As indicated in section 4.2 we test for outliers in the single difference observations. The first step is detection. For model 02 with C1-code there are no rejections at all. The values of the local overall model test T , divided by the critical value k , are given in figure 1.16. The detection is positive when this ratio exceeds 1.0. The redundancy equals 3 ($(m-1)=6$, $n=3$). The teststatistic values are rather small on the average; we expect $E\{\underline{T}^k\}=3$ and with $k=12.63$ we have $E\{\underline{T}^k/k\}=0.24$. The observed mean is 0.09. The mathematical model seems to be quite adequate, but the stochastic model is somewhat too loose. To obtain the expected mean, we should have used $\sigma_p=0.18$ m for the standard deviation of the undifferenced code, instead of 0.30 m.

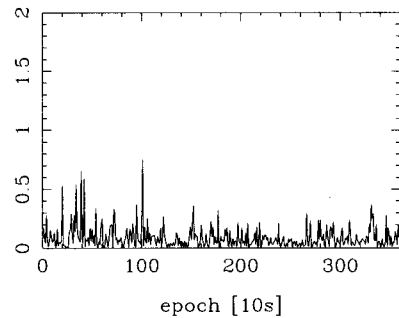


Figure 1.16: Local Overall Modelteststatistic divided by critical value T/k

example DIA procedure

By means of an example it will be shown, how the DIA-procedure for model validation performs in relative positioning with single frequency code observations. Model 02, full kinematic (thus single epoch solutions) is used, although the receivers were stationary.

- dataset

The original dataset - the data just as they were collected - was reasonably clean, see e.g. figure 1.15; quite ordinary stochastic behaviour, no large (systematic) biases. This dataset was corrupted by each time adding an outlier ∇ , $p=p+\nabla$, to a C1-code observation of the rover (YP09), at the epochs $k=5, 10, 15, \dots, 355$ (in total 71 epochs). The channel (satellite) was chosen arbitrarily (from a uniform distribution) and the outliers themselves were samples from a normal distribution $\nabla=N(0, \sigma^2)$, with $\sigma=4$ m; the probability that $\nabla \in [-4 \text{ m}, +4 \text{ m}]$ is 68.3%; finally 21 samples out of 71 lie outside this interval.

epoch	$k=15$	$k=45$	$k=65$	$k=105$	$k=155$	$k=175$	$k=285$
PRN	17	28	19	23	21	31	22
∇ [m]	2.6	-2.9	-4.4	6.2	3.6	7.3	3.1
est [m]	2.9	-3.3	-4.2	6.2	3.1	7.7	3.2
17	<u>4.0</u>	1.1	2.2	-9.5	-0.2	3.0	2.4
19	-1.3	-0.0	<u>-5.7</u>	0.3	0.4	-13.1	-1.3
21	2.7	-3.9	-0.1	-6.5	<u>4.2</u>	-1.2	-4.6
22	0.5	4.3	-3.4	-2.6	-3.1	-3.3	<u>4.9</u>
23	-4.0	0.4	0.7	<u>11.5</u>	-1.7	2.2	-0.4
31	0.7	2.2	5.3	2.9	-1.4	<u>14.0</u>	-0.4
28	-0.9	<u>-5.3</u>	0.2	-1.1	4.2	-8.3	0.4
∇N [m]	-1.0	0.2	1.2	-0.2	2.1	-0.1	2.1
∇E [m]	-1.1	-0.6	-0.0	-1.7	-0.2	2.4	0.5
∇H [m]	-1.1	2.2	-3.4	0.4	3.8	-0.8	0.8

Table 1.9: Slippage tests for outliers in each of the 7 satellites single frequency code; 7 epochs considered

This corrupted dataset was processed, once with detection and identification, but adaptation disabled (thus monitoring only) and once with full detection, identification and adaptation (monitoring *and* correcting). The DIA procedure for statistical testing was used with the default settings, discussed in chapter 4.

- detection and identification

In table 1.9, the testing results are given, as an example, for 7 epochs (one for each satellite). At these epochs the outlier was detected and the results of the consecutive identification are given: the values for the slippage teststatistics \underline{t}^k . The critical value for $|\underline{t}^k|$ is 3.29. The largest slippage teststatistic per epoch is underlined, and indicates the most likely alternative hypothesis (this identification is correct at the epochs given).

The correlation between the outlier hypotheses, discussed for single point positioning (cf. table 1.4), shows up in table 1.9, see between satellites PRN 19 and 31 at epochs $k=65$ and 175. The value for $\cos^2\phi$ is 0.752 (at $k=1$; $\phi \approx 30^\circ$). At epoch $k=65$ - outlier in 19 - also the test for 31 is quite large (opposite sign) and at epoch $k=175$, the situation is reversed. It should be kept in mind that the example concerns statistical testing based on a single epoch with only single frequency code data.

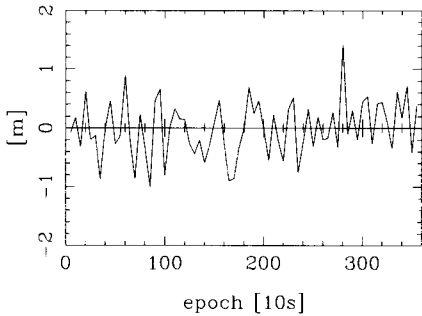


Figure 1.17: Difference of outlier and its estimate for the 71 errors

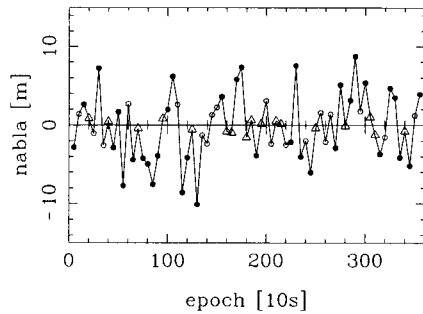


Figure 1.18: Statistical testing, outlier versus epoch, detection and identification

- (71) errors in total
- (35) detected and identified correctly
- (19) not detected, $T/k < 1.0$; the satellite with the error does however, show the largest value for $|\underline{t}^k|$, the channel-wise identification test, but the identification test is not rejected (the error is 'too small' for the statistical testing procedure to take action)
- △ (17) not detected, $T/k < 1.0$; the satellite with the error does *not* yield the largest $|\underline{t}^k|$ -value

In the figures 1.17 and 1.18 only the epochs with the additional errors ($\nabla \neq 0$) are given (none of the other epochs, $\nabla = 0$, were rejected). The figure on the left gives the (artificial) error ∇ put in the dataset, minus the outlier estimate $\hat{\nabla}$; the precision is at the few decimeter level, at $k=1$ the standard deviation $\sigma_{\hat{\nabla}}$ is between 0.55 m for PRN 23 and 0.86 m for PRN 21. The figure at right gives the size of the error; the symbols show the action of the DIA-procedure, see also the legend. Note that the errors of the last two categories (with 19 and 17 errors) are at the 1-2 meter level only, and thus smaller than the MDB values (2-3 m) in table 1.8.

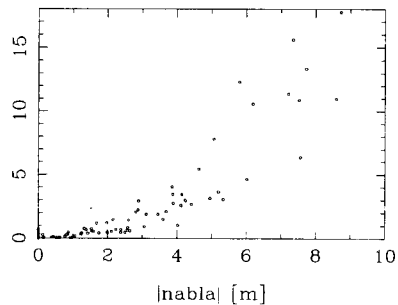


Figure 1.19: Value of teststatistic T/k versus size of outlier ∇ in m; all 359 epochs

From figure 1.19 the impression arises that the larger the outlier, the larger the value for the teststatistic; when $T/k > 1.0$ the detection is positive and the critical value is $k=12.63$. The relation shown between $|\nabla|$ and T/k seems a quadratic one and this is not surprisingly as the overall model teststatistic has expectation $E\{T_q\} = q + \lambda$ with $\lambda = \nabla^T Q_{\nabla}^{-1} \nabla$, see also eq. (7.10) in chapter 1.

- positioning

Also given in table 1.9, are the differences of the coordinate estimates with the reference values ∇N , ∇E and ∇H (adaptation disabled). The position is obviously biased by the outlier, when it is not corrected for. In general the effects agree with the analysis of external reliability, cf. table 1.8 and figure 1.13. For example, the outlier in PRN 23 at epoch $k=105$, has a large effect on the East coordinate, but only a small on the Height and North; the outlier in PRN 19, epoch $k=65$, largely effects the Height and also the North ($\nabla < 0$), but hardly the East.

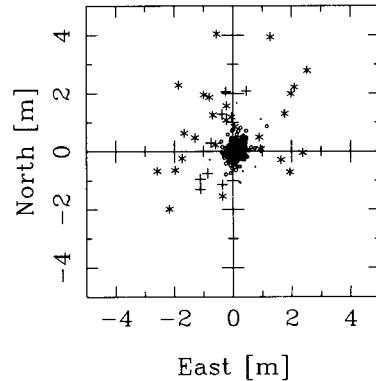


Figure 1.20: Position scatter for corrupted dataset (adaptation disabled), $T/k \in$
 $\circ [0, \frac{1}{2})$ $\cdot [\frac{1}{2}, 1)$
 $+$ $[1, 2)$ $*$ $[2, \infty)$

Figure 1.20 gives the scatter of all 359 position estimates in North and East. The symbols used are after the value for the detection teststatistic T/k . It can be seen that in general a larger deviation from the origin for the position corresponds to a larger value for the teststatistic.

- adaptation

The horizontal coordinate differences, North versus East, are plotted in figure 1.21; the position scatters are given for the original dataset (actually figure 1.15), the dataset with the outliers but adaptation disabled (actually figure 1.20) and with adaptation enabled.

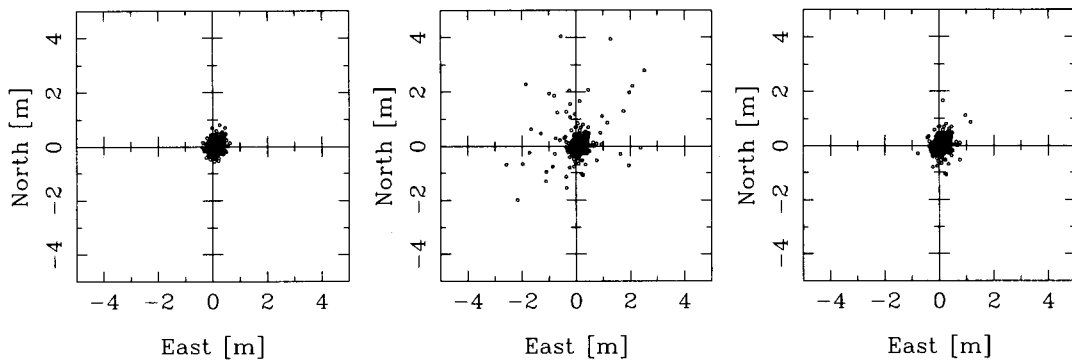


Figure 1.21: Position scatter of all 359 epochs with single frequency code,
 left original dataset, middle corrupted dataset,
 and right corrupted dataset but with adaptation enabled

For the original (clean) dataset there were no rejections at all. When adaptation was enabled, one step of correction was sufficient, there were no other errors found. After the adaptation, the remaining deviation in position is only at the few decimeter level. A few small outliers were not detected; the graph at right shows some positions that deviate at the 1-2 meter level.

As in fact single epoch solutions are computed, the graphs are all identical except for the 71 epochs (with each an additional error). In the figure at right, it can not really be noticed anymore that severe model errors - outliers up to 10 m - have occurred, cf. the figure at left. The example shows that the DIA-procedure is capable, in a fully automatic way, of accounting for the model errors.

5.1.2.3 Dual frequency code

In this section we will consider relative positioning with dual frequency code observations. With $m=7$ satellites, 7 C1 and 7 P2 observations per receiver per epoch were available. This yields $2(m-1)=12$ double difference observations per epoch. For the undifferenced code observable we took $\sigma_p = \sigma_{\bar{p}} = 0.3$ meter (and $\sigma_{p\bar{p}} = 0$).

In terms of a model with double difference observations there are only three coordinate unknowns. As compared with the single frequency case, the measurement scenario has been just doubled, $2(m-1)=12$ observations per epoch instead of $(m-1)=6$; the $(m-1)$ observation equations, have been just copied, to yield $2(m-1)$ observation equations for the same set of unknown parameters. Under the current mathematical model, the adjustment for this dual frequency case, could have been done in two steps. First, as $E\{p_{12}^{ii}\} = E\{\bar{p}_{12}^{ii}\}$ pivot 1, satellite i with $i=2, \dots, m$ ($(m-1)$ conditions; the double differences have to be equal on both frequencies), estimators \bar{p} are determined for the (double difference) code observables. The estimate is actually the average of p and \bar{p} : $\bar{p} = \frac{1}{2}(p + \bar{p})$. Next, these estimators are used in a single frequency adjustment to determine the baseline coordinates. The precision of these 'new' code observables is factor $\sqrt{2}$ better than of ordinary single frequency code observables: $Q_{\bar{p}} = \frac{1}{2}Q_p$; the dual frequency adjustment virtually is a single frequency adjustment with $\sigma \approx 0.21$ m instead of $\sigma = 0.30$ m as standard deviation for the undifferenced code observable.

precision

The behaviour of the precision is identical to the single frequency case. Only a scale factor of $\sqrt{2}$ has been applied. For model 02 (full kinematic), the standard deviations at epoch $k=1$ are $\sigma_N = 0.25$, $\sigma_E = 0.22$ and $\sigma_H = 0.50$ m, compare with table 1.7.

reliability

The Minimal Detectable Biases, for local model validation, concern outliers in the (single difference) code observations on both frequencies (thus a total of $2m$ hypotheses). The MDB-values are smaller than in the single frequency case (by a factor of about 1.1-1.5).

In table 1.10 reliability is considered for epoch $k=1$, it concerns internal reliability (MDBs) and external reliability. Note that $\sqrt{\lambda_{\hat{x}}} = \sqrt{\lambda_{\hat{x}_{NEH}}}$ as there are only three coordinate unknowns (in the double difference implementation). $\sqrt{\lambda_{\hat{x}_{NE}}}$ and $\sqrt{\lambda_{\hat{x}_{H}}}$ are significance measures for the effect of an undetected outlier (of size MDB) on the horizontal coordinates and the vertical coordinate respectively.

PRN	MDB [m]	$\sqrt{\lambda_{NEH}}$	$\sqrt{\lambda_{NE}}$	$\sqrt{\lambda_H}$
17	2.27	2.7	2.6	0.7
19	2.28	2.8	1.9	1.6
21	2.36	3.1	2.8	1.9
22	2.15	2.2	1.2	1.8
23	2.05	1.7	1.7	0.2
31	2.13	2.1	1.8	0.8
28	2.12	2.1	1.5	1.8

Table 1.10: Internal and external reliability for dual frequency code

Reliability for (outliers in) code observations is identical on L1 and on L2; table 1.10 therefore contains only seven items. As compared with the single frequency case, the vectors X have been halved (due to the averaging). The orientation is left unchanged. As the MDB values ∇ were reduced by a factor 1.1-1.5, the $\nabla\hat{x}=X\nabla$ -vectors (length) are smaller by a factor 2.2-3.0, see figure 1.22. Figure 1.22 shows the direct effect on the horizontal position of an outlier of size MDB (vectors $\nabla\hat{x}=X\nabla$, with the coordinates expressed in North, East and Height). The formal precision ellipse, $\alpha=0.05$, has been provided for reference. An outlier of $\nabla=2.27$ meter (MDB) in satellite 17 (C1 either P2), when left undetected, shifts the receiver position over 0.73 meters towards the (local) South-West. Compare with figure 1.13 of single frequency code relative positioning.

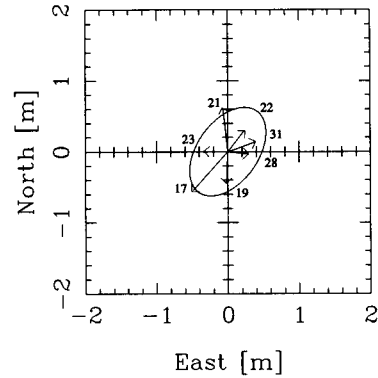


Figure 1.22: External reliability: bias in horizontal position

The precision has improved by $\sqrt{2}$; the scalar measures for external reliability $\sqrt{\lambda_x}$ are about 1.6-2.1 smaller than in the single frequency case.

PRN	17	19	21	22	23	31	28	17	19	21	22	23	31	28
17	1.000	.083	.000	.018	.135	.002	.035	.186	.002	.056	.008	.023	.072	.001
19		1.000	.011	.005	.013	.151	.018	.002	.202	.021	.091	.010	.026	.008
21			1.000	.037	.129	.066	.001	.057	.021	.311	.002	.018	.001	.068
22				1.000	.029	.030	.167	.008	.091	.002	.082	.001	.001	.039
23					1.000	.001	.005	.023	.010	.018	.001	.029	.032	.017
31						1.000	.063	.072	.026	.001	.001	.033	.070	.002
28							1.000	.001	.008	.068	.039	.017	.002	.064
17								1.000	.083	.000	.018	.135	.002	.035
19									1.000	.011	.006	.013	.151	.018
21										1.000	.037	.129	.066	.001
22											1.000	.029	.031	.168
23												1.000	.000	.005
31													1.000	.061
28														1.000

Table 1.11: Correlation-matrix for dual frequency code

With $m=7$ satellites, a total of $2m=14$ outlier hypotheses are to be considered; first 7 outliers on C1, next 7 on P2. The correlation matrix $\cos^2\phi$ is given in table 1.11 (ϕ is the angle between two alternative c_i -vectors). The correlation is low; one can discriminate well between the different hypotheses. Note that the correlation-blocks per observation type (C1 and P2) are identical (apart from some rounding effects, as the c_i -vectors were output at only 3 decimals). The full 6x6 C1-P2 correlation block is symmetric.

The overall conclusion is, that doubling the measurement scenario yields a significant improvement in the reliability of the measurement system.

example DIA-procedure: multiple model errors

The following example shows the procedure for quality control at work, when multiple (model) errors occur (nearly) simultaneously, as can be the case in practice. The first epoch $k=1$ is considered with 7 satellites dual frequency code (C1 and P2). Three (artificial) outliers, all of size $\nabla=10$ m, have been introduced in the P2 code observations of the rover station YP09; the satellites are PRNs 21, 22 and 23.

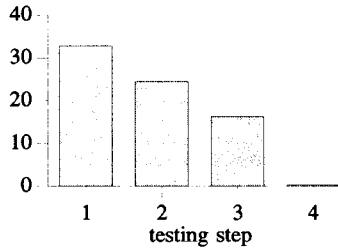


Figure 1.23: Overall model test T/k

The errors are handled by the detection, identification and adaptation in a stepwise manner. The procedure is recursive. As there are three model errors, we have four situations; the initial situation

step	q	T/k
1	9	32.9
2	8	24.5
3	7	16.3
4	6	0.3

Table 1.12: Overall model test T/k and redundancy q

and the situation after accounting for each model error. In the table, the redundancy q is given for the four testing steps, together with the value for the overall model teststatistic T divided by the critical value k . The

detection is positive in the first three steps, the value T/k largely exceeds the value 1.0. The value for T/k decreases as more errors are accounted for, see also figure 1.23. Finally in step 4, the detection is negative; no model error is suspected to be present anymore. Originally, without errors, the value was 0.30 (we expect $E\{\underline{T}^k\}=9$ and with $k=18.08$ we have $E\{\underline{T}^k/k\}=0.50$).

Table 1.13 gives the reliability for the four situations. Given are the MDBs for outliers in the code observations, in meters. Initially there are $m=12$ observations and $n=3$ unknowns. The redundancy equals $q=9$. By handling the errors, the redundancy decreases, and this is reflected in the quality. In the limit, the redundancy becomes zero and reliability will be infinitely poor. In this example with only one epoch of data, redundancy though seems to be still sufficient. The precision of the coordinates estimators deteriorates, but not by much. The standard deviations North, East and Height are 0.25, 0.22 and 0.50 m before (step1); 0.32, 0.24 and 0.58 m after (step4).

		step1	step2	step3	step4
17	C1	2.27	2.27	2.30	2.36
19		2.28	2.39	2.42	2.56
21		2.36	2.37	2.39	3.24
22		2.15	2.24	2.24	2.24
23		2.05	2.05	2.08	2.13
31		2.13	2.13	2.17	2.18
28		2.12	2.16	2.17	2.28
17	P2	2.27	2.29	2.49	2.57
19		2.28	2.29	2.30	2.32
21		2.36	2.41	2.64	-
22		2.15	-	-	-
23		2.05	2.08	-	-
31		2.13	2.16	2.17	2.32
28		2.12	2.32	2.35	2.37

Table 1.13: MDBs code outlier [m] during iterative adaptation, dual frequency code

For each step, the values of the identification teststatistics are given in figure 1.24. The critical value for the identification teststatistic is 3.29. The largest value (the satellite indicated by * *) points to the most likely alternative hypothesis and it is consequently accounted for first. Then testing is repeated. After three iterations, the three artificial outliers have been correctly detected, identified and adapted for. In the first testing step, the outlier in P2 of PRN 22 is identified and the error was estimated to be $\hat{V}=6.9$ m. In the second testing step, the outlier in P2 of PRN 23 was found, $\hat{V}=6.3$ m. And in the third testing step, the outlier in P2 of PRN 21 was found, $\hat{V}=10.3$ m. The latter estimate is fairly correct. At the time the other two estimates were computed, there was still at least one model error left unaccounted for; these estimates were biased. The standard deviations of the error estimators are about 0.5 to 0.8 m.

In the example, discrepancies between the data and the mathematical model are encountered. A re-measurement is practically not feasible or possible. The alternative taken, is to adapt the mathematical model, i.e. to take the occurred error explicitly into account in the functional model. By the iterative procedure, detection, identification and adaptation, the multiple errors were stepwise incorporated.

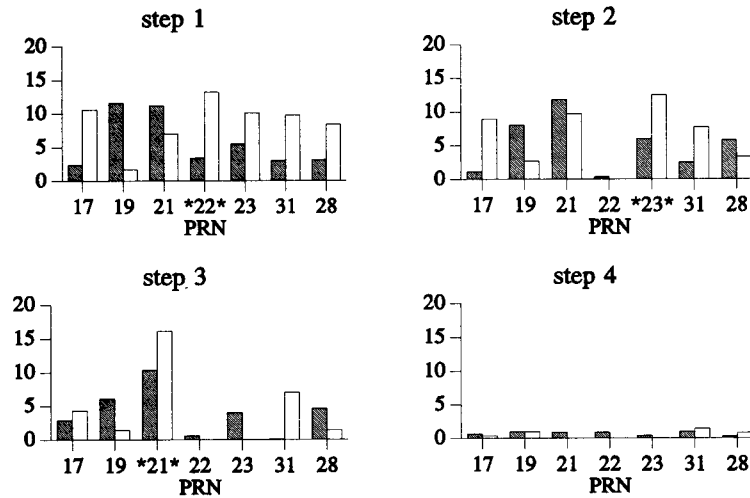


Figure 1.24: Slippage tests (absolute value) for outliers in the code, hatched C1, white P2 for iterative procedure of four testing steps, 1 and 2 (top), 3 and 4 (bottom)

5.1.2.4 Single frequency phase

The phase observable is about a one hundred times as precise as the code. Coordinates can be determined at the millimeter level. The phase comparison measurement technique however, causes that the phase observation is inherently ambiguous; an unknown number of cycles is involved. In order to enable high precision relative positioning, the ambiguities have to be resolved. In this section, the integer (double differenced) ambiguity values are known a-priori and used as such (i.e. constrained). The purpose is to analyse the quality of the coordinate estimators and the results of the actual data processing, based on single frequency phase observations (once the ambiguities are resolved).

The mathematical model for one epoch of data in terms of single differences was given by equation (5.5) in section 3.5. The $(m-1)$ double difference ambiguities are initially constrained to their reference values (integers; which can be assumed to be correct), see appendix A for development of the model in terms of single differences. As the ambiguities are known, there are only three unknown parameters, the (baseline) coordinates (per epoch for model 02, full kinematic). With $(m-1)=6$ double difference observations the redundancy equals 3. Single epoch positioning is possible now, when $m \geq 4$.

The resulting model has a structure identical to relative positioning with single frequency code and also to single point positioning. Once the ambiguities are (deterministically) known, the carrier phase measurements act as code measurements. They are however, more precise by two orders of magnitude ($\sigma_p=0.003$ m versus $\sigma_p=0.3$ m). In a qualitative sense, the conclusions for single point positioning and relative positioning with single frequency code, concerning precision and reliability will also apply here. The design matrix is identical and the variance covariance matrix is again taken a scaled unit matrix; only the scale factor differs. The results on design, precision and reliability, are easily predicted by the scale factor $\sigma_p/\sigma_c=1/100$.

precision

The standard deviations at epoch $k=1$ are $\sigma_N=0.004$, $\sigma_E=0.003$ and $\sigma_H=0.007$ m. The rankdeficient receiver-satellites geometries discussed for single point positioning, also hold for relative positioning with carrier phases. The design matrices are similar. For relative positioning the geometry concerns receiver r2.

reliability

The Minimal Detectable Biases, for local model validation, concern slips in the (single difference) phase observations. When the (cycle) slip has the size of the MDB, it can be detected with power

$\gamma=0.8$ probability. The level of significance was set to $\alpha=0.001$ ($q=1$). As we do consider only one epoch of data at a time, there is no difference between a slip and an outlier. The MDB-values can thus also be derived from the code positioning results (factor 1/100). Table 1.14 concerns internal reliability (MDBs) and external reliability, for model 02 at the first epoch $k=1$. The MDB values are given in (L1) cycles, as well as in meters.

PRN	MDB [cyc]	MDB [m]	$\sqrt{\lambda_{\hat{x}_{NEH}}}$	$\sqrt{\lambda_{NE}}$	$\sqrt{\lambda_H}$
17	0.16	0.030	5.1	4.8	1.3
19	0.16	0.031	5.3	3.6	3.0
21	0.19	0.036	6.6	5.9	4.1
22	0.13	0.025	3.7	2.1	3.0
23	0.12	0.022	2.7	2.6	0.4
31	0.13	0.025	3.5	2.9	1.3
28	0.13	0.025	3.4	2.4	2.9

Table 1.14: Internal and external reliability for model 02

reliability: external

Note that $\sqrt{\lambda_{\hat{x}}} = \sqrt{\lambda_{\hat{x}_{NEH}}}$ (only three coordinate unknowns). $\sqrt{\lambda_{\hat{x}_{NE}}}$ and $\sqrt{\lambda_{\hat{x}_H}}$ are significance measures for the effect of an undetected slip (of size MDB) on the horizontal coordinates and the vertical coordinate respectively. The above scalar measures for external reliability ($\lambda_{\hat{x}}$) are identical to the single point positioning case, cf. figure 1.2; the scale factor cancels.

PRN	position bias [m]
17	0.123
19	0.074
21	0.097
22	0.063
23	0.062
31	0.072
28	0.051

Table 1.15: Bias in horizontal position by a one cycle slip

We consider the propagation of cycle slips on the estimated position; $\nabla\hat{x} = X\nabla$ where X is a 3x1-vector (for the baseline coordinates; the ambiguities were constrained). Note that vector X is identical as to code positioning, apart from the scale factor λ , as the MDBs are expressed here in cycles rather than in meters. The bias in the horizontal position $\sqrt{\nabla N^2 + \nabla E^2}$ (North and East) is given in table 1.15 for a one cycle slip ($\nabla=1$), for all seven satellites.

Figure 1.25 shows the direct effect of a slip of size MDB (thus not a 1 cycle slip) on the horizontal position. The formal precision ellipse, $\alpha=0.05$, has been provided for reference.

reliability: internal

The MDBs in table 1.14 are all in the order of 0.1 to 0.2 cycles. When a true cycle slip (1 full cycle) occurs, it can be found with high probability, $\gamma > \gamma_o$.

The slippage teststatistics correlation matrix is identical to code positioning (only one epoch considered (outlier=slip); the scale factor cancels in the ratio for $\cos^2\phi$), see table 1.4 for single point positioning.

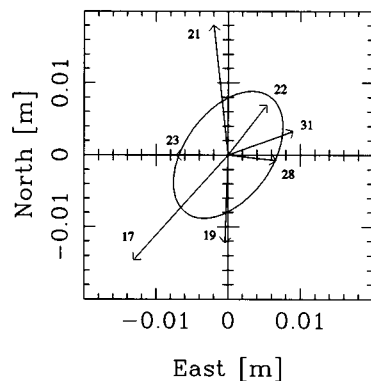


Figure 1.25: External reliability: bias in horizontal position

estimation results and model validation

Reference values for the coordinates are available, they are at the cm-level (stationary receivers). The estimated coordinates per epoch (full kinematic solution) are differenced with the reference values. This difference vector is expressed in a local topocentric system. This system is centered at the reference coordinates of receiver r2. The horizontal coordinate differences, North versus East, are plotted in figure 1.26; a 4x4 cm area is depicted. The estimation results, figures 1.26 and 1.27, are also given for the L2 phase.

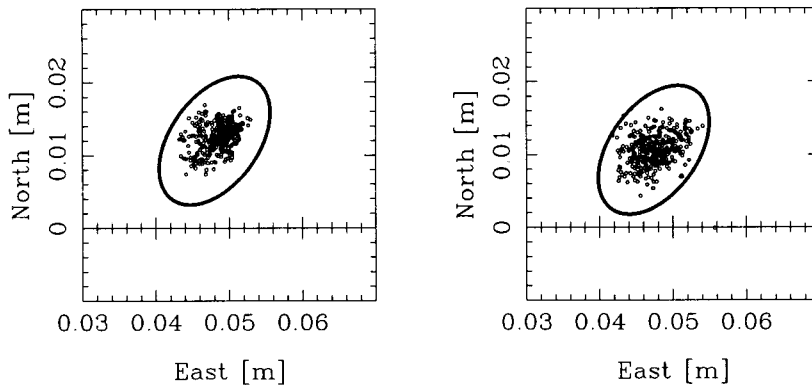


Figure 1.26: Coordinate differences North vs East, L1 phase left, L2 phase right

In figure 1.26 also the two-dimensional formal precision ellipse is given with $\chi^2=5.99$, $\alpha=0.05$. The ellipse has been centered at the mean values. Each of the 359 little dots represents one single epoch solution and they all (but one for the L2 phase) lie inside the ellipse; It seems that the current stochastic model is a too pessimistic description of the data.

In figure 1.27, one can notice some long term trend in the coordinate differences for the East (a few millimeters over the 1 hour time span). One can suspect also some dependence over time from the shorter term fluctuations. These effects are not necessarily due to the receiver (tracking loop, interchannel delays). At this millimeter level, unmodelled differential atmospheric delays may play a role as well; neither can multipath be excluded.

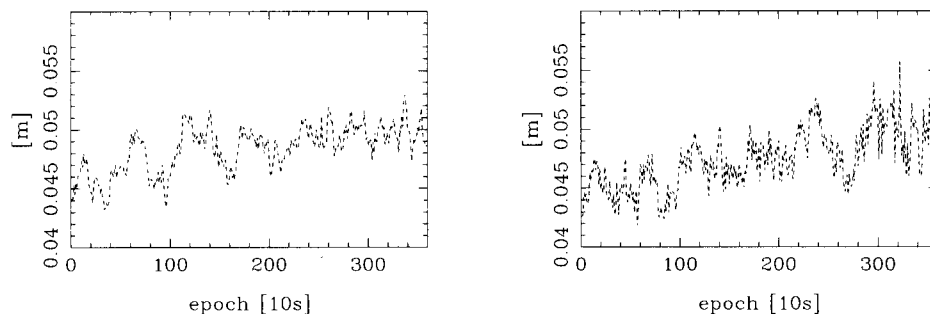


Figure 1.27: Coordinate-differences in East, L1 phase left, L2 phase right

The observations were made under Anti-Spoofing; L1 was obtained after true code correlation on L1, and L2 by cross correlation of L1 and L2. The L2 observable, seems to be more noisier than the L1 observable.

With L1 phase observations there are no rejections at all in the detection step. The values of the local overall model test T , divided by the critical value k , are given in figure 1.28. The teststatistic values are rather small on the average. For model 02 the redundancy equals 3; $(m-1)=6$, $n=3$. We expect $E\{\underline{T}^k\}=3$ and with $k=12.63$ we have $E\{\underline{T}^k/k\}=0.24$. The observed mean is smaller, namely 0.08. The stochastic model is somewhat too pessimistic. To obtain the expected mean, we should have used a standard deviation of $\sigma_p=1.7$ mm instead of 3.0 mm.

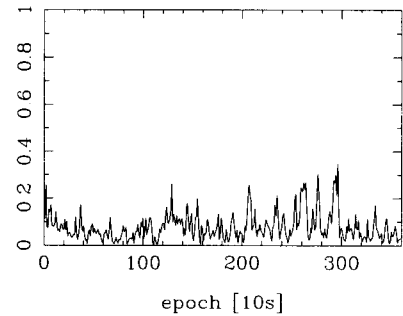


Figure 1.28: Local Overall Model teststatistic divided by critical value T/k ; L1-phase

example DIA procedure

By means of an example it will be shown, how the testing-procedure performs in relative positioning with single frequency phase observations, once the ambiguities have been resolved. At each epoch, all channels will be inspected for cycle slips. Model 02 - single epoch solutions - is used, but a corrupted observation file was provided. It contains seven artificial slips at the rover site (a slip for one epoch only, thus actually an outlier; we use single epoch solutions). The slips, all of one cycle, are listed in table 1.16. Each satellite, also the pivot, is tried once.

The MDB values are about 0.1-0.2 cycle, cf. table 1.14. The slips of one cycle should be easily found. This is the case indeed. In the identification, the model error is estimated. The estimates $\hat{\nabla}$ are also listed in table 1.16. They are all very close to the value of 1.0 cycle; their precision is at the level of 0.03-0.04 cycle.

epoch	PRN	∇ [cyc]	est. [cyc]
$k=50$	17	1.0	0.99
$k=100$	19	1.0	0.96
$k=150$	21	1.0	1.00
$k=200$	22	1.0	1.00
$k=250$	23	1.0	1.00
$k=300$	31	1.0	0.98
$k=350$	28	1.0	1.02

Table 1.16: Validation for cycle slips

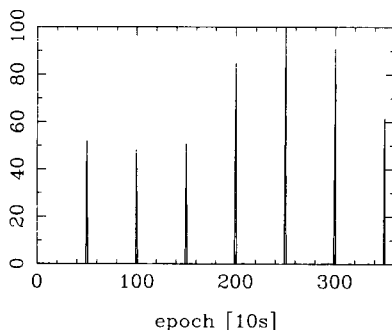


Figure 1.29: Local Overall Model teststatistic divided by critical value T/k

The detection test is depicted in figure 1.29; clearly some model error has occurred at the seven respective epochs. The test ratio largely exceeds the value of 1.0. The detection for cycle slips is very powerful. There were no other epochs rejected.

All seven artificial cycle slips were detected and correctly identified, even for this single frequency, single epoch example. The effect of the cycle slips, when not corrected for, on the estimated coordinates, corresponds quite well to the figures given in table 1.15 concerning the size, and to the vectors depicted in figure 1.25, concerning the direction (external reliability).

5.1.2.5 Dual frequency phase

Previously it has been discussed what happens to the quality and data processing results, when the single frequency system is augmented by a second frequency. It concerned C1 and P2 code observations. Here we will analyse the quality of the coordinate estimators, based on dual frequency phase observations (once the ambiguities are resolved).

Relative positioning with dual frequency phase observations was carried out. With $m=7$ satellites, 7 L1 and 7 L2 observations per receiver per epoch were available. This yields a total of $2(m-1)=12$ double difference observations per epoch. The $2(m-1)$ double difference ambiguities are initially constrained to their reference values (integers, which can be assumed to be correct). The variance covariance matrix for the single differences is a scaled unit matrix. The standard deviation for the undifferenced phase observable is taken $\sigma_p = \sigma_{\bar{p}} = 0.003$ m (and $\sigma_{p\bar{p}} = 0$).

The model has a structure, identical to relative positioning with dual frequency code, see section 5.1.2.3. The observables are just more precise by a factor 100. As compared with the single frequency case (in terms of double differences), the $(m-1)$ observation equations, have been just copied, to yield $2(m-1)$ observation equations (instead of $(m-1)=6$) for the same set of unknown parameters (the three baseline coordinates). The redundancy equals $12-3=9$. According to the same reasoning as in section 5.1.2.3 The dual frequency adjustment virtually is a single frequency adjustment with $\sigma \approx 2.1$ mm instead of $\sigma = 3.0$ mm as standard deviation for the undifferenced phase observable.

precision

The standard deviations of the coordinates at epoch $k=1$ are $\sigma_N=0.003$, $\sigma_E=0.002$ and $\sigma_H=0.005$ m. The behaviour of the precision is identical to the single frequency case. Only a scale factor of $\sqrt{2}$ has been applied. For comparison with the dual frequency code case, a scale factor of $\sigma_p/\sigma_{\bar{p}}=1/100$ is needed.

reliability

The Minimal Detectable Biases, for local model validation, concern slips in the (single difference) phase observations on both frequencies (thus a total of $2m$ hypotheses). As compared with the single frequency phase case, the MDB-values are smaller by a factor of about 1.1-1.5.

Reliability is considered for epoch $k=1$ for model 02. Table 1.17 concerns internal reliability (MDBs) and external reliability. The MDB values are given in (L1 and L2) cycles, as well as in meters. Reliability for (slips in) phase observations is identical on L1 and on L2, when expressed in meters; table 1.17 therefore contains only seven items.

Figure 1.30 shows the direct effect on the horizontal position, vectors $\nabla \hat{x} = X \nabla$, of a slip of size MDB (thus not a 1 cycle slip) with the coordinates expressed in North, East and Height. The vectors are identical for L1 and L2. Note however, that in practice, a full 1 cycle slip on L2 corresponds to a larger range error (0.24 m) than one on L1 (0.19 m). The formal precision ellipse, $\alpha=0.05$, has been provided for reference. Compare with figure 1.25 of single frequency phase relative positioning.

The scalar measures for external reliability $\sqrt{\lambda_x}$ are identical to the dual frequency case with codes. For the correlation matrix $\cos^2 \phi$, see also the dual frequency code case.

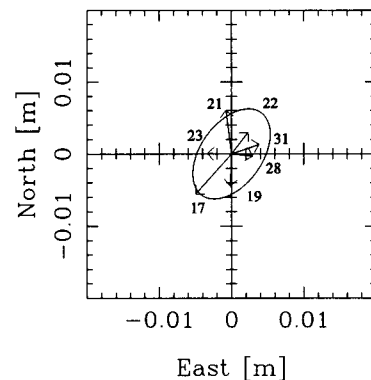


Figure 1.30: External reliability: bias in horizontal position, dual frequency phase

PRN	MDB (L1)	MDB (L2)	MDB [m]	$\sqrt{\lambda_{NEH}}$	$\sqrt{\lambda_{NE}}$	$\sqrt{\lambda_H}$
17	0.12	0.09	0.023	2.7	2.6	0.7
19	0.12	0.09	0.023	2.8	1.9	1.6
21	0.12	0.10	0.024	3.1	2.8	1.9
22	0.11	0.09	0.022	2.2	1.2	1.8
23	0.11	0.08	0.021	1.7	1.7	0.2
31	0.11	0.09	0.021	2.1	1.8	0.8
28	0.11	0.09	0.021	2.1	1.5	1.8

Table 1.17: Internal and external reliability for model 02, dual frequency phase

Doubling the measurement scenario yields a significant improvement in the reliability.

5.1.2.6 Single frequency code and phase

Relative positioning with GPS yields much higher accuracies than single point positioning. The quality of GPS relative positioning has been analysed in previous sections for different observation types. Code observations were used as well as phase observations; the latter with the (double difference) ambiguities constrained (fixed). In this section, the case is considered with code and phase observations together. The phase difference measurement is ambiguous; the carrier phase ambiguity is an additional unknown parameter. The double differenced ambiguity is an *integer* number and should be estimated as such. In the following analysis we will distinguish between the cases float ambiguities (ambiguities treated as real valued quantities) and fixed ambiguities (ambiguities constrained, after estimating them as integers).

With $m=7$ satellites, 7 C1 (code) and 7 L1 (phase) observations per receiver per epoch are available. In addition to the three coordinates of receiver r2, also carrier phase ambiguities, $(m-1)$ double difference ambiguities, are unknown parameters. Two different mathematical models are used in relative positioning. In model 02 (full kinematic) new coordinate unknowns are introduced for each epoch, whereas in model 00 (static) receiver r2 is assumed to be stationary, so there are only three coordinate unknowns for the whole session. In both models, the ambiguities are constants (for the whole session).

The (single frequency) measurement scenarios that will be considered and compared are:

- code only, see also section 5.1.2.2
- code and phase, with
 - ambiguities float
 - ambiguities resolved at epoch $k=3$
 - ambiguities fixed
- phase only, with ambiguities fixed, see also section 5.1.2.4

For the code and phase case, three scenarios are considered. In the float scenario, no attempt is made to fix the ambiguities; they are just real valued unknown parameters. In the fixed scenario, they are (correctly) estimated as integers and consequently constrained from the first epoch $k=1$ onwards. The scenario 'resolve at $k=3$ ' is in between; at that epoch, the correct integer estimate does represent sufficient probability; it is considered non-stochastic. The ambiguities are then constrained and kept fixed from $k=3$ onwards.

Note that with code and phase observations, the scenarios 'resolve at $k=3$ ' and ambiguities fixed, yield identical results, once the ambiguities are fixed, thus from epoch $k=3$ onwards. We consider only 10 epochs of data (from 16:45:10 on), spaced by 10 seconds.

The above five measurement scenarios are combined with the two mathematical models, kinematic and static. The computations for the scenario phase only with ambiguities fixed, were carried out however, only for the kinematic case, not for the static case. When figures (on precision and reliability) are given for the static case, they have been derived from the scenario code only (scale factor $\sigma_p/\sigma_p=1/100$).

precision

The precision is described by the standard deviation of the estimator. In table 1.18 we give the σ_N , σ_E and σ_H for all scenarios at epoch $k=3$. This is the epoch, at which the ambiguities, after estimating them as integers, can be reliably fixed. From then on, they are known deterministically; the variance covariance matrix $Q_{\hat{x}_2}$ is actually a *conditional* variance covariance matrix, see [Teunissen, 1997b].

The most important feature of table 1.18, is the difference in precision between the ambiguities fixed and other scenarios (ambiguities float and code-only).

For the code-only scenario, the precision of the coordinate estimators is determined by the measurement precision (decimeter-level) and the instantaneous geometry. No change in receiver-satellite geometry is needed. In the kinematic case, actually single epoch solutions are computed.

	k i n e m a t i c					s t a t i c				
	code	float	code&phase k=3	fixed	phase	code	float	code&phase k=3	fixed	phase
σ_N [m]	0.360	0.206	0.004	0.004	0.004	0.208	0.205	0.002	0.002	0.002
σ_E [m]	0.310	0.178	0.003	0.003	0.003	0.179	0.178	0.002	0.002	0.002
σ_H [m]	0.710	0.404	0.007	0.007	0.007	0.409	0.395	0.004	0.004	0.004

Table 1.18: Precision, standard deviation of coordinates in meters

When only phase observations are available, the geometry must change, in order not to be bothered by a rankdeficient normal matrix, due to the presence of the additional unknown, but time constant, ambiguities. In that case the coordinate estimators of the float solution would have infinitely poor precision. The precision of the (baseline) coordinate estimators, with the ambiguities float and ambiguities fixed, is studied in detail in section 3 of [ibid]. For the code&phase scenarios, it can be seen in table 1.18, that the precision largely improves by fixing the ambiguities.

In figure 1.31 we give for all scenarios, the standard deviation of the North σ_N as function of time. The horizontal axis represents 10 epochs of 10 seconds. The standard deviation is given along the vertical axis with a logarithmic scale, that ranges from 1 millimeter to 1 meter. The kinematic case is at left, the static at right.

We will now discuss the precision of several individual scenarios. With the code-only scenario, single epoch solutions are computed in the kinematic case. In the static case, a recursive adjustment is made on the coordinates, and the precision behaves as $1/\sqrt{k}$, with k the number of epochs; the number of observations increases as time proceeds. During the short time span we consider, the geometry at $k=1$ does not differ much from the geometry at $k=10$. As a consequence of the very slow change in geometry, the measurement scenario is actually doubled (or generally multiplied) in time. To a good approx-

imation the estimated coordinates will be just the cumulative average of the coordinates obtained epochwise with the kinematic model.

The standard deviations for the code-only scenario, do equal those for the phase-only scenario with ambiguities fixed, after a scaling by $\sigma_p/\sigma_c=1/100$, both for the kinematic and static case, see also figure 1.31. The coordinates variance covariance matrix of the phase-only fixed case is a downscaled version of the code-only variance covariance matrix [ibid]. The precision for the phase-only scenario with ambiguities fixed, is determined by the instantaneous geometry and the measurement precision (millimeter level).

For the kinematic case, the float (code&phase) solution has better precision than the code-only solution. New coordinate unknowns are introduced epochwise, but the ambiguities are constant over the epochs. The ambiguities are estimated with the aid of the code observations. For a short time span, like a few tens of seconds, we can give as a rough indication, that the precision of the ambiguity estimator improves by \sqrt{k} with k the number of epochs. The change in receiver-satellites geometry is small for the time span considered here. This $1/\sqrt{k}$ behaviour can be seen also in figure 1.31. When the time span is enlarged, also the phase observations will start to contribute to the estimation. For very long spans, they will even take the lead. In the experiments shown here, the float solution is determined mainly by the code observations (with only one epoch of data, it is the presence of the code observations, that enables the coordinate estimation). The (small) contribution of the phase observations can be seen, by comparison of the code-only and code&phase float scenario for the static case (figure 1.31 right). On the other hand, once the ambiguities are fixed, the code observations do not contribute much anymore (just a very little bit), compare the code&phase fixed scenarios with the phase-only ones; they coincide (the lower line in figure 1.31). This is caused by the large difference in measurement precision between code and phase, see section 5 of [ibid].

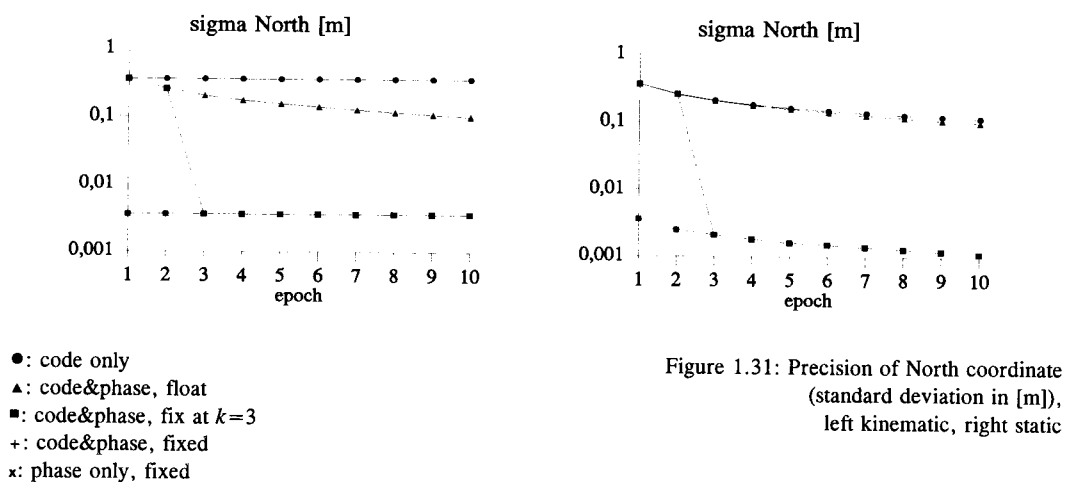


Figure 1.31: Precision of North coordinate (standard deviation in [m]), left kinematic, right static

The most important finding concerning the precision of the coordinate estimators, is thus the large improvement by fixing the ambiguities, see table 1.18 and figure 1.31. The gain in (baseline) precision is treated in section 4 of [ibid].

parameter estimation

Figure 1.32 gives, to get insight in the parameter estimation problem, both the standard deviation $\sigma_{\hat{x}_i}$ (dashed) and the conditional standard deviation $\sigma_{\hat{x}_i|t+1,\dots,r}$ (solid), with

$i=1, \dots, n$ and $n=9$, as we have $n=3+6$ unknown parameters (first three coordinates XYZ and then six double difference ambiguities). The (conditional) standard deviations of the ambiguities are expressed in meters rather than in cycles.

The conditional standard deviation $\sigma_{\hat{x}_{i|i+1, \dots, n}}$ gives the standard deviation of the estimator \hat{x}_i with the other unknown parameters x_{i+1} through x_n constrained (fixed). It can be seen that, for a baseline, once three parameters (three ambiguities in this case) are known (fixed), the remaining unknowns can be estimated very precisely (at the millimeter level, i.e. the measurement noise). The conditional standard deviation in relation with the GPS ambiguity resolution problem is discussed in [Teunissen et al, 1994].

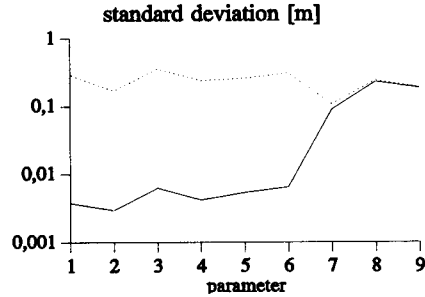


Figure 1.32: Precision of estimators, at epoch $k=3$ for the kinematic case, code&phase float
dashed: standard deviation
solid: conditional standard deviation

ambiguity estimation

Above we have analysed the structure of the overall parameter estimation problem. We will now detail on the integer estimation of the six ambiguities, for the kinematic code&phase scenario at $k=3$. The integer estimate for the vector of ambiguities, results from a discrete search over the ellipsoidal region prescribed by the float estimate and the variance covariance matrix [Teunissen, 1993]. The eigenvalues λ_i with $i=1, \dots, 6$ of the matrix yield the lengths of the principal axes of the ellipsoid, see table 1.19 and figure 1.33. There are 3 large axes (typically for precise GPS positioning); the remaining ones are very small (at the mm-level). Note that in comparing the lengths of the large and small axes, the factor 100 (approximately) shows up, i.e. σ_p/σ_p .

	λ [cyc ²]	$\sqrt{\lambda\alpha}$ [cyc]	$\sqrt{\lambda\alpha}$ [m]
1	1.66E-4	0.05	0.01
2	1.66E-4	0.05	0.01
3	3.38E-4	0.08	0.01
4	1.61	5.20	0.99
5	1.65	5.27	1.00
6	5.59	9.69	1.84

Table 1.19: Ambiguity search ellipsoid: eigenvalues λ of variance covariance matrix and length of the axes $\sqrt{\lambda\alpha}$ with $\alpha=0.01$

In addition, the ambiguities are correlated, see the histogram of the (absolute) correlation coefficients $|\rho_{\hat{x}_i, \hat{x}_j}|$ with $1 \leq j < i \leq 6$ in figure 1.34. With 6 ambiguities there are 15 coefficients. The ambiguity search ellipsoid is thus elongated and rotated with respect to the grid axes; a straightforward search would be inefficient. The LAMBDA method for integer ambiguity estimation, first decorrelates the ambiguities prior to the search and is thereby able to provide the integer estimate in a quick and efficient way.

For the validation of the integer ambiguity estimate, we may consider the volume of the ambiguity search ellipsoid [Teunissen et al, 1996]. For the kinematic code&phase scenario it equals $V_6=0.29 \text{ cyc}^6$ for $\chi^2=16.81$ ($\alpha=0.01$) and can be interpreted as that the ellipsoid contains no, one or at maximum only a few candidates, which gives hope for a positive validation. In [Teunissen, 1997c] the ADOP (ambiguity DOP) is proposed. It is, like the volume, also a function of the determinant of the variance covariance matrix: $\text{ADOP} = \sqrt{|Q_{\hat{x}_i}|}^{1/n}$. For the example at hand $\text{ADOP}=0.15 \text{ cycle}$. As an approximation (the transformed ambiguities are assumed to be fully decorrelated and to have all equal variance) the ADOP is the standard deviation of the transformed (decorrelated) ambiguity;

it can be referred to as generalized standard deviation. If the ADOP is, as such, much smaller than 1.0 cycle (e.g. 0.1 cycle), the validation can be expected to be successful.

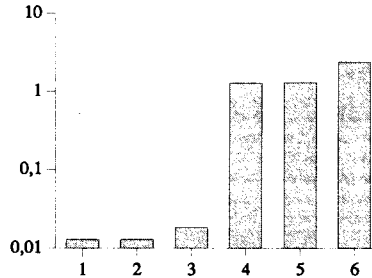


Figure 1.33: Eigenvalues of variance covariance matrix $\sqrt{\lambda}$ [cyc]

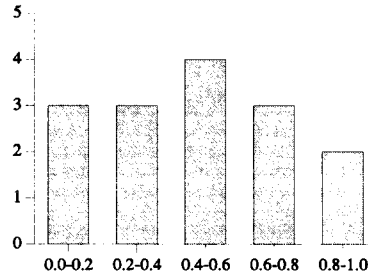


Figure 1.34: Histogram of (absolute) correlation coefficients

The ADOP (and the volume) should thus be as small as possible, from the viewpoint of validation (no other likely candidates). On the other hand, section 4 in [ibid], the reliability of the integer ambiguity solution (the volume) competes with the gain in baseline precision. From an economic point of view, we would like to occupy the point to be surveyed as short as possible, in order to maximize surveying productivity. To meet the requirements on precision for the surveyed coordinates, we need then a large gain. In practice, validation has to take priority over the gain in this. It is preferred not to fix the ambiguities over fixing them possibly incorrectly, which leads to (large) biases in the coordinate estimates. The surveyor has to be satisfied with a less spectacular gain; he has to wait until reliability turns the light to green. (For kinematic surveying, with the data processed in the field, this can be monitored in real time).

internal reliability

For the reliability, we consider the Minimal Detectable Biases for outliers in the code-observations and slips in the phase observations (local model validation). The observations of satellite PRN22 will be taken as an example.

The MDBs are given in figure 1.35. On top those for an outlier in the code observation, the y-axis ranges from 1.6 to 2.8 meter, at bottom those for a slip in the phase observation, the y-axis ranges from 1 to 4 centimeter.

PRN	17	19	21	22	23	31	28	17	19	21	22	23	31	28
17	1.000	.056	.007	.021	.082	.002	.031	.000	.003	.000	.005	.000	.001	.002
19		1.000	.017	.001	.018	.089	.022	.001	.000	.000	.000	.000	.001	.000
21			1.000	.033	.078	.046	.003	.000	.002	.000	.006	.002	.001	.004
22				1.000	.029	.030	.098	.001	.000	.000	.000	.001	.000	.001
23					1.000	.006	.012	.000	.000	.000	.000	.000	.000	.000
31						1.000	.048	.000	.001	.000	.001	.000	.000	.001
28							1.000	.001	.000	.000	.001	.001	.000	.001
17								1.000	.368	.200	.004	.573	.231	.054
19									1.000	.007	.353	.000	.752	.003
21										1.000	.074	.665	.241	.266
22											1.000	.028	.034	.684
23												1.000	.041	.004
31													1.000	.159
28														1.000

Table 1.20: Correlation matrix, code&phase float kinematic case at $k=3$

The MDBs for outliers in the code remain at (about) the same level for the kinematic code-only case (top, left). The MDBs (outlier and slip) of the code&phase float scenario (both kinematic and static), decrease as function of time, like there is an improvement in precision of the coordinate estimator. Note that with only one epoch of data, a slip in a phase observation at this first epoch can not be detected (it can not be separated from the ambiguity); the MDB is infinite.

Once the ambiguities are fixed, the MDBs are constant, for an outlier in the code. The MDB value equals 1.89 m (for all satellites), both for the kinematic and static case. The phase observations actually determine the coordinates precisely. In terms of single differences, the code observations have to determine only one unknown parameter, namely their clock error per epoch. The constant code MDB value is (practically) independent of the precision of the phase data (as long as this precision is some orders of magnitude better than of the code).

With the ambiguities fixed in the kinematic case, the MDBs for a slip in the phase are constant as well (code&phase and phase-only coincide in figure 1.35, graph bottom at left). The MDB value equals 2.5 cm. Note that for an outlier in the code, the MDB was 2.5 m in the code-only scenario. For the static case (ambiguities fixed), the MDB decreases as function of time, as the precision improves, see figure 1.31 right. The MDB will tend towards the value 1.9 cm (there is a new clock error per epoch).

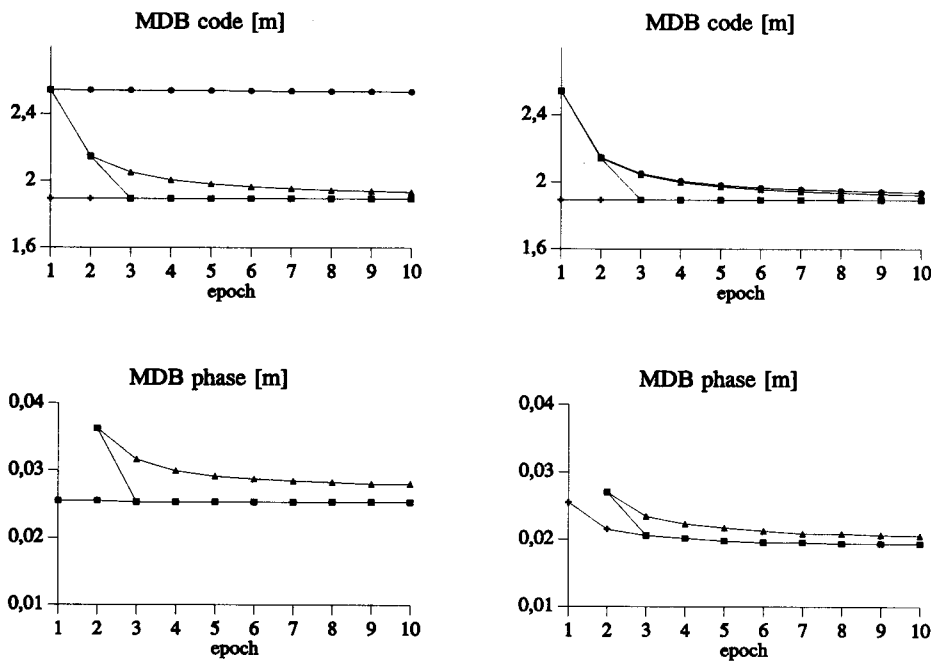


Figure 1.35: Internal reliability, Minimal Detectable Bias in [m], left kinematic, right static top outlier code, bottom slip phase satellite PRN22

As an example of separability between alternative hypotheses, we consider the correlation matrix of the one-dimensional teststatistics for the code&phase scenario with ambiguities

float for the kinematic case at epoch $k=3$. With 7 code and 7 phase (single difference) observations, the matrix is 14×14 , see table 1.20.

Between outlier hypotheses, the correlation is small. Correlation is also minimal between outliers in the code and slips in the phase. The 7×7 correlation matrix for the slip hypotheses very much looks like the one for the single frequency phase case, but with the ambiguities fixed, section 5.1.2.4, given at epoch $k=1$, cf. table 1.4.

external reliability

External reliability concerns the effect of undetected model errors on the estimators for the unknown parameters. We will consider the model errors outlier in code and slip in phase of size MDB. In the analysis below the ambiguity parameters are left out of consideration, as they are nuisance parameters. Only the three coordinates remain.

PRN	k i n e m a t i c					s t a t i c				
	code	code&phase			phase	code	code&phase			phase
		float	$k=3$	fixed			float	$k=3$	fixed	
17	5.1	2.0	0.0	0.0	-	2.1	2.0	0.0	0.0	-
19	5.3	2.1	0.0	0.0	-	2.1	2.1	0.0	0.0	-
21	6.6	2.3	0.0	0.0	-	2.3	2.2	0.0	0.0	-
22	3.7	1.7	0.0	0.0	-	1.7	1.7	0.0	0.0	-
23	2.7	1.4	0.0	0.0	-	1.4	1.3	0.0	0.0	-
31	3.5	1.6	0.0	0.0	-	1.7	1.6	0.0	0.0	-
28	3.4	1.6	0.0	0.0	-	1.6	1.6	0.0	0.0	-

Table 1.21: External reliability epoch $k=3$, scalar measure $\sqrt{\lambda_{NEH}}$ for outlier in code observation (kinematic and static)

In the tables 1.21 and 1.22, the values for $\sqrt{\lambda_{\hat{x}_{NEH}}}$ are given. They are significance measures for the effect of an undetected outlier or slip (of size MDB) on the three-dimensional coordinates.

The most remarkable feature of the above table is that once the ambiguities are fixed, the $\sqrt{\lambda_{\hat{x}_{NEH}}}$ -values are very small. They are about 0.03 for code&phase fixed in the kinematic case and about 0.02 in the static case. The code observations do not contribute very much to the coordinate estimators. An interpretation of the scalar measure $\sqrt{\lambda_{\hat{x}}}$ is given by equation (8.7) in chapter 1. In the fixed solution, the coordinate precision is at the 10^{-2} - 10^{-3} m level, implying an upperbound for the bias in this parameter in the order of 10^{-4} m or 0.1 mm. Note that column ' $k=3$ ' is redundant; at and after $k=3$, thus once the ambiguities are resolved, this scenario equals the fixed scenario.

Although the phase observations contain the additional ambiguity unknown, they link the successive epochs and thereby help to reduce the MDBs for outliers in the code observations in the kinematic case. This was also the case for the precision of the coordinates. As such, they improve, even with float ambiguities, the external reliability of the coordinate estimators. In the static case the values for the code-only scenario are about equal to those for code&phase float scenario. Introducing the phase observations in the static case does not aid much. The $\sqrt{\lambda_{\hat{x}_{NEH}}}$ -values are just slightly smaller. There is not much difference between the kinematic and static case for the code&phase float scenario.

For the code&phase float scenario, in both the kinematic and static case (outliers in the code), we have $\sqrt{\lambda_{\hat{x}_{NEH}}} \approx \sqrt{\lambda_{\hat{x}}}$ (the significance measure for the full vector of unknowns, coordinates and ambiguities).

For the code&phase float scenarios the $\sqrt{\lambda_{\hat{x}_{NEH}}}$ is small for slips in the phase observation. The phase observations do not contribute much to coordinates (short time spans). The values are not equal for the kinematic and static case, but they are at the same level 0.2-0.7. When the full vector of unknowns is considered (coordinates and ambiguities), the $\sqrt{\lambda_{\hat{x}}}$ -values are much larger, in the order of 5 to 7 for the kinematic case and about 3 for the static case.

PRN	code	k i n e m a t i c				code	s t a t i c			
		float	code&phase k=3	fixed	phase		float	code&phase k=3	fixed	phase
17	-	0.4	5.1	5.1	5.1	-	0.7	2.1	2.1	2.1
19	-	0.5	5.3	5.3	5.3	-	0.4	2.1	2.1	2.1
21	-	0.2	6.6	6.6	6.6	-	0.4	2.3	2.3	2.3
22	-	0.7	3.7	3.7	3.7	-	0.6	1.7	1.7	1.7
23	-	0.4	2.7	2.7	2.7	-	0.3	1.4	1.4	1.4
31	-	0.3	3.5	3.5	3.5	-	0.4	1.7	1.7	1.7
28	-	0.6	3.4	3.4	3.4	-	0.2	1.6	1.6	1.6

Table 1.22: External reliability epoch $k=3$, scalar measure $\sqrt{\lambda_{NEH}}$ for slip in phase observation (kinematic and static)

When fixed, the phase observations, instead of the code observations, do determine the coordinates. Undetected slips in phase observations have a large impact on the coordinates: the coordinate estimators are very precise, as compared with the float solution.

Note that the $\sqrt{\lambda_{\hat{x}_{NEH}}}$ values for phase-only fixed equal those for outliers in the code-only scenario in the kinematic case. For the static case, they were not computed. The values will be identical to code-only scenario of the static case. These values have been substituted in the table above.

5.1.3 Summary

Various measurement scenarios for relative positioning were considered, code and/or phase observations, single and dual frequency, ambiguities float and fixed. The interrelationships between these scenarios were discussed. The chapter started however with the case of single point positioning.

summary

This study made us acquainted with the quality that can be achieved with kinematic GPS positioning, or more general with precise relative GPS positioning on a local scale. The quality was analysed in terms of precision and reliability. The purpose in addition, was to identify a workable set of parameters to represent the quality of the measurement system.

- precision

Precision describes the quality of the estimator \hat{x} under the working mathematical model, the null hypothesis H_0 . The dispersion is given by the variance covariance matrix. The estimators for the coordinate unknowns x_2 are of primary interest. The coordinates are expressed in WGS84 XYZ (geocentric coordinate system) or in local North, East, Height (Up) (topocentric coordinate system). We considered the standard deviation of each coordinate estimator individually, as they are easy to interpret. The smaller the value for the standard deviation, the better the precision of the estimator. The precision ellipse, section 4.1.2, (in two dimensions) has also been considered; it visualizes the full information content of the variance covariance matrix.

- reliability

Parallel to the recursive estimation, the validity of the working mathematical model is checked. The validation concerned misspecifications in the functional model, namely outliers in code observations and (cycle) slips in phase observations. Slippage tests are performed. The nominal performance of the testing procedure is expressed by reliability.

The MDBs ∇ give the error that can be found with a certain probability, equation (8.2) in chapter 1. The above model errors directly concern one or one sequence of observations and are expressed in unit meters for outliers in the code and unit cycles for slips in the phase. For good reliability the MDBs should be small. The size of the ∇ can be judged with respect to the standard deviation of the observable.

As more than one model error might occur (possibly simultaneously), it is important to consider also the separability between the various specified errors. Separability, as correlation between the teststatistics, is expressed by $\rho_{ii}^2 = \cos^2\phi$, equation (8.4) in chapter 1. There is optimal separability between two errors when $\rho_{ii}^2 = 0$.

External reliability is the propagation of the model error, when it remains undetected, into the estimator for the vector of unknown parameters. Of particular interest for positioning of course, is the bias caused in the (three) coordinate estimators. The ambiguities are nuisance parameters (knowing the actual values is of no use; they have no physical meaning). The significance of the propagation is expressed by the bias to noise ratio $\sqrt{\lambda_x}$, equation (8.6) in chapter 1. The smaller $\sqrt{\lambda_x}$, the better reliability. For its interpretation, the value for $\sqrt{\lambda_x}$ (when it concerns the three coordinates) can be compared with the value χ for the three-dimensional precision ellipsoid.

conclusions

An analysis on quality, the design computations as they were made for the Ypenburg 94 campaign, can be made prior to actual field operation (no real observations are needed). Evidently, the analysis is based on the assumed modelling; the mathematical model must be adequate.

- precision

For the precision, it can be concluded that in general, σ_H is about two times the σ for the horizontal coordinates North and East. Usually the σ_E is slightly smaller than σ_N . This holds for GPS positioning at the mid-latitudes on Earth, with code observations only, or with phase observations (and the ambiguities fixed). The configuration of the Ypenburg 94 experiment turned out to be a representative one.

By fixing the carrier phase ambiguities, the precision of the coordinate estimators improves. This gain is large, in particular when only short observation time spans are used, as is the case in kinematic GPS surveying. Using carrier phases and consequently fixing the ambiguities, are prerequisites for achieving the precision desired in GPS surveying.

- reliability

Increasing the redundancy of the measurement system by using more satellites and in particular using dual frequency data over single frequency (doubling the measurements), is very beneficial for reliability. It results in smaller MDBs, better separability and smaller $\sqrt{\lambda_x}$'s.

- estimation results

In the estimation results (small) systematic effects in the measurement system were encountered several times. For the Trimble 4000 SSE receiver, predecessor of nowadays 4000 SSI, interchannel time varying hardware delays (or multipath) could be suspected to affect the code measurements, at the 1-2 dm level.

- model validation

The settings for the statistical testing procedure discussed in section 4.2 were used and seem to yield satisfying results for kinematic GPS surveying. Due to the recursive estimation, the redundancy never becomes extremely large (think of 10^1 - 10^2). The testing procedure performed well. Outliers in the code, and cycle slips in the phase were detected, correctly identified and estimated.

5.2 Analysis of GPS code and phase observables

In chapter 3, the mathematical model for the GPS observables was developed to comply also with the Rinex standard. For geodetic purposes, there are however, several different receivers available and they employ different measurement techniques to provide dual frequency phase and code observations, see e.g. [Dierendonck, 1994], and this will be directly reflected in different stochastic properties of their observables. By means of the data of a zero baseline per receiver pair, we will attempt to reveal these properties. In this analysis we will try not to digress to a ranking of the receivers in terms of better and best. We will on the other hand, not refrain from clearly pointing out the differences in the stochastic properties of the observables of the different receivers. The zero baseline data are referred to as the UNAVCO 95 campaign.

For the interpretation of the zero baseline data analysis, it is important to realize that the resulting figures may deviate from those that would have been obtained under operational (practical) circumstances (two receivers with two antennas). The distinct difference in the measurement set up is that for the zero baseline only *one* antenna and Low Noise Amplifier (LNA) are used. The LNA may be responsible for a part of the noise of the observable. In this set up, the same LNA is used for both receivers and the noise may therefore largely cancel in relative positioning. On the other hand, the signal from the amplifier is split over two receivers and may therefore suffer from some loss in power, resulting in a weaker signal (lower signal strength) and thus in more noise for the observable. With one of the receivers, to anticipate on this, also a short baseline with two receivers and two antennas was measured in Delft. The experiment is described and the results are analysed and discussed in section 5.2.2.7.

5.2.1 Experiment description

The data were collected in a GPS equipment test, carried out by the University NAVSTAR Consortium (UNAVCO). The consortium provides information, technical support and equipment to investigators using the Global Positioning System satellites for high-accuracy geosciences research. The test is described in full detail in [UNAVCO, 1995].

Four sets of equipment, suited for scientific applications, were tested: the 4000 SSI from Trimble Navigation Ltd, the Z-XII3 from Ashtech, the SR399 from Leica Inc and the SNR-8000 from Allen Osborne Associates Inc, see also table 2.2. These receivers yield

dual frequency pseudo-range data and full wavelength carrier phases under both A/S and non A/S conditions; the so-called Y-buster receivers.

Various aspects of the GPS equipment were tested by UNAVCO. In this study we use the data from the zero baseline 1 second sampling test. Two receivers of the same make and type are connected to the one antenna and low-noise amplifier (LNA). The test was conducted to examine receiver performance. The measurements with the four receiver pairs have been carried out simultaneously and at the same site (Table Mountain, $\varphi=40^\circ$ $\lambda=-105^\circ$, at Boulder, Colorado, US), see figure 2.2. The markers are Diamond North DN, East DE, West DW and South DS. The receiver-pairs thus operated under identical circumstances. During the test A/S Anti-Spoofing was on. Autumn 1995 was a period near the solar minimum (ionosphere).

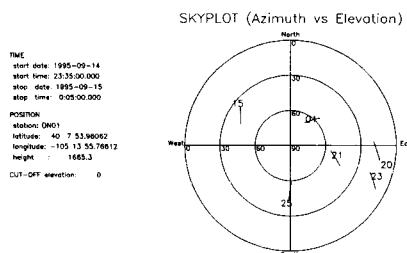


Figure 2.1: Skyplot at DN, UNAVCO 95, Table Mountain, Boulder, Colorado, US

```

number of satellites: 6 (all Block II and IIA)
PRNs: 01 15 25 23 20 21
pivot: 21 (double differencing)
number of receivers: 2 per make (stationary, zero baseline)
receiver type: see below, table 2.2
date: September 14th, 1995 (GPS week 818; day 257)

observation session: ~1 hour
start: 23:15:00 GPS; 429300 seconds in GPS week
end: 00:15:00 GPS ; 432900 seconds in GPS week
sampling interval: 1 second

processing session: 30 minutes (181 epochs)
start: 23:35:00 GPS ; 430500 seconds
end: 00:05:00 GPS ; 432300 seconds
sampling interval: 10 seconds ' GPS = UTC + n [s] with n=10

```

A skyplot for the 30 minutes processing session is given in figure 2.1. Some receivers did track in addition two or three low elevation satellites, but these did never reach the 15° elevation. PRN 23 sets (after 23:45 it is below 15°) and PRN 20 rises (it is below 15° before 23:45). These two are nevertheless tracked for the whole observation session.

	DN01 Trimble	DE01 Ashtech	DW01 Leica	DS01 Turbo Rogue
X [m]	-1283327.1182	-1283324.2669	-1283331.1012	-1283328.2540
Y [m]	-4712971.7753	-4712974.8025	-4712973.2709	-4712976.4440
Z [m]	4090247.3114	4090244.6509	4090244.5048	4090241.7175

Table 2.1: Stations and coordinates of markers in WGS84

The Rinex files were created with the Bernese translator for Trimble and Ashtech, with Leica's own translator for Leica and with the JPL-translator for Turbo-Rogue, see [ibid].

receiver	Trimble	Ashtech	Leica	Turbo Rogue
type	4000 SSI	Z-XII3	SR399	SNR-8000
antenna	compact L1/L2 gr-pl removable	choke-ring Dorne Margolin	external with gr-pl	choke-ring Dorne Margolin
obs types	C1 P2 L1 L2	C1 (P) P2 L1 L2	C1 P2 L1 L2	C1 P2 L1 L2
technique	cross-correlation	P-W tracking	P-code aided squaring	cross-correlation

Table 2.2: Receiver characteristics

5.2.2 Results and analysis

For a zero baseline, two receivers are both connected to one antenna. The baseline coordinates are deterministically known: $x_{12}=0$, $y_{12}=0$ and $z_{12}=0$. In principle, the propagation delays completely cancel and so do the effects of satellite position and reference receiver coordinates. Also site-related disturbances are in principle common. By means of the zero baselines, the geodetic performance with code and phase observations will be assessed of four state of the art receiver-pairs. The data, C1-code and L1-phase, of the zero baselines are processed in the ordinary way to provide relative positioning results, which are thus known a-priori to be zero, section 1 and 2. Note however, that the performance is assessed here under favourable conditions; performance may be somewhat less under true operational conditions (as for instance each receiver then uses its own antenna and may be moving instead of stationary). Then the observation types, code and phase on both frequencies L1 and L2, are treated separately; the sections 3 through 6. Introducing the a-priori known baseline, the coordinates are constrained, yields a very powerful tool for analysing the (raw) observables, see appendix A.

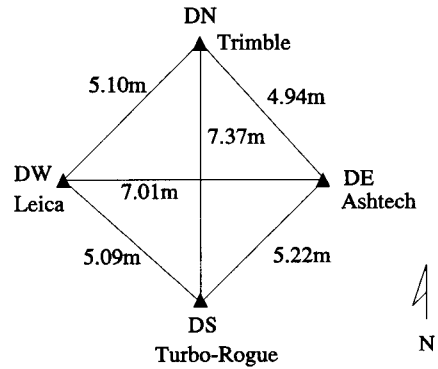


Figure 2.2: Measurement location at Table Mountain with 4 stations

5.2.2.1 Positioning: C1-code

Ordinary relative positioning with L1-code observations was carried out. With $m=6$ satellites, there are $(m-1)=5$ double difference observations per epoch. Although the baselines are static, kinematic solutions were computed: new coordinate unknowns are estimated for each epoch (actually processing on single epoch basis). The standard deviation of the undifferenced code observable was taken $\sigma_p=0.3$ meter.

single point positioning: receiver clock estimates

For all 2x4 receivers, first single point solutions were determined on single epoch basis. The variance covariance matrix was taken a scaled unit matrix with $\sigma=20.6m$. Note that for the Ashtech, P1-code data were used, not C1-code.

We will omit the coordinate estimates and consider, as a side step in the analysis, the estimates for the receiver clock errors. In figure 2.3 for each pair, the estimates are given for the second receiver, expressed (using the speed of light) in units of range, nl. meters (at $k=1$ $\sigma=27.4m$). The receiver clock error estimates are different for the four receivers, note the difference in vertical scales, 3×10^5 m \equiv 1 ms and 300 m \equiv 1 μ s. This shows that different techniques are used by the receivers to keep the receiver clock (approximately) synchronized with the (transmitted) GPS time (the receiver computes a navigation solution in real time). In table 2.3 we give the size of the total drift over the 30 minutes period and the resulting drift rate (as experienced by the user).

		drift (30 min) [s]	drift rate [s/s]
DN02	Trimble	7.7×10^{-4}	0.4×10^{-6}
DE02	Ashtech	2.6×10^{-4}	0.1×10^{-6}
DW02	Leica	1.9×10^{-7}	0.1×10^{-9}
DS02	T-Rogue	1.0×10^{-7}	0.6×10^{-10}

Table 2.3: Receiver clock behaviour

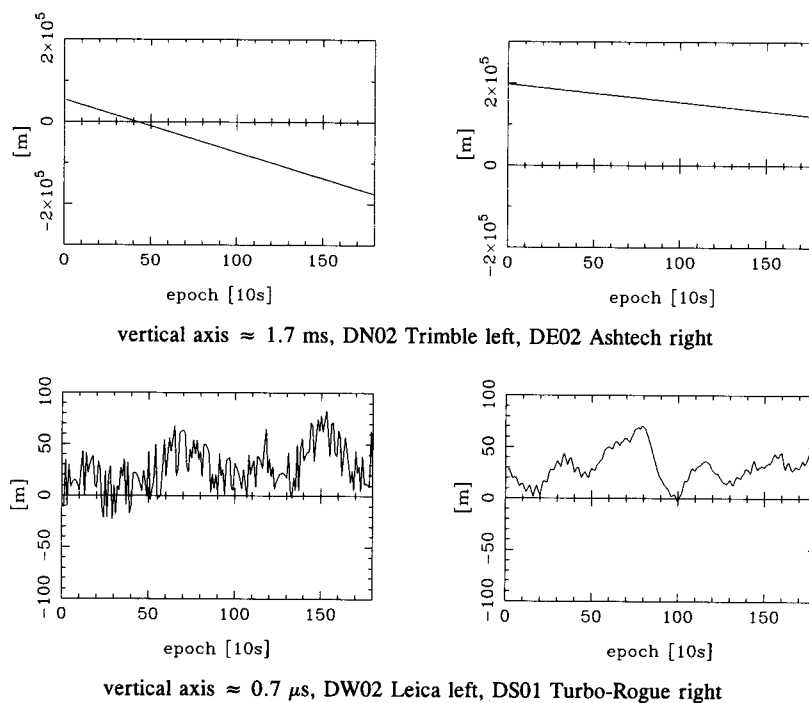


Figure 2.3: Clock error estimates $c\delta\hat{t}$ for second receiver

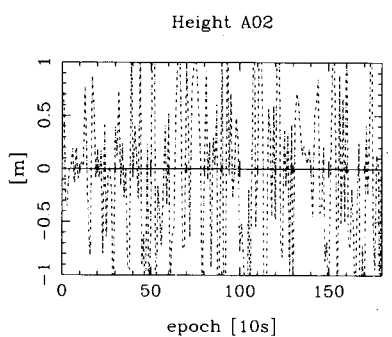
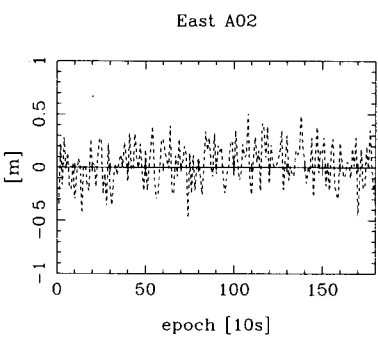
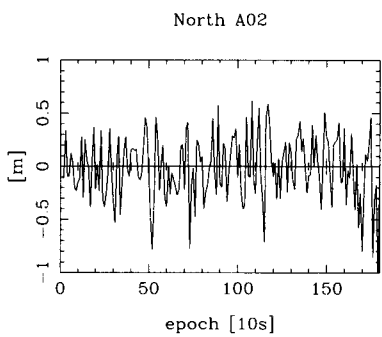
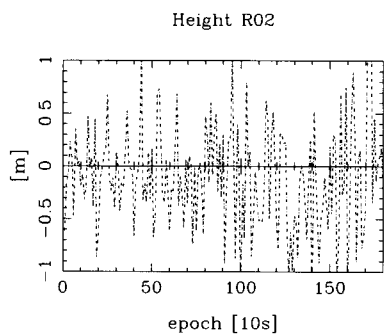
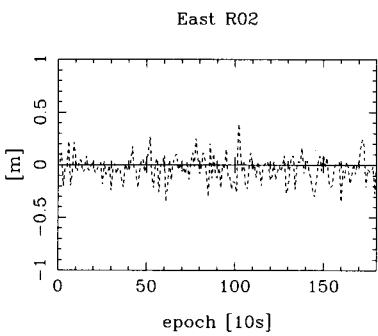
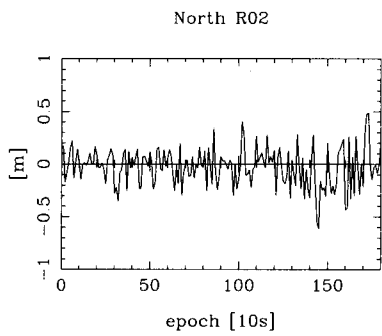
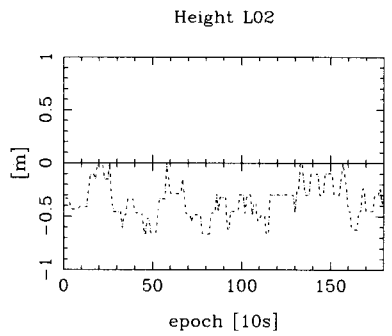
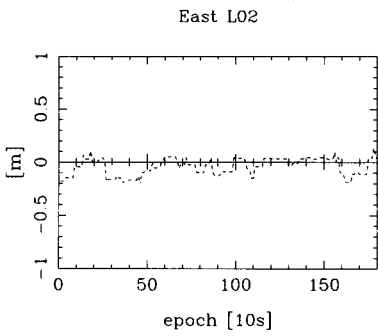
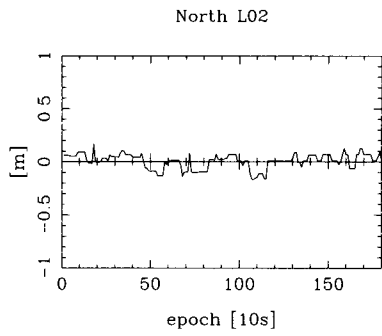
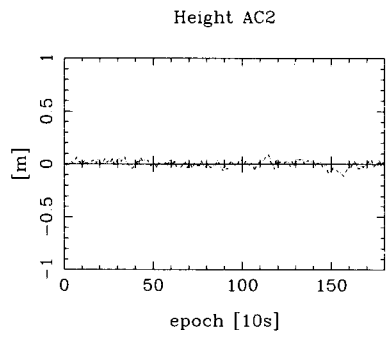
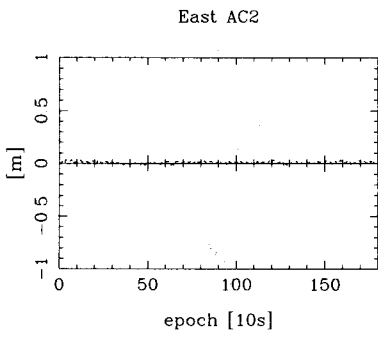
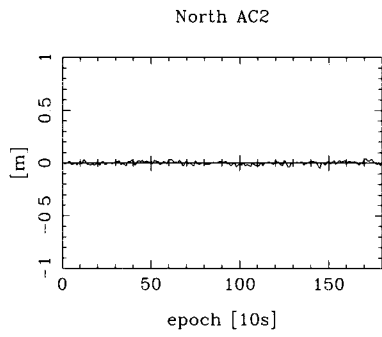
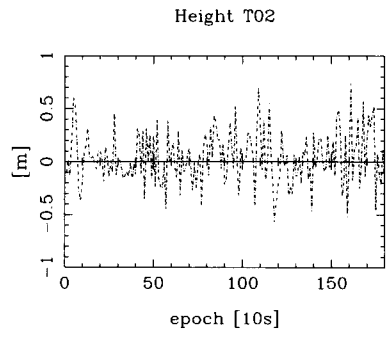
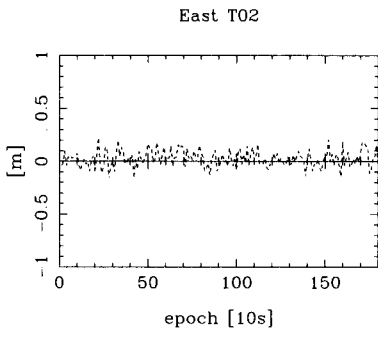
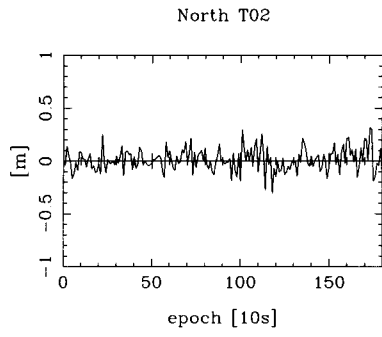
The clock of the Trimble has a typical quartz-oscillator drift rate of 10^{-6} s/s. The clock is left running free and kept synchronous to GPS time within 1 ms by clock resets (actually one such reset occurred for DN02, but it has been undone by the Rinex conversion). The oscillator of the Ashtech seems to have a somewhat better stability (no clock jumps occurred).

The Leica and Turbo Rogue seem to steer the receiver clock rate continuously during the measurement session. In this way they keep the clock synchronized without discrete clock jumps. The resulting drifts are very small. The steering of the Turbo-Rogue seems to be long-term (the drift rate smoothly varies over time), whereas it of the Leica seems to be very short-term (there is a correlation with the estimated height). From [Sandholzer, 1992] we cite, that for the Leica SR299, 'The clock-steering is designed to hold the receiver clock to within 100 ns (standard deviation) of the transmitted GPS time'; 100 ns is equivalent to 30 m, cf. figure 2.3.

relative positioning: coordinates

The coordinate estimates (for the marker underneath receiver 2), obtained with relative positioning with single frequency code observations, are differenced with the reference values and expressed in a local topocentric system. We have a perfect ground truth available: the estimates for the coordinates of receiver r2 have to be equal to the coordinate-values we fix the reference receiver to, or in other words, the baseline coordinate estimators are expected to have zero mean.

Figure 2.4 (right page): Relative positioning (C1) coordinate-differences in North, East, Height
T Trimble, A Ashtech, L Leica, R Turbo-Rogue and A Ashtech (P1)



By means of single epoch solutions, we analyse the overall geodetic performance of the receiver-pair (not antenna). We cite from [UNAVCO, 1995]: 'Each receiver type was tested on a zero baseline with their respective antenna. Data were sampled at a 1 second interval. The resulting observations reflect receiver noise, with minimum phase or code averaging.'. GPS receivers usually use the carrier phase and averaging to smooth the pseudo-range observations. 'At one second sampling, the averaging time is minimized for each receiver, and observations are minimally correlated from epoch to epoch.'

Each receiver provides CA-code observations (C1 obtained by code-correlation). In addition the Ashtech provides P1-code observations (obtained by P-W tracking). We will thus consider five cases.

In figure 2.4, the coordinate differences, estimated - reference, are given, in terms of local North, East and Height. The y-axis ranges from -1 to +1 meter. The precision of the height is worse than the precision of the horizontal coordinates.

Per coordinate North, East and Height, the 181 estimates for the difference with the reference value, are assumed to be samples of independent (in time) random variables with zero mean. Per coordinate, the mean and empirical standard deviation are given in table 2.4 below. Also the formal precision at the first epoch $k=1$ is given.

	mean					standard deviation					formal
	DN	DE	DW	DS	DE*	DN	DE	DW	DS	DE*	
North	0.01	0.00	0.01	-0.03	-0.02	0.11	0.02	0.07	0.18	0.30	0.48
East	0.02	0.01	-0.04	-0.04	0.03	0.08	0.02	0.09	0.13	0.20	0.38
Height	0.04	0.00	-0.36	-0.10	-0.06	0.25	0.03	0.39	0.50	0.81	0.79

* by P1 observations

Table 2.4: Mean and standard deviation per coordinate in meter

For the Trimble (DN) the mean per coordinate does not really deviate from zero. In figure 2.4 no severe (long term) fluctuations in the series can be noticed. The noise is likely to originate from raw code measurements.

The figures of the Ashtech (DE) for the mean (very close to zero) and standard deviation (a few centimeters only) are very impressive. With single frequency code observations actually surveying precision is achieved. The receiver probably uses though some averaging and/or carrier phase to smooth the code observations. When the coordinates are determined with the P1-code observations (P-W tracking, instead of code correlation), the graphs (figure 2.4) are similar to those of the Trimble. They are however, much noisier (about three times).

For the Leica (DW), the Height does significantly deviate from zero and it is not an error in the antenna-height. Some bias is also noticed in [UNAVCO, 1995]. The edge-shaped graphs in figure 2.4 show that severe data processing is carried out inside the receiver. Probably a Kalman filter is used for the dual frequency phase and code observations together, per satellite (channel). According to [Euler, 1997], the receiver has run in compacted data mode (as opposed to sampled data mode). The code observations are severely smoothed and the phase observations slightly; the latter within one second, so that sampling at 1 Hz yields phase observables which practically are not time-correlated. Another feature is that the (double difference) ambiguities have small values (for this zero baseline between -10 and +10); other receivers do have here ambiguity values on the order of 10^5 , and Trimble even 10^6 .

Although somewhat noisier (almost a factor 2), the graphs of the Turbo-Rogue (DS) are similar to those of the Trimble.

relative positioning: model validation

There are no rejections at all, for all receiver pairs, except for the Ashtech when the P1 observations are used instead of the C1 (a few outliers in the low elevation satellites PRNs 20 and 23); adaptation was disabled. The values of the local overall model test T , divided by the critical value k , are given in figure 2.5. The detection is positive when this ratio exceeds 1.0. The teststatistic values are rather small on the average. For model 02, the redundancy equals 2, we expect $E\{\underline{T}^k\}=2$ and with $k=11.73$ we have $E\{\underline{T}^k/k\}=0.17$. The observed means are given below. We also give the standard deviation of unit weight for the (undifferenced) code observable to achieve the expected mean of the local overall model test. For CA-code correlation, they all are much smaller than the a-priori value of 0.30 m.

	mean T/k	σ [m]
DN Trimble	0.02	0.10
DE Ashtech	0.00	<0.05
DW Leica	0.00	<0.05
DS T-Rogue	0.06	0.18
DE Ashtech	0.20	0.33

* by P1 observations

Table 2.5: Local overall model test

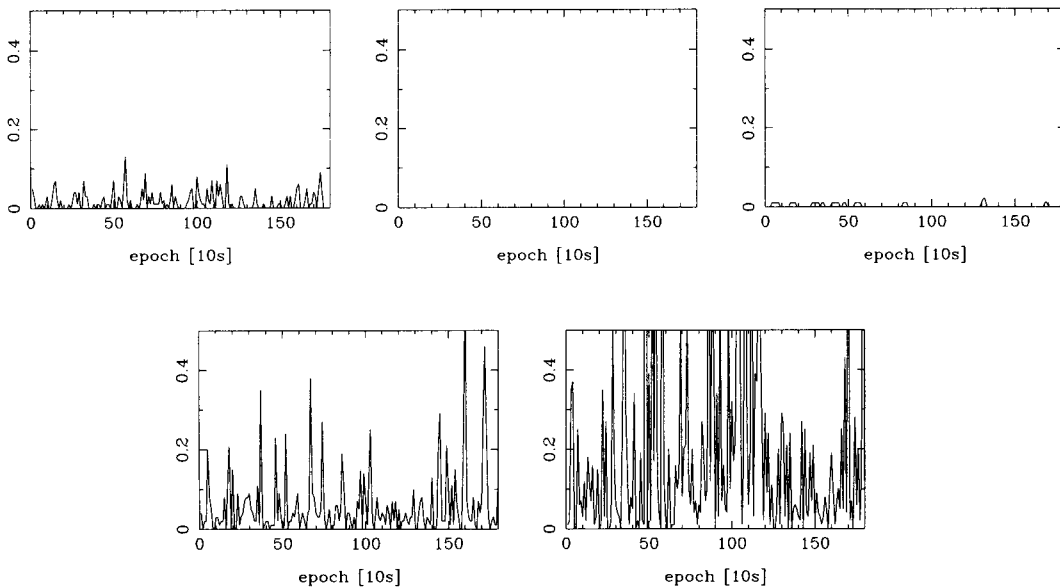


Figure 2.5: Local Overall Model teststatistic divided by critical value T/k
Trimble, Ashtech, Leica
Turbo-Rogue and Ashtech (P1)

5.2.2.2 Positioning: L1-phase

Relative positioning with L1-phase observations was carried out. The double difference ambiguities have been constrained (fixed) to their integer values. Only three coordinate unknowns are left. The data have been processed on single epoch basis, new coordinate unknowns are introduced for each epoch. The standard deviation for the undifferenced phase observable was taken $\sigma_p = 0.003$ meter.

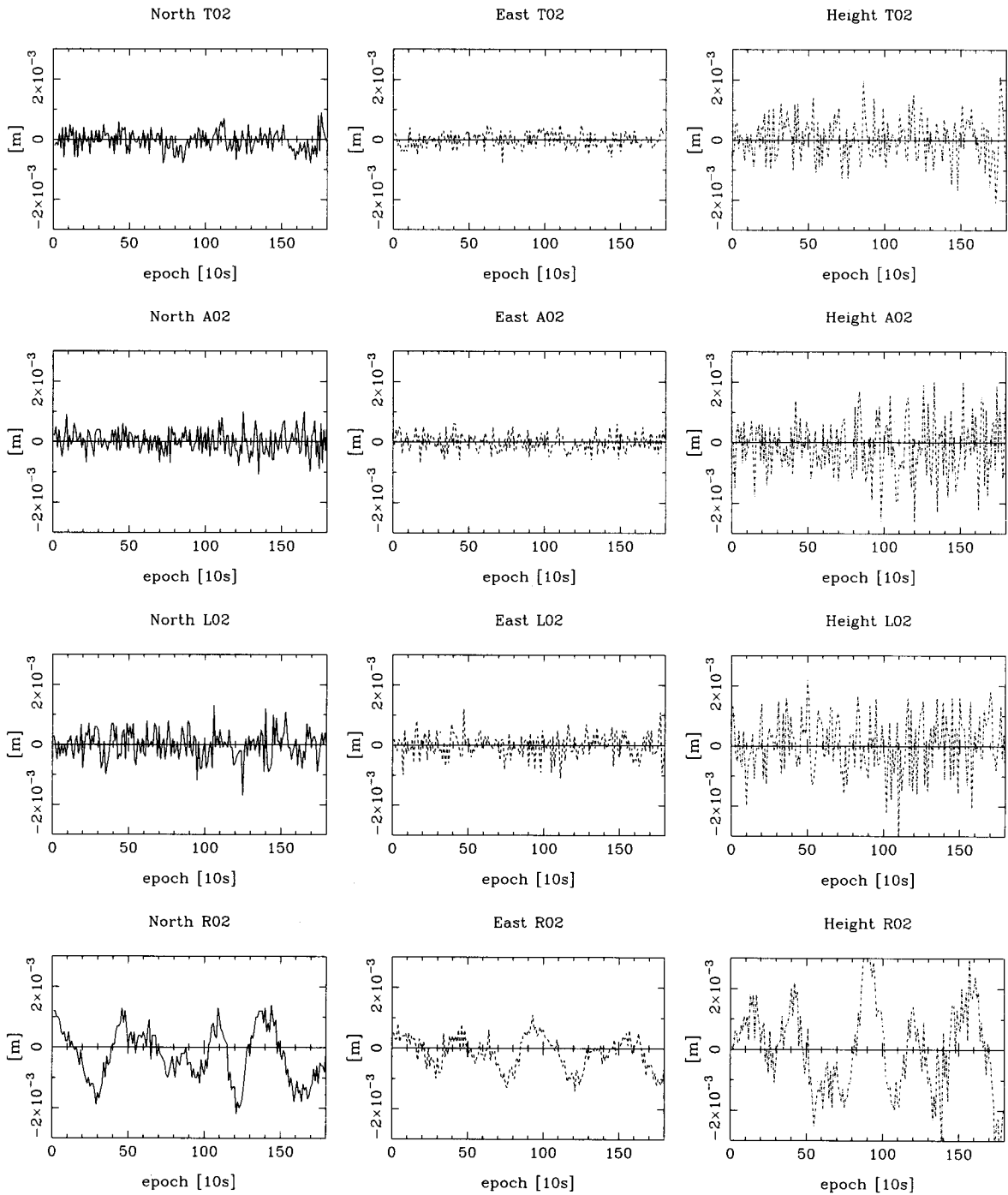


Figure 2.6: Relative positioning (L1) coordinate-differences in North, East, Height
T Trimble, A Ashtech, L Leica, R Turbo-Rogue

relative positioning: coordinates

The coordinate estimates obtained with relative positioning with single frequency phase observations (ambiguities fixed), are differenced with the reference values and expressed in a local topocentric system, see figure 2.6. The y-axis ranges from -3 to +3 millimeter. The precision of the height is worse than the precision of the horizontal coordinates. The coordinates were output at 0.1 mm resolution.

	mean				standard deviation				formal
	DN	DE	DW	DS	DN	DE	DW	DS	
North	-0.1	0.0	-0.0	-0.3	0.3	0.4	0.5	0.9	4.8
East	-0.0	-0.0	-0.0	-0.2	0.2	0.3	0.4	0.5	3.8
Height	0.0	-0.2	0.1	0.0	0.7	0.9	0.9	1.4	7.9

Table 2.6: Mean and standard deviation per coordinate in 10^{-3} m or millimeter

Per coordinate, the mean and empirical standard deviation are given in table 2.6. Also the formal precision at the first epoch $k=1$ is given.

The coordinates do not really deviate from zero, for any receiver-pair. The variations in the coordinate estimates over about half a centimeter, as were observed for the baseline with Trimble 4000 SSE receivers, figure 1.27 in section 5.1.2.4, can be a receiver effect or a differential atmospheric delay. On a zero baseline, the differential delays are in principle zero, $I_{12}^s=0$ and $T_{12}^s=0$. Long term variations are indeed practically absent in figure 2.6, except for the Turbo-Rogue.

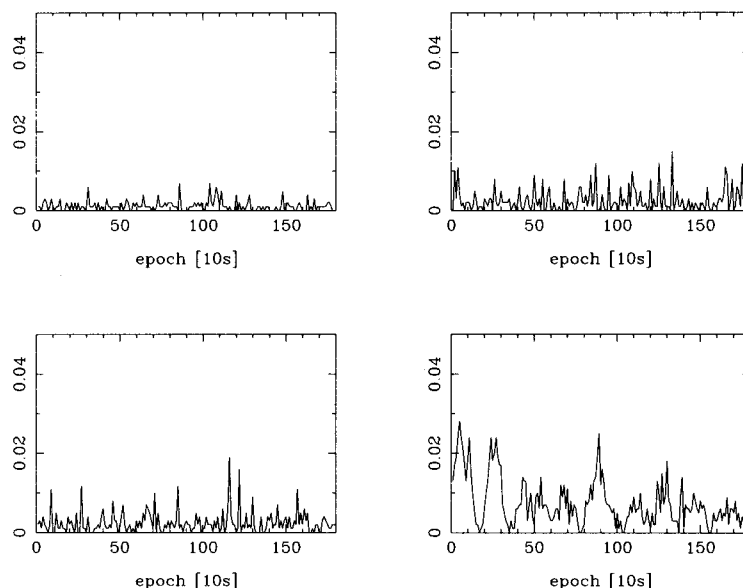


Figure 2.7: Local Overall Model teststatistic divided by critical value T/k
 Trimble Ashtech
 Leica Turbo-Rogue

The noise level shown in figure 2.6, is thought to represent the receiver noise in making the L1 phase observation. For all receiver pairs, it holds that the noise is much smaller than assumed a priori ($\sigma=3\text{mm}$).

relative positioning: model validation

For all four receiver pairs, there are no rejections at all. The values of the local overall model test T , divided by the critical value k , are given in figure 2.7. The teststatistic values are rather small on the average. The y-axis ranges up to only 0.05. We expect $E\{\underline{T}^k\}=2$ and with $k=11.73$ we have $E\{\underline{T}^k/k\}=0.17$. The observed means are given in table 2.7. We also give the standard

	mean T/k	σ [m]
DN Trimble	0.0012	0.0003
DE Ashtech	0.0025	0.0004
DW Leica	0.0025	0.0004
DS T-Rogue	0.0074	0.0006

Table 2.7: Local overall model test

deviation of unit weight for the (undifferenced) phase observable to achieve the expected mean for the local overall model test. They all are much smaller, up to ten times, than the a-priori value of $\sigma=0.003$ m, see also the considerations in [Langley, 1997].

5.2.2.3 Analysis: C1-code

The GPS observables will be analysed in detail in the next four sections. This analysis is made in order to get acquainted with the stochastic properties (and possibly some unmodelled functional ones as well) of the GPS code and phase observables. By means of analysing error estimates we will check whether the currently assumed mathematical modelling is adequate.

The analysis is made per observation type, C1-code, P2-code, L1-phase and L2-phase, one observation type at a time. For the L1 and L2 phases, the ambiguities are kept fixed. The standard deviation of the undifferenced observable is taken 0.30 m for the code, and 0.003 m for the phase. We will use 10 minutes (23:35:00-23:45:00 or in seconds 430500-431100) of data at 1 second sampling interval. This yields 601 epochs. The adaptation of the model validation was disabled; the data were analysed just as they have come in.

We will constrain the baseline coordinates (model C1). As only one antenna is used, it is known a-priori that these coordinates are zero. When the coordinates are constrained, we get a better insight in the receiver performance on channel basis. In terms of the model with single difference observations, there is only one unknown per epoch, namely the receiver clock and it is common to all channels (satellites) via (the same) coefficient 1.0, see appendix A for a derivation. In this experiment with 6 satellites, there are $m=6$ observations and there is one unknown $n=1$. The redundancy per epoch equals $m-n=5$. Per epoch $m=6$ outlier estimators are computed, based on $m-n=5$ residuals. Under the null hypothesis the error estimators have zero mean and their mutual correlation is $\rho_{\hat{v}_i \hat{v}_j} = -\frac{1}{5}$. The formal standard deviation equals $\sigma_{\hat{v}} = \sqrt{\frac{m}{m-1}} \sqrt{2} \sigma_p \approx 0.46$ m for the code and 4.6 mm for the phase.

Per observation type and per channel/satellite, a time series of error estimates forms the basis of the analysis. The following empirical figures will be considered for these series:

- mean
- standard deviation
- mutual correlation (between channels), for C1-code and for L1-phase

and in addition the

- cross correlation (between observation types; same channel/satellite), for the pairs C1-P2-code and L1-L2-phase, and for the pair C1-code and L1-phase

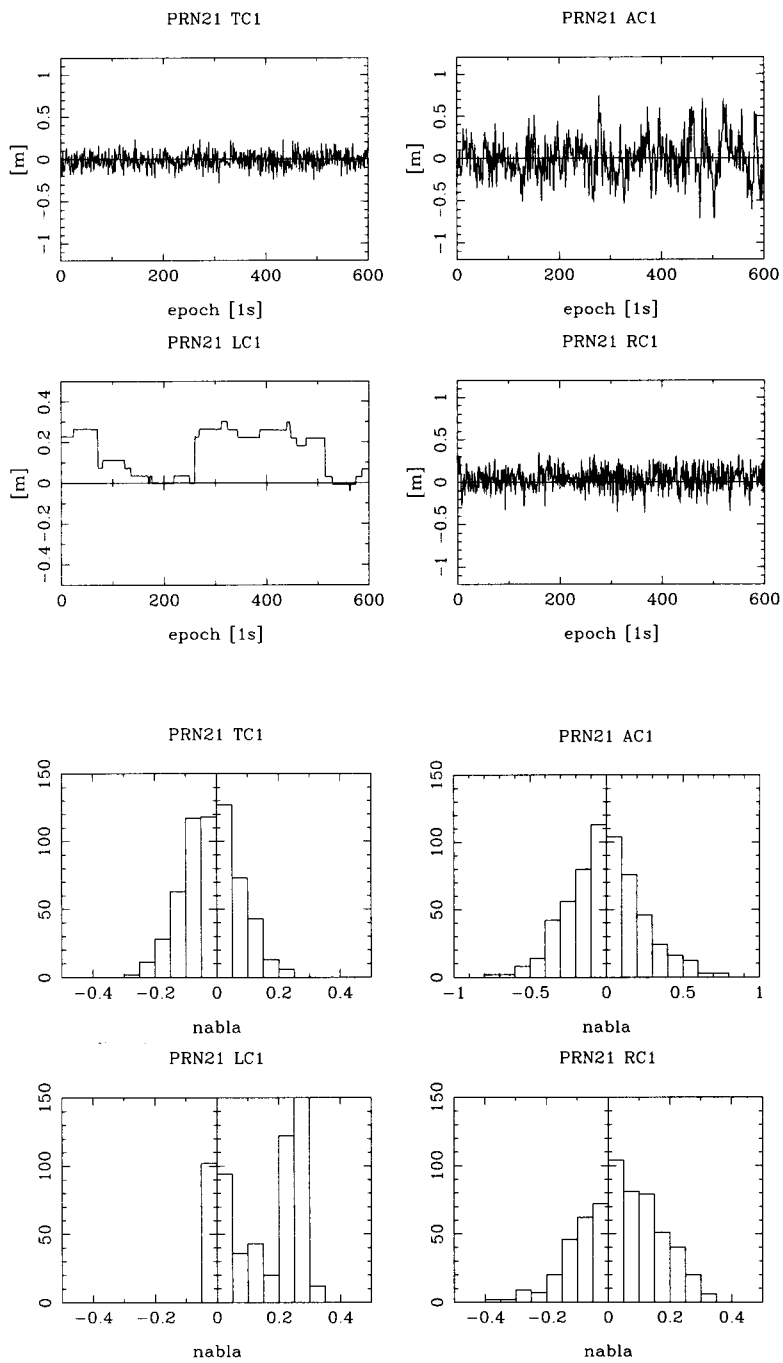
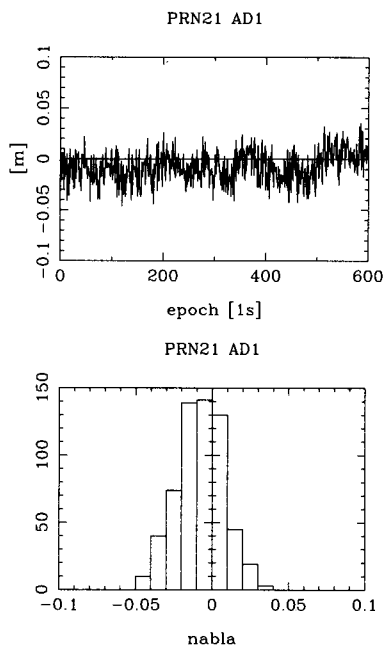


Figure 2.8: Error estimates for C1-code; Trimble, Ashtech (P1), Leica and Turbo-Rogue satellite PRN 21

Visual inspection of the data will concern plots of the time series, histograms (distribution) and correlograms (time correlation). The latter will be given for all satellites, the first two only for one satellite, namely PRN 21; representative for reasonable to high elevations, in this configuration it has the one but highest elevation.



For the C1-code, the means are given in table 2.8, the empirical standard deviations in table 2.9. The error estimates $\hat{\nabla}$ are plotted as a time series in figure 2.8 for the code on the L1-frequency. Note that a different scaling is used for the Ashtech C1-code (figure 2.8a), its P1-histogram and the Leica time-series.

The mean of the error estimate-series per satellite is quite close to zero, for all receivers, except for the Leica SR399 (DW). Further analysis of the stochastic model can thus be based on 'clean' data; in general no severe anomalies (concerning the functional model) were encountered (e.g. a significant deviation of the mean from zero).

Figure 2.8a: Ashtech C1-code (C1)

The standard deviations are very small (2 cm) for the Ashtech (C1, with CA-code). Those for the Trimble 4000 SSI (DN) are in the range 10-20 cm, for the Turbo-Rogue SNR-8000 (DS) 15-35 cm and for the Ashtech with P1-code 20-65 cm. The dependence on the elevation is clear for all receivers, except for the Leica. The figures given and the dependence may be different when two antennas are used instead of one. In appendix B a brief description is given of the elevation dependence for the observation precision.

PRN	elevation		DN	empirical mean				
	k=1	k=601		DE	DW	DS	DE'	
23	18.7	15.3	0.01	0.00	-0.11	0.01	-0.01	
20	12.9	15.2	-0.01	0.00	-0.05	-0.01	0.01	
15	36.4	39.4	0.01	0.01	-0.08	-0.02	0.01	
21	55.3	51.6	-0.02	-0.01	0.15	0.04	-0.01	
25	44.2	49.1	0.01	0.00	0.03	-0.02	0.00	
01	67.2	63.4	-0.00	-0.01	0.07	0.01	-0.00	

* by P1 observations

Table 2.8: Empirical mean [m] of outlier estimates, C1-code

PRN	elevation		DN	empirical standard deviation				
	k=1	k=601		DE	DW	DS	DE'	
23	18.7	15.3	0.21	0.02	0.15	0.36	0.63	
20	12.9	15.2	0.20	0.02	0.12	0.33	0.60	
15	36.4	39.4	0.10	0.02	0.14	0.16	0.32	
21	55.3	51.6	0.09	0.02	0.18	0.13	0.24	
25	44.2	49.1	0.09	0.02	0.05	0.14	0.25	
01	67.2	63.4	0.09	0.02	0.11	0.13	0.20	

* by P1 observations

Table 2.9: Empirical standard deviation [m] of outlier estimates, C1-code

DN	PRN	01	15	25	23	20	21
C1	01	1.000	.178	.246	-.377	-.341	.149
	15		1.000	.162	-.353	-.337	.070
	25			1.000	-.338	-.366	.158
	23				1.000	-.371	-.352
	20					1.000	-.263
	21						1.000
DE'	PRN	01	15	25	23	20	21
P1	01	1.000	.219	.493	-.459	-.402	.556
	15		1.000	.038	-.354	-.300	.119
	25			1.000	-.406	-.332	.373
	23				1.000	-.382	-.402
	20					1.000	-.386
	21						1.000
DW	PRN	01	15	25	23	20	21
C1	01	1.000	-.222	.339	-.718	-.690	.498
	15		1.000	-.384	-.418	.053	-.873
	25			1.000	-.600	-.269	.476
	23				1.000	.224	-.676
	20					1.000	-.371
	21						1.000
DS	PRN	01	15	25	23	20	21
C1	01	1.000	.187	.243	-.430	-.286	.427
	15		1.000	.190	-.318	-.354	.134
	25			1.000	-.369	-.309	.241
	23				1.000	-.438	-.409
	20					1.000	-.287
	21						1.000

* by P1 observations

Table 2.10: Mutual channel (satellite) correlation, C1 code

Under the null-hypothesis the error estimator is normally distributed: $\hat{\nabla} \sim N(0, \sigma_{\hat{\nabla}}^2)$. In figure 2.8 also the histograms are given. For all receivers, except for the Leica, it holds that a normal distribution for the error estimator is not unlikely indeed.

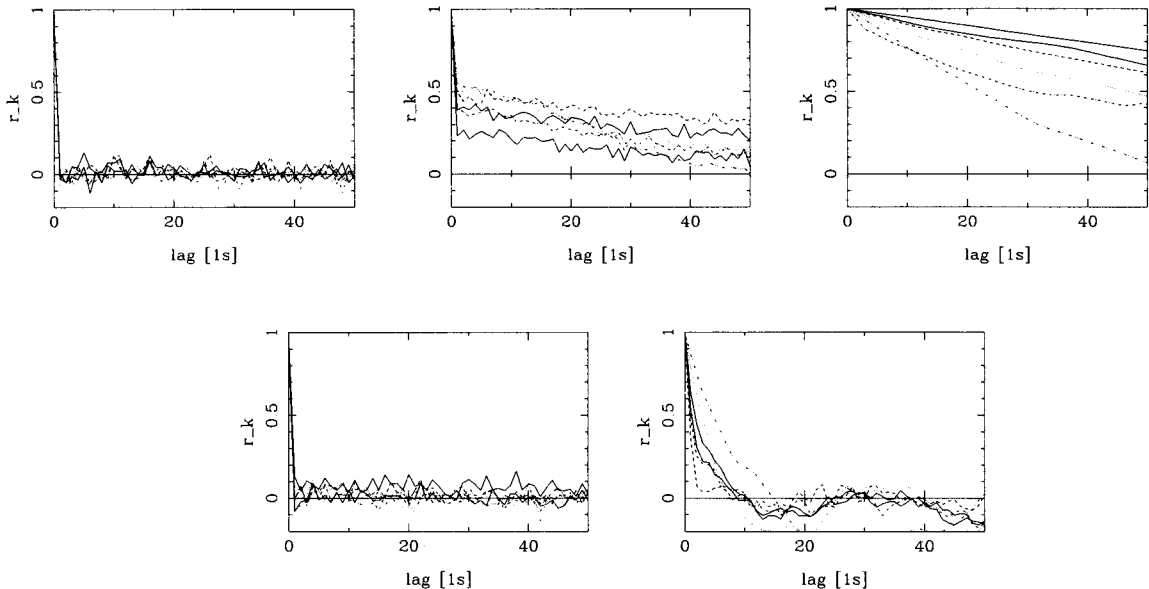


Figure 2.9: Correlograms C1-code: Trimble, Ashtech, Leica, Turbo-Rogue and Ashtech (P1)

For the outlier estimate series (601 samples), the cross-correlation between different satellites has been determined. This was done for the C1-code for all four receiver pairs, table 2.10. Zero mean was assumed. On the average the empirical correlation coefficients

agree on the formal $\rho = -1/5 = -0.200$. The spread is however quite large. It is interesting to note that all receivers, apart from the Leica (internal filtering), show identical behaviour with positive and negative correlation coefficients, e.g. $\rho_{01-25} > 0$ and $\rho_{15-23} < 0$; there are 6 positive and 9 negative ones. Correlation for pseudo-range (code) observations between satellites (spatial correlation) is suggested also in [Roberts et al, 1997].

Figure 2.9 gives the correlograms, see e.g. [Chatfield, 1989]: the auto-correlation-coefficients r_k versus lag k for the error estimates (all satellites), cf. figure 2.8. They were computed under the assumption of zero mean; see table 2.8 for the empirical means. $N=601$ samples were used. The epochs are spaced by 1 second.

If a time series is completely random (no time correlation), the coefficients r_k , for $k \geq 1$, will all be close to zero, taking into account the standard deviation of $\sigma_{r_k} \approx \frac{1}{\sqrt{N}} \approx 0.04$. The graphs for the Trimble and Turbo-Rogue do show such correlograms. For the other receivers, Ashtech and Leica, time correlation seems to be present.

For the C1-code of the Ashtech, the observed (positive) time correlation is thought to be caused by some averaging and/or carrier aiding to smooth the code observations. For the reconstructed P1-code observable, there is some time correlation, but it is less severe. The graphs for the Leica in figure 2.8, already made us suspect the worst. Note that the zero mean assumption does not hold for the Leica.

5.2.2.4 Analysis: P2-code

The data of UNAVCO 95 were collected under Anti-Spoofing. C1 code observations were obtained by CA-code correlation on L1. Code observations are made on L2, although the signal contains only the encrypted P-code. The Trimble and Turbo-Rogue use cross-correlation (the cross-correlation measurement technique is hypothesized in appendix C), the Leica uses P-code aided squaring and the Ashtech uses P-W tracking. The latter yields two code observations P1 and P2.

For the (reconstructed) code observation on the second frequency, referred to as P2, the error estimates \hat{V} are plotted as a time series in figure 2.10. Note that as compared with figure 2.8 in the previous section, the range for the y-axis has been doubled: now from -2.4 to +2.4 meter.

PRN	elevation		empirical mean			
	$k=1$	$k=601$	DN	DE	DW	DS
23	18.7	15.3	-0.11	-0.02	0.01	0.54
20	12.9	15.2	0.16	-0.02	-0.01	-0.91
15	36.4	39.4	-0.03	0.00	-0.03	0.11
21	55.3	51.6	-0.02	0.01	0.00	0.15
25	44.2	49.1	-0.01	0.01	0.01	0.04
01	67.2	63.4	0.01	0.02	0.02	0.07

Table 2.11: Empirical mean [m] of outlier estimates, P2 code

For the tables 2.11 and 2.12, beside the mean, also the empirical standard deviation has been determined for each series of \hat{V} (per satellite, over 601 samples).

The mean of the error estimate-series per satellite is close to zero, for the Ashtech and Leica. Note that for the Leica (DW), the deviations were somewhat larger for the C1-code, cf. table 2.8. The means for the Trimble (DN) are small as well; only the low

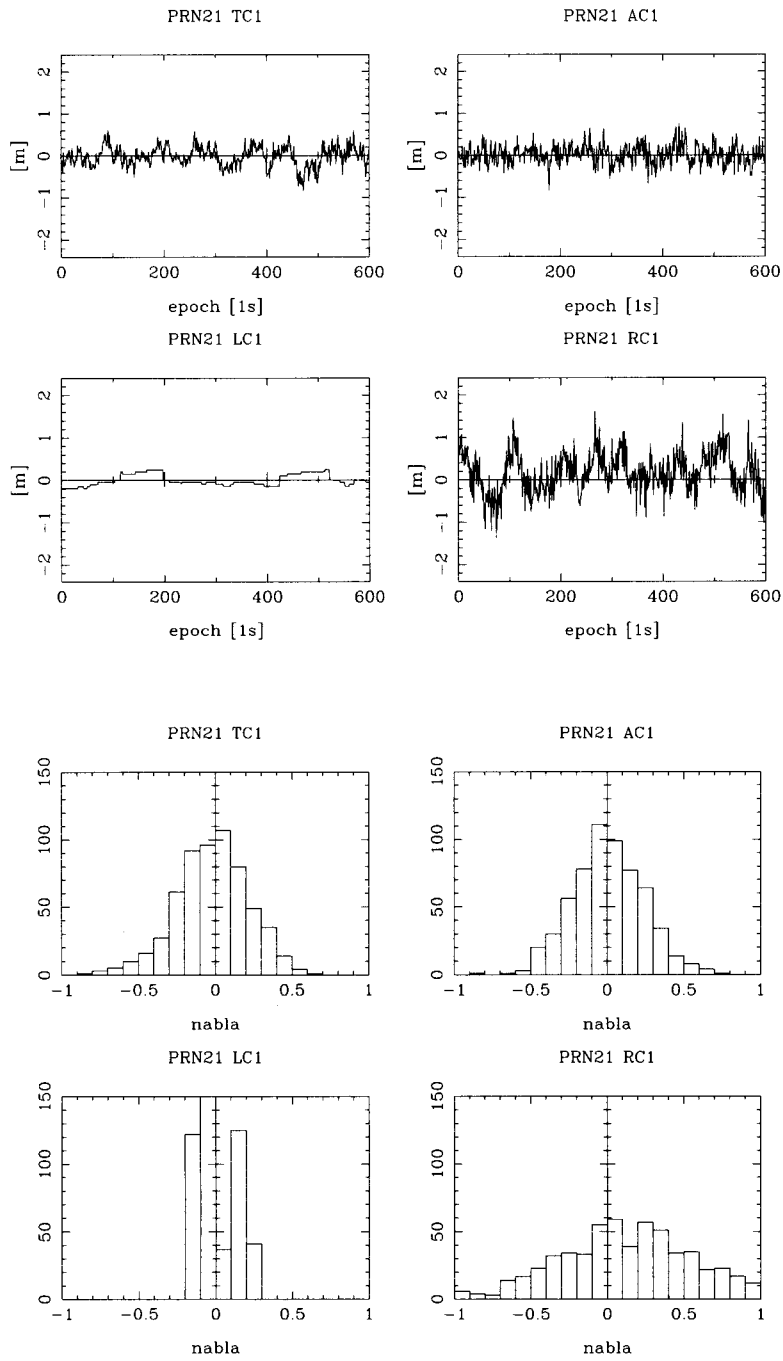


Figure 2.10: Error estimates for P2-code, Trimble, Ashtech, Leica and Turbo-Rogue satellite PRN 21

PRN	elevation		empirical standard deviation			
	k=1	k=601	DN	DE	DW	DS
23	18.7	15.3	0.73	0.63	0.11	1.80
20	12.9	15.2	0.85	0.55	0.13	2.15
15	36.4	39.4	0.27	0.32	0.12	0.62
21	55.3	51.6	0.24	0.23	0.13	0.50
25	44.2	49.1	0.24	0.25	0.12	0.52
01	67.2	63.4	0.24	0.20	0.12	0.48

Table 2.12: Empirical standard deviation [m] of outlier estimates, P2 code

PRN	elevation		correlation C1-P2 ρ			
	k=1	k=601	DN	DE	DW	DS
23	18.7	15.3	0.27	0.06	-0.08	0.29
20	12.9	15.2	0.18	0.09	-0.01	0.19
15	36.4	39.4	0.42	-0.04	0.19	0.25
21	55.3	51.6	0.34	-0.04	-0.20	0.29
25	44.2	49.1	0.32	-0.05	0.04	0.21
01	67.2	63.4	0.36	-0.03	0.34	0.30

Table 2.13: Empirical correlation outlier estimates C1 and P2

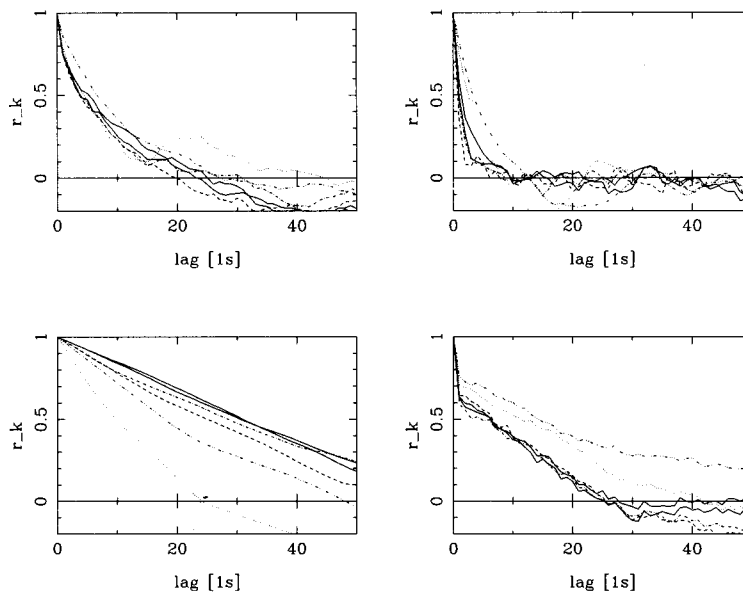


Figure 2.11: Correlograms P2-code: Trimble, Ashtech, Leica and Turbo-Rogue

elevation satellites PRNs 23 and 20 do show some larger deviation. The behaviour of the Turbo-Rogue is like the Trimble, but much worse.

The standard deviations are in the range 10-15 cm for the Leica SR 399 (DW); the same level as for the C1-observations, cf. table 2.9. Those for the Ashtech (DE) and Trimble (DN) are larger, in the range 20-65 cm and 25-85 cm respectively. For the Turbo-Rogue (DS) they are from 50 cm to over 200 cm for low elevation satellites. Note that the values for the Ashtech Z-12 (DE) look very much like those for P1 in table 2.9, column DE'. The standard deviations for the P2 of the Trimble 4000 SSI and Turbo-Rogue SNR-8000 are much larger than for the corresponding C1; as a rough indication we may give

$\sigma_{\bar{p}} \approx 3 \sigma_p$ for the Trimble and $\sigma_{\bar{p}} \approx 4 \sigma_p$ for the Turbo-Rogue. The dependence on the elevation is clear for all receivers, except for the Leica. For the cross-correlating receivers, Trimble and Turbo-Rogue, the elevation dependence seem to be somewhat stronger for the P2-observations than for the C1. The figures given and the dependence may be different when two antennas are used instead of one.

The error estimators \hat{V} for the C1 (P1) code and those for the P2 code are uncorrelated (null-hypothesis). The empirical correlation is determined. As expected, there is (positive) correlation between the C1 and P2 observations for the cross-correlation receivers: Trimble and Turbo-Rogue, see also appendix C. The correlation coefficient is about $\rho_{\bar{p}\bar{p}} \approx \frac{1}{3}$ for the Trimble (DN) and $\rho_{\bar{p}\bar{p}} \approx \frac{1}{4}$ for the Turbo-Rogue (DS). These values do not contradict the stochastic model hypothesized in appendix C, when the above indications are used $\sigma_{\bar{p}} \approx 3 \sigma_p$ for the Trimble and $\sigma_{\bar{p}} \approx 4 \sigma_p$ for the Turbo-Rogue. The correlation is very small for the Ashtech (we used P1 and P2 observations) and it varies but is not large for most satellites for the Leica.

Under the null-hypothesis the error estimator is normally distributed. In figure 2.10 also the histograms are given. For all receivers, except for the Leica, it holds that a normal distribution for the error estimator is not unlikely indeed. Note that compared with the C1-code histograms in figure 2.8, the range for the horizontal axis has been doubled in figure 2.10: now from -1.0 to +1.0 meter.

Figure 2.11 gives the correlograms, auto-correlation-coefficients r_k versus lag k , for the error estimates, cf. figure 2.10, for all satellites. If a time series is completely random (no time correlation), the coefficients r_k , for $k \geq 1$, will all be close to zero, taking into account the standard deviation of $\sigma_{r_k} \approx \frac{1}{\sqrt{k}} \approx 0.04$. In figure 2.11 there are no such correlograms. For all receivers, time correlation seems to be present. For the Ashtech, the correlation concerns about 10 seconds, some 20 seconds for the Trimble and slightly larger for the Turbo-Rogue. Note again that for the Ashtech, the behaviour of the P2-observations is very similar to the P1, cf. figure 2.9, and that the correlation coefficient $\rho_{\bar{p}\bar{p}}$ is very small, table 2.13.

5.2.2.5 Analysis: L1-phase

For model validation, slips in the (single difference) phase observations are considered. With local model validation however, a slip can not be distinguished from an outlier yet. The slip estimate equals the outlier estimate. The error estimates \hat{V} for the L1-phase are plotted as a time series in figure 2.12. The y-axis ranges from -0.02 to +0.02 cycles (\approx -/+ 4 millimeter). The error estimates were output at 0.001 cycle resolution.

The tables 2.14 and 2.15 give the mean and the empirical standard deviation, respectively. They have been determined for each series of \hat{V} (per satellite, over the full 601 samples). The mean and empirical standard deviation are expressed in milli-cycles (0.001 cycle \approx 0.2 millimeter).

The mean of the error estimate-series per satellite is close to zero, for the Trimble, Ashtech and Leica (less than 0.1 mm). The means for the Turbo-Rogue (DS) are somewhat larger. For the Turbo-Rogue, a long term variation can be observed in figure 2.12. This could be a receiver effect (hardware delay) or caused by multipath.

PRN	elevation		empirical mean			
	k=1	k=601	DN	DE	DW	DS
23	18.7	15.3	-0.1	0.2	0.1	2.1
20	12.9	15.2	0.3	-0.2	0.2	-0.6
15	36.4	39.4	0.0	-0.4	0.0	-0.9
21	55.3	51.6	0.1	-0.1	0.0	-0.7
25	44.2	49.1	-0.3	-0.0	-0.2	-0.8
01	67.2	63.4	0.0	0.4	-0.2	0.9

0.001 cycle = 0.2 mm

Table 2.14: Empirical mean [milli-cycle] of outlier estimates, L1 phase

PRN	elevation		empirical standard deviation			
	k=1	k=601	DN	DE	DW	DS
23	18.7	15.3	2.4	3.6	3.5	6.2
20	12.9	15.2	2.1	3.9	3.5	5.4
15	36.4	39.4	1.5	1.9	2.4	2.4
21	55.3	51.6	1.4	1.7	2.3	5.5
25	44.2	49.1	1.5	1.8	2.2	3.9
01	67.2	63.4	1.5	1.6	2.4	2.5

0.001 cycle = 0.2 mm

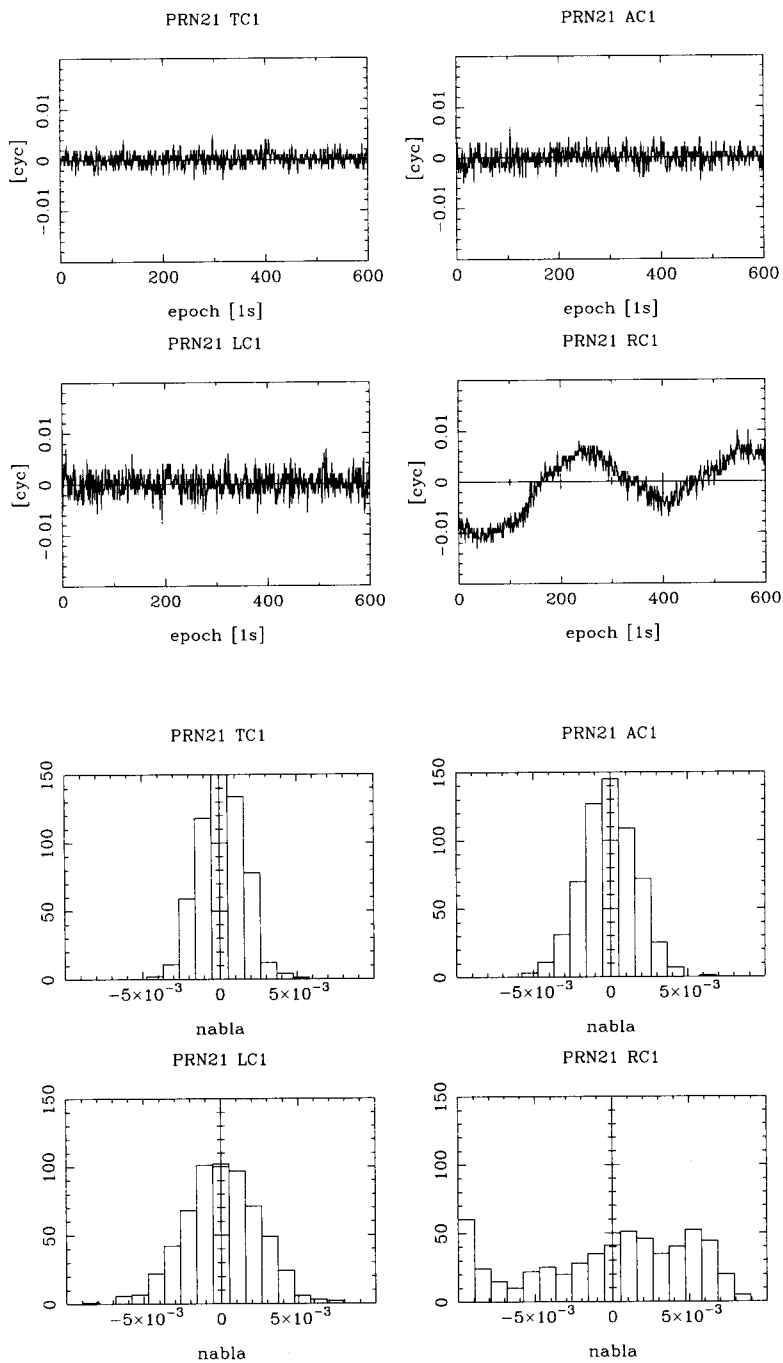
Table 2.15: Empirical standard deviation [milli-cycle] outlier estimates, L1

DN	PRN	01	15	25	23	20	21
L1	01	1.000	-.033	-.083	-.289	-.260	-.044
	15		1.000	.025	-.347	-.164	-.125
	25			1.000	-.273	-.251	-.121
	23				1.000	-.355	-.182
	20					1.000	-.193
	21						1.000
DE	PRN	01	15	25	23	20	21
L1	01	1.000	.130	.203	-.281	-.400	.215
	15		1.000	.183	-.327	-.370	.149
	25			1.000	-.373	-.354	.161
	23				1.000	-.337	-.319
	20					1.000	-.375
	21						1.000
DW	PRN	01	15	25	23	20	21
L1	01	1.000	-.055	-.059	-.262	-.284	-.080
	15		1.000	-.073	-.280	-.290	-.045
	25			1.000	-.253	-.234	-.066
	23				1.000	-.292	-.270
	20					1.000	-.235
	21						1.000
DS	PRN	01	15	25	23	20	21
L1	01	1.000	-.509	.131	.234	-.202	-.394
	15		1.000	-.312	-.520	.442	.186
	25			1.000	.563	-.645	-.629
	23				1.000	-.785	-.627
	20					1.000	.257
	21						1.000

Table 2.16: Mutual channel (satellite correlation), L1 phase

The standard deviations are in the range 0.3-0.7 mm for the Trimble, Ashtech and Leica; those for the Turbo-Rogue are larger, up to 1.2 mm. The dependence on the elevation is clear for all receivers, except the Turbo-Rogue). The figures given and the dependence may be different when two antennas are used instead of one.

Under the null-hypothesis the error estimator is normally distributed. In figure 2.12 also the histograms are given. For all receivers, except for the Turbo-Rogue, it holds that a normal distribution for the error estimator is not unlikely indeed. The range for the horizontal axis is from -0.01 to +0.01 cycle (\approx +/-2 mm).



0.01 cycle \approx 2 mm

Figure 2.12 Error estimates for L1-phase, Trimble, Ashtech, Leica and Turbo-Rogue satellite PRN 21

For the outlier estimate series, the cross-correlation between different satellites has been determined, table 2.16. This has been done for the L1-phase observations, for all four receiver-pairs. Zero mean was assumed.

The pattern found with C1(P1) code observations in section 5.2.2.3, shows up again for the L1 phase observations for the Ashtech. Also for the Trimble and Leica it seems present, although the positive values have become small negative ones. For these three receivers holds that the large negative coefficients all belong to the satellites PRN 20 and 23. The formal coefficient is $\rho = -1/5 = -0.200$. The agreement of the empirical coefficients is better (than with the code observations). The spread is small for the Leica and Trimble.

The observed behaviour can make one question about the diagonal structure of the variance covariance matrix of the undifferenced (or single differenced) observables per observation type. Further investigations are needed.

PRN	elevation		DN	correlation C1-L1 ρ		
	k=1	k=601		DE'	DW	DS
23	18.7	15.3	0.04	-0.03	-0.05	0.03
20	12.9	15.2	0.01	-0.03	0.00	0.03
15	36.4	39.4	0.03	-0.04	0.06	0.03
21	55.3	51.6	0.00	0.01	-0.01	0.03
25	44.2	49.1	-0.08	-0.01	-0.12	0.07
01	67.2	63.4	0.11	-0.06	-0.02	0.01

* by P1 observations

Table 2.17: Empirical correlation outlier estimates C1 and L1

Correlation between code C1 (P1 for Ashtech) and phase L1 has also been considered; it is practically absent in the data of all four receivers, see also the discussion in [Eissfeller, 1997]. The correlation coefficients ρ , expected to be zero, are given in table 2.17.

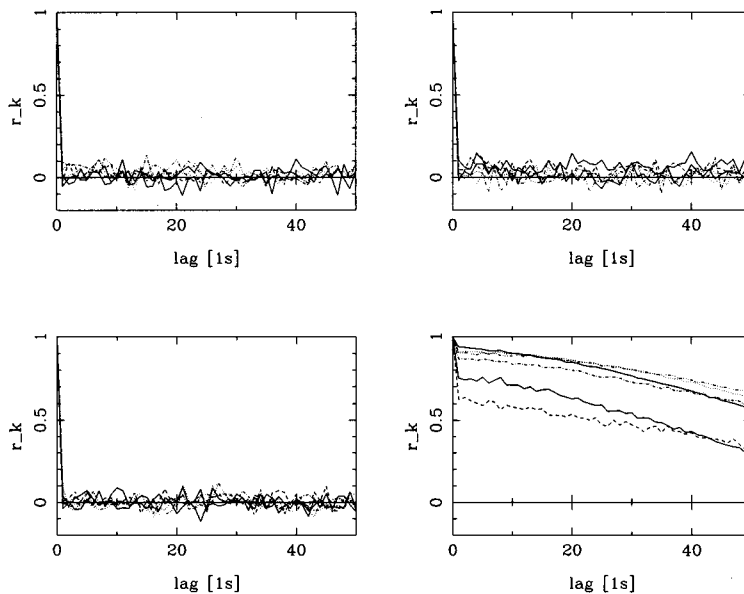


Figure 2.13: Correlograms L1-phase: Trimble, Ashtech, Leica and Turbo-Rogue

Figure 2.13 gives the correlograms, auto-correlation-coefficients r_k versus lag k , for the error estimates, cf. figure 2.12, for all satellites. In figure 2.13, the Trimble, Ashtech and Leica do show 'no time-correlation' correlograms. For the Turbo-Rogue time correlation could be expected already, due to the long term variation in figure 2.12.

From this analysis on L1 phase observations, it can be concluded that the Trimble 4000 SSI, the Ashtech Z-XII and the Leica SR399 perform equally well. As opposed to the code observations (sections 5.2.2.3 and 5.2.2.4), the phase observations of the Leica seem to result from raw measurements indeed.

5.2.2.6 Analysis: L2-phase

The UNAVCO 95 data were collected under Anti-Spoofing. Phase observations are made on L2, although the signal contains only the encrypted P-code. All four receivers provide full wavelength L2 phase observations: the Trimble and Turbo-Rogue use cross-correlation, the Leica P-code aided squaring (with polarity determination) and the Ashtech P-W tracking. The reconstructed phase observation on the second frequency is referred to as L2.

PRN	elevation		empirical mean			
	k=1	k=601	DN	DE	DW	DS
23	18.7	15.3	1.5	0.8	-0.0	1.5
20	12.9	15.2	1.9	-0.1	-0.4	-4.8
15	36.4	39.4	-0.8	-0.7	0.2	-0.3
21	55.3	51.6	-0.8	-0.2	0.2	0.8
25	44.2	49.1	-1.1	-0.1	-0.2	0.9
01	67.2	63.4	-0.8	0.2	0.1	2.0

0.001 cycle = 0.2 mm

Table 2.18: Empirical mean [milli-cycle] of outlier estimates, L2 phase

PRN	elevation		empirical standard deviation			
	k=1	k=601	DN	DE	DW	DS
23	18.7	15.3	9.4	6.3	9.3	72.1
20	12.9	15.2	10.3	5.5	11.4	78.5
15	36.4	39.4	4.0	3.2	5.2	23.6
21	55.3	51.6	3.4	2.5	4.7	22.9
25	44.2	49.1	3.4	2.5	5.8	23.2
01	67.2	63.4	3.4	2.2	4.9	22.1

0.001 cycle = 0.2 mm

Table 2.19: Empirical standard deviation [milli-cycle] outlier estimates, L2

The error (outlier=slip) estimates \hat{V} are plotted as a time series in figure 2.14. The y-axis ranges from -0.04 to +0.04 cycles (\approx -/+10 millimeter) and -0.4 to +0.4 cycles (\approx -/+10 centimeter) for the Turbo-Rogue. The error estimates were output at 0.001 cycle resolution.

The tables 2.18, 2.19 and 2.20 give the mean, the empirical standard deviation and the correlation between L1 and L2, respectively. They have been determined for each series of \hat{V} (per satellite, over 601 samples). The mean and empirical standard deviation are expressed in milli-cycles (0.001 cycle \approx 0.2 millimeter).

The mean of the error estimate-series per satellite is close to zero, for the Ashtech and Leica (less than 0.2 mm). The deviations are a bit larger for the Trimble, in particular for the two low elevation satellites. The Turbo-Rogue is much worse.

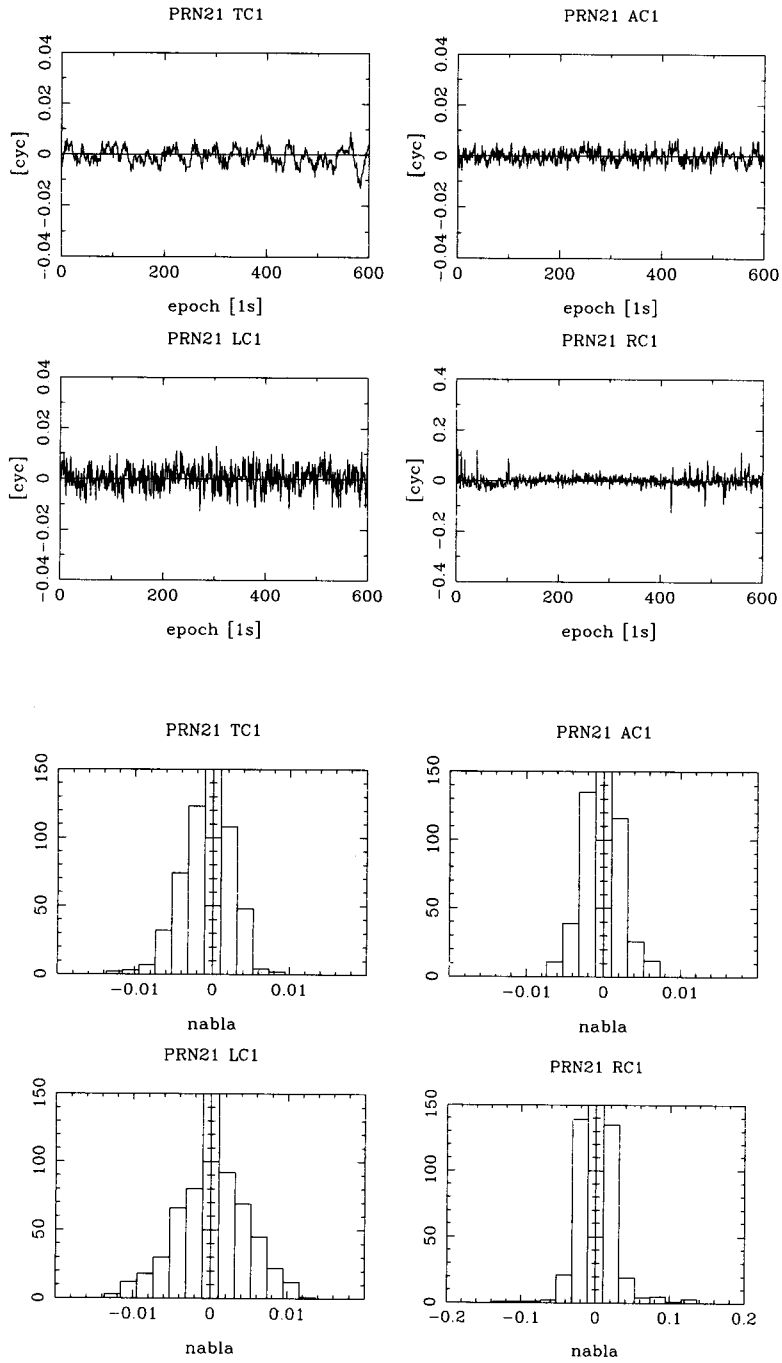


Figure 2.14: Error estimates for L2-phase, Trimble, Ashtech, Leica and Turbo-Rogue satellite PRN 21

PRN	elevation		DN	correlation L1-L2 ρ		
	k=1	k=601		DE	DW	DS
23	18.7	15.3	0.19	0.44	0.27	0.10
20	12.9	15.2	0.21	0.54	0.28	0.06
15	36.4	39.4	0.25	0.40	0.35	0.01
21	55.3	51.6	0.25	0.48	0.36	0.17
25	44.2	49.1	0.30	0.51	0.20	0.15
01	67.2	63.4	0.19	0.44	0.38	0.13

Table 2.20: Empirical correlation of outlier estimates, L1 and L2 phase

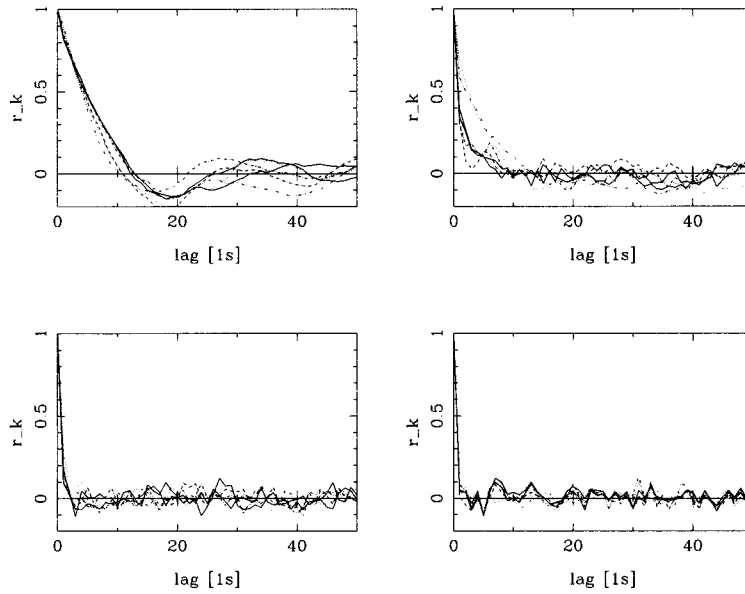


Figure 2.15: Correlograms L2-phase: Trimble, Ashtech, Leica and Turbo-Rogue

For the higher elevation satellites, the standard deviation is about 0.6 mm for the Ashtech, 0.9 mm for the Trimble, 1.3 mm for the Leica and 5.6 mm for the Turbo-Rogue. The standard deviations in table 2.19 are larger than with the L1 phase observations, cf. table 2.15. For the Ashtech we have $\sigma_{\bar{p}} \approx 2\sigma_p$, for the Trimble and Leica $\sigma_{\bar{p}} \approx 3\sigma_p$, and $\sigma_{\bar{p}} \approx 8\sigma_p$ for the Turbo-Rogue. The dependence on the elevation is clearly stronger on L2 than on L1 for all receivers, except for the Ashtech. The figures given and the dependence may be different when two antennas are used instead of one.

The error estimators $\hat{\nabla}$ for L1 and L2 are uncorrelated (null-hypothesis). The empirical correlation has been determined. For all receivers, it holds that there is a positive correlation between the phase observables L1 and L2. It is largest for the Ashtech, about 0.5 (which indicates that, concerning the L2 phase observation, Ashtech’s P-W tracking is based also on cross-correlation), moderate for the Leica and Trimble and small for the Turbo-Rogue. With the reconstruction by cross-correlation, hypothesized in appendix C, and $\sigma_{\bar{p}} \approx 3\sigma_p$ for the Trimble, we expect $\rho=0.43$. The values in table 2.20 are smaller (between 0.2 and 0.3). Based on $\sigma_{\bar{p}} \approx 8\sigma_p$ we expect $\rho=0.16$ for the Turbo-Rogue.

In figure 2.14 the histograms for the error estimates are given. For all receivers, it holds that a normal distribution for the error estimator is not unlikely indeed. The range for the

horizontal axis is from -0.02 to +0.02 cycle (\approx \pm 5 mm) and from -0.2 to +0.2 cycle (\approx \pm 5 cm) for the Turbo-Rogue.

Figure 2.15 gives the correlograms for the error estimates. Time correlation is practically absent for the Leica and Turbo-Rogue. For the Ashtech the time correlation concerns about 10 seconds, and some 20 seconds for the Trimble.

5.2.2.7 Short baseline

In this section, the data measured on a short baseline (3 meter; both receivers static) are used, for analysis of receiver performance. Usually a zero baseline is measured for this purpose: two receivers are connected to *one* antenna (with *one* low-noise-amplifier). For a short baseline, each receiver is connected to its own antenna; thus two receivers and two antennas (of the same make and type). The receivers are operated like in a typical high accuracy (stationary) GPS surveying application. This experiment and analysis is meant to see whether and how, for one of the receiver pairs, the zero baseline results transfer to a short baseline.

First a description of the experiment is given, then the results and analysis, it parallels the one for the zero baselines of the previous sections. The section ends with a discussion of the results.

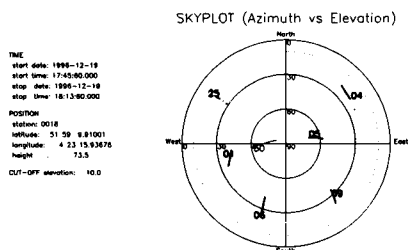


Figure 2.16: Skyplot at 18, for short baseline, Delft, The Netherlands

```

number of satellites: 7 (all Block IIA)
PRNs: 01 04 05 06 09 25 30
pivot: 30 (double differencing)
number of receivers: 2 (stationary)
receiver type: Trimble 4000SSI Geodetic Surveyor
antenna type: Trimble Geodetic Compact L1/L2 with groundplane
               the antennas were equally oriented (and levelled)
date: December 19th, 1996 (GPS week 884; day 354)

observation session: -1 hour
start: 17:30:04 GPS ; 408604 seconds in GPS week
end: 18:29:59 GPS ; 412199 seconds in GPS week
sampling interval: 1 second

processing session: 28 minutes (1681 epochs)
start: 17:46:00 GPS ; 409560 seconds
end: 18:14:00 GPS ; 411240 seconds
sampling interval: 1 second * GPS = UTC + n [s] with n=11

coordinates of marker #18 X = 3924689.291 m
(reference receiver r1): Y = 301145.322 m
in WGS84 Z = 5001908.641 m

```

experiment description

The data were collected on the observation platform on top of the Department's building in Delft, with the Trimble 4000 receivers, after they had been upgraded to SSIs. They provide dual frequency pseudo-range data and full wavelength carrier phases under both A/S and non A/S conditions.

A skyplot for the processing session is given in figure 2.16. One channel of receiver r1 was malfunctioning and did therefore not track satellite PRN24; it has been left out. The elevation cut-off was 10°. The receivers occupied the markers #18 and #19; a 3 meter baseline.

results and analysis

For the error analysis, the baseline coordinates have been determined very precisely and are treated as deterministically known. Although the baselinelength is not zero, it is very short and differential propagation delays will be minimal and so are the effects of satellite position and reference receiver coordinates. The short baseline, in addition to the zero baseline, enables us to assess the geodetic performance of the receiver pair. With the short baseline, the performance of the *full* system, thus antennas, amplifiers, cables and receivers, is assessed under true operational conditions.

- reference solution

The coordinates for receiver r2 were obtained from the L1-phase reference solution over a 28 minutes period. The ambiguities were constrained. A sequential adjustment was made for the coordinates (stationary receiver). With $m=7$ satellites, 7 observations per receiver yields $(m-1)=6$ double difference observations per epoch. 1681 epochs of data are used at 1 second interval.

The estimated coordinates of marker #19 are:

```
X = 3924691.0402 m
Y = 301143.2502 m
Z = 5001907.4010 m
```

and this yields a baseline length of 2.982 m between the markers #18 and #19. The formal precision of the coordinate-estimators (expressed in NEH) is $\sigma_N=0.08$, $\sigma_E=0.07$, $\sigma_H=0.18$ mm. This description is probably too optimistic.

PRN	elev. k=301	empirical mean			
		C1	P2	L1	L2
25	19.5	0.07	0.12	-4.5	-0.6
04	22.4	0.06	-0.11	4.3	-5.0
06	30.1	-0.04	-0.31	-9.8	12.5
09	32.2	0.00	0.14	5.4	0.5
01	41.8	0.02	-0.01	4.9	5.2
05	67.7	-0.05	0.12	-0.1	-9.8
30	71.2	-0.07	0.05	-0.2	-3.0

Table 2.21: Empirical mean of error estimates in [m] for code, in [millicycle] for phase; 1 millicycle \approx 0.2 mm

PRN	elev. k=301	empirical standard deviation			
		C1	P2	L1	L2
25	19.5	0.32	0.70	7.7	14.7
04	22.4	0.31	0.83	9.7	11.7
06	30.1	0.27	0.51	12.6	14.9
09	32.2	0.23	0.37	8.1	6.4
01	41.8	0.18	0.28	6.4	7.4
05	67.7	0.17	0.31	5.7	10.6
30	71.2	0.18	0.25	4.2	5.3

Table 2.22: Empirical standard deviation of error estimates in [m] for code, in [millicycle] for phase; 1 millicycle \approx 0.2 mm

- error analysis

The four observation types (code on L1 and L2 and phase on L1 and L2) are processed individually. In terms of a single difference model, the coordinates are constrained for this error analysis and, in case of L1 and L2 phase data, the ambiguities too. The (differential) receiver clock error is free (one new unknown per epoch). The redundancy per epoch equals $m-n=6$. Per epoch $m=7$ error estimators are computed, based on $m-n=6$ residuals. For the error analysis we consider on epoch basis, thus local model

validation, errors in the (single difference) observations (per satellite): outliers in the code-observations C1 and P2 and slips (=outliers) in the phase observations L1 and L2. Adaptation was disabled. The standard deviation for the undifferenced code observable was taken $\sigma_p = \sigma_{\bar{p}} = 0.3$ meter and for the phase $\sigma_p = \sigma_{\bar{p}} = 0.003$ meter.

For this analysis, again 10 minutes of data were used (601 epochs), to facilitate comparison to the previous sections. The period is 17:46:00-17:56:00 (or in seconds 409560-410160) at one second interval.

For the tables 2.21, 2.22 and 2.23, the mean, the empirical standard deviation and the correlation have been determined for each series of \hat{V} (per satellite, over the full session). The satellites were sorted after increasing elevation (given in 360° degrees for epoch 17:51, $k=301$).

From table 2.21 it can be seen that the deviations of the mean from zero, are quite large for the P2 code observations. This was also the case for the low elevation satellites PRNs 23 and 20 in table 2.11. For the C1 code, the deviations are not really significant. The deviations for the phase observations L1 and L2 are up to 10 times larger than for the zero baseline, tables 2.14 and 2.18. The deviations now reach the 0.01 cycle, which corresponds to about 2 mm.

The (formal) standard deviations (on all channels) are constant (in time) and equal $\sigma_{\hat{v}} \approx 0.46$ m for the codes both C1 and P2, $\sigma_{\hat{v}} \approx 24.1$ millicycle for L1 and $\sigma_{\hat{v}} \approx 18.8$ millicycle for L2. The empirical standard deviations for the error estimates are in the range 15-30 cm for C1, 25-85 cm for P2, 0.8-2.5 mm for L1 and 1.2-3.7 mm for L2. The standard deviations for the codes C1 and P2 are at the same level as for the zero baseline. For the phases L1 and L2, the standard deviations are larger, in particular for the L1.

The Trimble 4000 SSI is a cross-correlating receiver and as shown in the previous sections, positive correlation is present between the observables on L1 and L2. The empirical correlation between the error estimates \hat{V} on both frequencies is determined both for code and phase, see table 2.23. For the codes it holds that the correlation is slightly larger than found for the zero baseline. For the phases there are some disturbances here (e.g. $\rho < 0$).

PRN	elev. $k=301$	emp. correlation C1-P2	L1-L2
25	19.5	0.40	0.14
04	22.4	0.28	0.08
06	30.1	0.48	-0.52
09	32.2	0.47	0.25
01	41.8	0.61	0.68
05	67.7	0.26	-0.00
30	71.2	0.50	0.30

Table 2.23: Empirical correlation of error estimates

Per observation type, the error estimates \hat{V} are plotted in figures 2.17 for one satellite, PRN01, at reasonable elevation; the estimates as time series are on top and the histograms at bottom. The estimates for the codes C1 and P2 are expressed in meters. For the C1-code the vertical axis ranges from -1.2 m to +1.2 m and the horizontal axis from -0.5 m to +0.5 m. For the P2-code these scales are doubled. For the L1-phase, the vertical axis ranges from -0.02 cycle to +0.02 cycle (thus over ~ 8 mm) and the horizontal axis from -0.01 cycle to +0.01 cycle. For the L2-phase these scales are doubled. The same scalings were used for the zero baselines, figures 2.8, 2.10, 2.12 and 2.14.

Under the null-hypothesis $\hat{V} \sim N(0, \sigma_{\hat{v}}^2)$. Figure 2.17 gives the histograms. In most figures for the codes C1 and P2, the normal distribution can be recognized. The histograms for

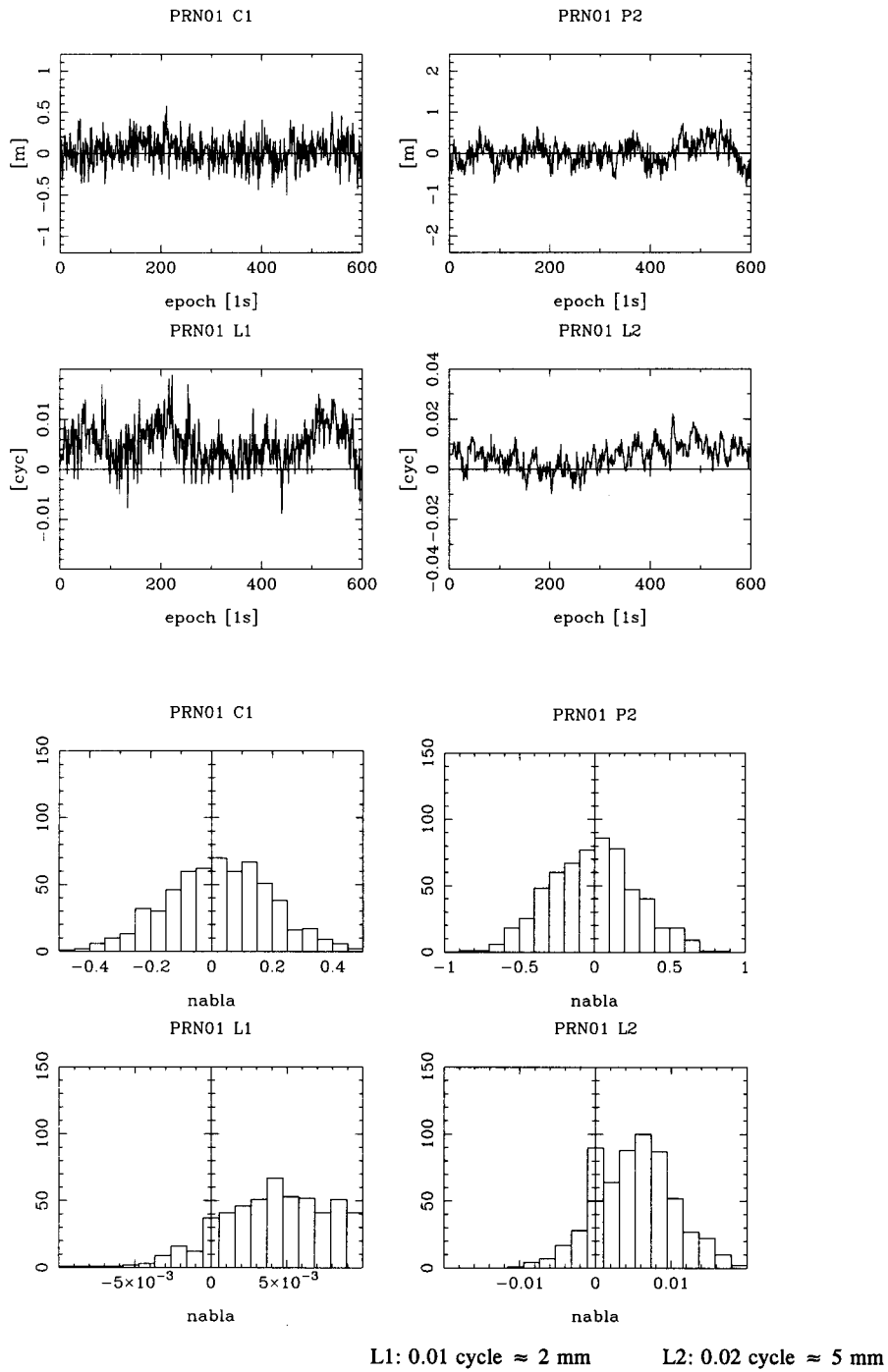


Figure 2.17: Error estimates for satellite PRN01; code C1, code P2, phase L1 and phase L2

the L1 phase seem disturbed and some of those for the L2 phase are offset. Some systematic effect is thought to be present.

- discussion

Compared with the zero baseline, the characteristics of especially the phase observables are different for this 3 meter baseline: deviations of the mean, larger standard deviations and time correlation in particular for the phase observations. Noise involved in making GPS code and phase observations can originate from different sources; there are the satellite's transmission, the sky, the ground and environment (objects in the vicinity of the antenna) and the receiving system itself, see the discussion in [Langley, 1997]. Beside 'true' noise, also functionally unmodelled effects can be present.

The cause can here be instrumental as well as lie in the fact that now two (antenna) locations are involved instead of one. On the instrumental side, the amplifier is suspected, as now two are used instead of one (common), see also [Nolan et al, 1992]. Environmental effects may be different at the two sites, even when they are close together. This holds in particular for multipath, the principal suspect. The antennas were on top of the building with no obstruction at positive elevation angle. Signals reflected by the roof and its sidewalls may however, reach the antenna from below and though affect the measurements. The location is not a favourable one. For multipath by reflection from below (ground bounce) see the discussion in [Weill, 1997]. A second environmental effect is the atmospheric delay, to be further divided into tropospheric and ionospheric. Concerning the latter, it should be remarked that the magnitude of the delay is small (~ 3 meter zenith delay). Short term (both in space and time) irregularities in the delay (scintillation, which can also effect the signal) can not be excluded, as the measurements took place in the early evening, about two hours after sunset.

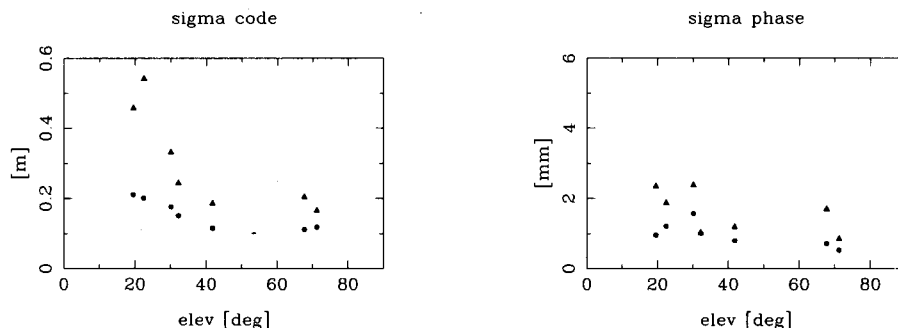


Figure 2.18: Standard deviation versus elevation angle
left: code • C1 and ▲ P2 right: phase • L1 ▲ L2

The empirical standard deviations in table 2.22 are graphically presented in figure 2.18. For this figure, they have been normalized to the standard deviation of the undifferenced observable. The standard deviation in figure 2.18 is given as function of the elevation angle. In particular the standard deviation of the P2 code observable shows a strong dependence. The a-priori assumed values are $\sigma_p = \sigma_{\bar{p}} = 0.3$ m and $\sigma_p = \sigma_{\bar{p}} = 3$ mm.

In this experiment (and also for the zero baselines), two identical receivers and antennas were used (same make and model). All results are obtained with an a-priori stochastic model, in which it is assumed that the observables of both receivers possess identical

stochastic behaviour, for instance $\sigma_{p r1} = \sigma_{p r2}$. The null-hypothesis furthermore prescribes equal standard deviation (over all epochs) on all channels for the observation type at hand and no mutual nor time correlation (for the undifferenced observables).

conclusion

We have assessed the performance of the full measurement system, two receivers with two antennas, under operational conditions, or in other words, the performance in the field. This short baseline is just one trial. It must be kept in mind that the conditions, e.g. concerning multipath, may greatly vary from one location to the other, see also the discussion in [Weill, 1997].

5.2.3 Summary

A rigorous application of the model validation in the processing of the data from a known short (or zero) baseline, provides the opportunity of a powerful analysis of the GPS code and phase observables. The different geodetic receivers employ different measurement techniques to provide dual frequency phase and code observations and this is directly reflected in different stochastic properties of their observables, which were clearly revealed. In this summary only main findings will be given. A direct comparison of the various receivers in respect of GPS surveying, is not made as many more aspects are then involved.

From the results, it can be concluded that in principle, a geodetic GPS receiver together with its antenna, is capable of providing raw data, code and phase observables, apparently normally distributed, with no (or only little) time correlation (the normal-distribution assumption was 'checked' only by graphical inspection).

Dependent on the measurement technique employed by the receiver, the noise characteristics can be different for the observables on the two frequencies, thus code C1 and P2 and phase L1 and L2. Apart from the measurement technique, the noise turned out to be a function of the elevation angle, under which the satellite is observed. The standard deviation of an observable is small for a zenith satellite, and increases as the elevation decreases, see appendix B for a discussion of the effect. The dependence may differ for different observation types.

The default stochastic model, specified by $\sigma=0.3$ m for the code and $\sigma=3$ mm for the phase (both undifferenced), is a conservative one; nowadays receivers can do better.

recommendation: tune stochastic model

For precise relative GPS positioning (surveying/navigation), it is important to get to know the receivers (and their antennas) before the units are used in the field for production work (and maybe, even before purchasing the receivers). The mathematical model, functional and stochastic, to be used in later data processing should be adequate. Estimation and model validation results are based on this model. The estimates should be unbiased and the quality description must be realistic.

The data should be examined on systematic effects, not captured by the current functional model. In particular with the zero baselines, the purpose was to model *receiver* noise (not the noise when additional, unmodelled effects are present). The simple stochastic model (scaled unit matrix for the variance covariance matrix per (undifferenced) observation type) most likely needs to be refined: it should take into account elevation dependence

and (if appropriate) cross-correlation. Indications were given for these first steps. Further refinements, via a more rigorous approach, may be needed, e.g. mutual channel/satellite correlation.

The mathematical model was developed in chapter 3. Symbolically it reads $E\{\mathbf{y}\} = A\mathbf{x}$; $D\{\mathbf{y}\} = Q_y$. It was thus assumed that both functional and stochastic model were completely known and hence, could be fully specified. The results in this section indicated that the current simple stochastic model should be refined. It could be that unknown parameters x_s are involved $D\{\mathbf{y}\} = Q_y(x_s)$. These parameters x_s should be solved for during the data processing or may be recovered from an a-priori calibration. The first approach could be referred to as in the field calibration (permanent); components of the stochastic model are estimated directly from the data. Equivalently to functional model validation, alternative hypotheses could be set up; the data then decide which model to use.

recommendation: receiver calibration

For the second approach it is recommended to 'calibrate' the receiver-pair by both a *zero* baseline test and a (known) *short* baseline test. These tests should be run at a high sampling rate (e.g. 1 second).

For a zero baseline only one antenna (with one amplifier) is used. The signal is then split over two receivers. The baseline is physically (0,0,0). This constraint (deterministically known) is applied in the subsequent data processing and thereby allows a very powerful analysis. The zero baseline can be used to check on receiver defects. The functional model commonly used in relative positioning is applicable and assumes e.g. no inter-channel biases. The analysis also allows for setting the stochastic model for the receiver at hand. Different receivers namely use different measurement techniques and each antenna type has its own gain pattern, which is of direct influence on the relation between elevation and measurement noise. The observation noise (standard deviation) can be quantified, the stochastic distribution of the observable can be revealed together with time correlation and mutual correlation (e.g. between observation types).

For the short baseline, 'short' means a few meters, so that the differential atmospheric delays are still zero. This test may lead to some tuning of the findings of the zero baseline test. For both tests it holds that they should be run under representative conditions, thus representative atmosphere and configuration (a satellite geometry with both high and low elevation satellites) and, for the short baseline, on a representative location (multipath); the two receivers with two antennas should be set up as under true operational conditions.

The need for such a calibration stems from the fact that GPS equipment manufacturers usually do not reveal all details and that the properties may vary with changing circumstances. It is suggested to carry out the calibration on a regular basis (circumstances may change such as atmospheric (ionospheric) conditions and new satellites) and whenever modifications to the equipment are made (e.g. upgrade; the stochastics may depend for instance on how the internal receiver software is configured).

In this section, receiver calibration was carried out by means of a zero and a short receiver baseline. Concerning the zero baseline, it should be noted that it is not necessarily observed with static receivers. A zero baseline can be measured also on a moving vehicle, in order to infer the impact of kinematics on the receiver noise in code and phase (kinematic zero baseline). Single receiver analysis is, in principle also possible, when

5.3.1 Experiment description

Four geodetic dual frequency receivers were out in the Flevopolder. The measurements took place on the Oostvaardersdijk from Almere to Lelystad, along the Markermeer. Two receivers were placed stationary on parking-lots, about 12.7 km apart, figure 3.1. The

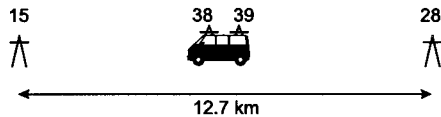


Figure 3.1: Flevo 96 local network; 4 receivers

kinematic part of the experiment was carried out with the Department's VW-van. Two receivers were inside the van; their antennas were rigidly mounted on a wooden bar, which was attached to the roof of the van (in the middle; lengthwise).

In this section a major part of the first one-hour session, at one second sampling rate, is used. The skyplot is given in figure 3.2. The survey starts static, then the van is driven on the dike at about 40 km/h (a two-way trip, with a static period at the turning point) and finally the survey ends static.

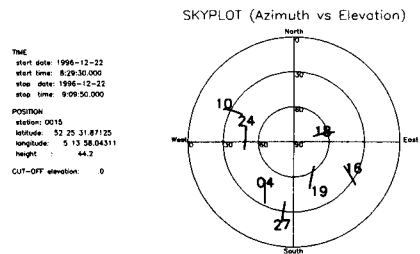


Figure 3.2: Skyplot at 15 for Flevo 96

The circumstances during the experiment concerned typical weather for this season of the year: temperature -4° C, open sky, pressure 1020 hPa, relative humidity about 70% and a strong wind blowing from the North-East. The Sun Spot Number was low, about 20-30; the (absolute) ionospheric delay was small.

5.3.2 Results and analysis

The purpose of relative positioning is to estimate the coordinates of the second receiver with respect to those of the first one r1. With kinematic surveying the second receiver can be in motion. For this kinematic GPS experiment, an analysis on quality of the measurement system is given in the second section. The sections 3 and 4 then concern practical results on positioning and ambiguity resolution, respectively. The last section discusses the limitations of the current mathematical model. We start off in the first section with a brief side step on single point positioning.

5.3.2.1 Single point positioning

For the two stationary receivers we will first have a look at the single point solutions. They were determined on single epoch basis with the CA-code observations. The standard deviation was taken $\sigma=20.6$ m. For these reference stations 15 and 28, reference coordinates are available. The coordinate estimates obtained were differenced with these reference values and then expressed in local North, East and Height. In figure 3.3 the scatters of the 2421 position estimates are given for the horizontal coordinates North and East. Note that for both stations the signature is very similar, it is the SA-effect.

The receiver clock error estimates are given in the figure 3.4 (expressed in meters). The vertical axis represents 7×10^5 m for station 15 and 2×10^5 m for station 28. The drift of the oscillator at 15 is about 0.8×10^{-6} s/s (the typical drift of a quartz-oscillator).

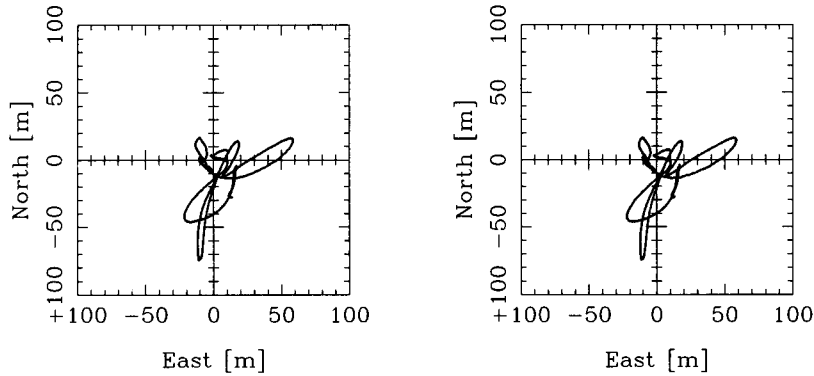
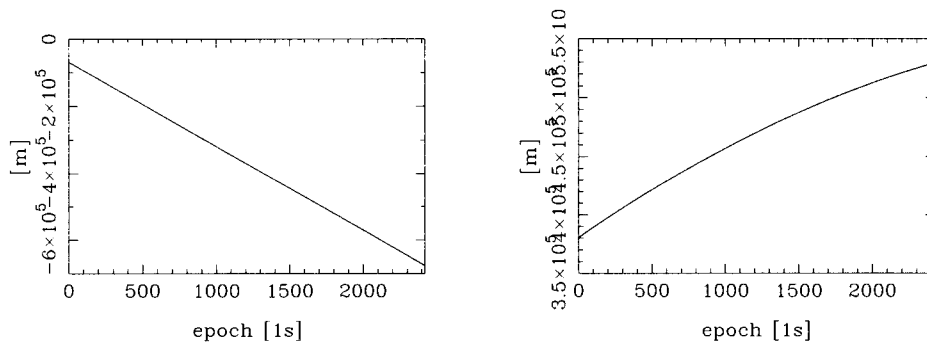


Figure 3.3: Single point positioning, station 15 left, station 28 right

Figure 3.4: Receiver clock error $c\delta t$, station 15 left, station 28 right

5.3.2.2 Quality: precision and reliability

The purpose of relative positioning is to estimate the coordinates of the rover with respect to those of the reference. The rover may be stationary or in (permanent) motion, full kinematic. There is one coordinate-triplet in the first case and three new coordinate unknowns are introduced for each epoch in the second case. If carrier phase observations are used, the vector of unknowns may additionally contain the (integer) double difference carrier phase ambiguities. The baselines are typically short ones; the two reference receivers 15 and 28 are 12.7 km apart. Differential atmospheric delays are assumed to be zero (in the model).

Observing m satellites gives $(m-1)$ double differences per epoch, per observation type, with $m=7$ in this experiment, unless stated otherwise. Satellite PRN 18 was taken as the pivot. For the stochastic model the standard deviation for the undifferenced code observable was taken $\sigma_p = \sigma_{\bar{p}} = 0.3$ meter and for the phase $\sigma_p = \sigma_{\bar{p}} = 0.003$ meter.

In this section we will analyse the quality of the measurement system in terms of precision and reliability for various scenarios. The baseline from reference station 15 to rover 39 is taken (about 2 km baseline). At the beginning of the session the rover is in principle stationary, but the data are processed as if it was kinematic. 31 epochs of data were considered (08:29:30 - 08:30:00).

The following three aspects were varied to obtain 16 different measurement scenarios:

- number of satellites 7 / 6 / 5 / 4
- ambiguities float or fixed f1/fx
- single or dual frequency data (C1+L1 vs C1&P2+L1&L2) sg/dl

With different numbers of satellites, the configurations are

PRN 04 10 16 19 24 27 and 18 (pivot)	7 satellites
PRN 04 10 16 19 27 and 18 (pivot)	6 satellites
PRN 04 10 16 27 and 18 (pivot)	5 satellites
PRN 04 10 16 and 18 (pivot)	4 satellites

Out of the originally 7, satellites were removed such that the final configuration with 4 satellites was not too bad.

precision

In table 3.1 below is given the precision in terms of standard deviations σ_N , σ_E and σ_H at the two epochs $k=1$ and $k=31$. The coordinates (of 28 with respect to 15) were transformed to a local topocentric system (at 15): North, East and Height (or Up).

svs	f1/fx	dl/sg	sigma at k=1			sigma at k=31		
			N	E	H	N	E	H
7	f1	dl	0.3099	0.3023	0.7009	0.0552	0.0536	0.1230
7	fx	dl				0.0031	0.0030	0.0071
7	f1	sg	0.4383	0.4275	0.9913	0.0781	0.0759	0.1739
7	fx	sg				0.0044	0.0043	0.0100

Table 3.1: Precision, standard deviation of North, East and Height in [m]

In figure 3.5 the precision of the fixed solution is given as function of the number of satellites, both for the single and dual frequency case. Below we will discuss the precision of the coordinate estimators for the cases in table 3.1 and figure 3.5 and analyse the consequences with respect to the three aspects.

- single vs dual frequency

With dual frequency data the measurement scenario has been just doubled as compared with the single frequency scenario (C1+L1 vs. C1+L1&P2+L2). The precision of the coordinate estimators improves by a factor $\sqrt{2}$ (exactly), compare the two float and the two fixed solutions in table 3.1 and see also figure 3.5.

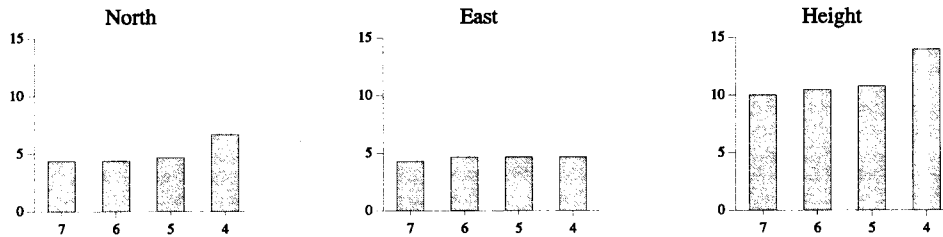
- number of satellites

Less satellites yields less precise coordinate estimators (for float and fixed). The differences are quite marginal. The differences are somewhat larger for the step from 5 back to the minimum of 4 satellites.

- gain in precision: float vs fixed

For the float solution with 1 epoch of data, the standard deviation is typically several decimeters to up and over 1 meter. After 31 epochs it is typically at the 1 dm level. For the fixed solution it is at the few mm level up to 1 cm. Fixing the ambiguities yields a large gain in precision (for these short observation time spans) see [Teunissen, 1995]. The conclusion reads that fixing the ambiguities is a prerequisite for achieving the precision desired in precise surveying, using only short time spans (by employing a fast surveying measurement technique).

single frequency



dual frequency

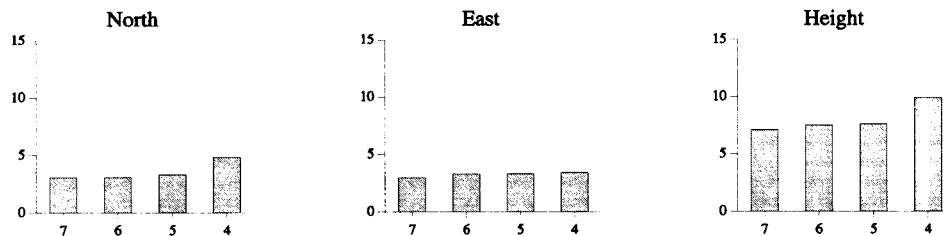


Figure 3.5: Precision of coordinates North, East, Height of fixed solution: standard deviation in millimeter versus number of satellites.

Further conclusions that can be drawn from table 3.1 concern how the precision behaves as function of time. First it seems that the (instantaneous) receiver-satellite geometry determines the precision. In the float solution for $k=1$, the phase observations do not contribute to the coordinate estimates (they determine their own ambiguities). Thus actually a code-only solution is available that determines the coordinates.

New coordinate unknowns are introduced for each epoch (kinematic receiver), but the ambiguities are constant. They allow to carry over the information from one epoch to the next in the recursive adjustment. This causes the precision improvement over time in the float solution. The standard deviation improves by slightly over a factor \sqrt{k} : $\sigma(k=31) \approx 1/\sqrt{k=31} * \sigma(k=1)$. For a static receiver and a frozen geometry, this relation would hold exactly. The change in receiver-satellite geometry over these 30 seconds is still too small to have the phase observations contribute significantly. The precision of the coordinate estimators is governed by almost solely the code observables.

For the fixed solution, the precision is about equal for all epochs (kinematic receiver). It is namely determined by the (instantaneous) satellite-receiver geometry and this does not change much during the 30 seconds time span. As such we have an epochwise coordinate estimation. Therefore the standard deviations are given only once in table 3.1, at $k=31$ (the σ 's at $k=1$ are about equal to the σ 's at $k=31$).

Once the ambiguities are fixed, the code observables do not really contribute much to the coordinate estimators anymore, due to the difference in measurement precision, $\sigma=30$ cm vs. $\sigma=3$ mm. The phase observables (now act as very precise code observables and) determine the coordinate estimators epochwise. We practically have a phase-only case to determine the coordinates.

Finally note the relation in standard deviations between the fixed and float solution ($k=1$). There is a factor 1/100 and this is the difference in measurement precision between code and phase, 30 cm vs 3 mm.

reliability

In table 3.2 the internal reliability is given in terms of Minimal Detectable Biases at the two epochs $k=1$ and $k=31$. We consider, for local model validation, outliers in the code observations and (cycle) slips in the phase observations. The MDBs outlier code and slip phase are given per satellite (channel, actually per single difference observation). The MDBs code are in [m], the MDBs phase in [cyc] (L1). Figures 3.6 through 3.8 concern internal reliability for one representative satellite, namely PRN04.

We will discuss the internal reliability for the cases in table 3.2 and figures 3.6 through 3.8 and analyse the consequences with respect to the three aspects.

svs	fl/fx	dl/sg	PRN	MDBs at $k=1$		MDBs at $k=31$	
				code [m]	phase [cyc]	code [m]	phase [cyc]
7	fl	dl	04	2.182	-	1.901	0.116
			10	2.405	-	1.905	0.129
			16	2.271	-	1.903	0.121
			19	1.986	-	1.896	0.106
			24	2.072	-	1.899	0.111
			27	2.320	-	1.903	0.124
			18	2.157	-	1.900	0.115
7	fx	dl	04			1.894	0.114
			10			=	0.126
			16			=	0.119
			19			=	0.104
			24			=	0.109
			27			=	0.122
			18			=	0.113
7	fl	sg	04	2.661	-	1.908	0.142
			10	3.866	-	1.917	0.207
			16	3.030	-	1.912	0.162
			19	2.093	-	1.899	0.112
			24	2.312	-	1.903	0.124
			27	3.286	-	1.913	0.175
			18	2.574	-	1.907	0.138
7	fx	sg	04			1.894	0.139
			10			=	0.204
			16			=	0.159
			19			=	0.110
			24			=	0.122
			27			=	0.172
			18			=	0.136

- : infinity = : equal to value above

Table 3.2: Internal reliability, Minimal Detectable Biases in meters for code and cycles for phase

- single vs dual frequency

With dual frequency data, the MDBs code are equal on the two frequencies L1 and L2 (and therefore only the C1 code observations are given). The MDBs phase (if expressed in meters, not in cycles) are also equal on L1 and L2 (and therefore only the L1 phase observations are given, in cycles).

As is clear from the table, using dual frequency data over single frequency is very beneficial for (internal) reliability. The MDBs are smaller (note in particular PRN 10).

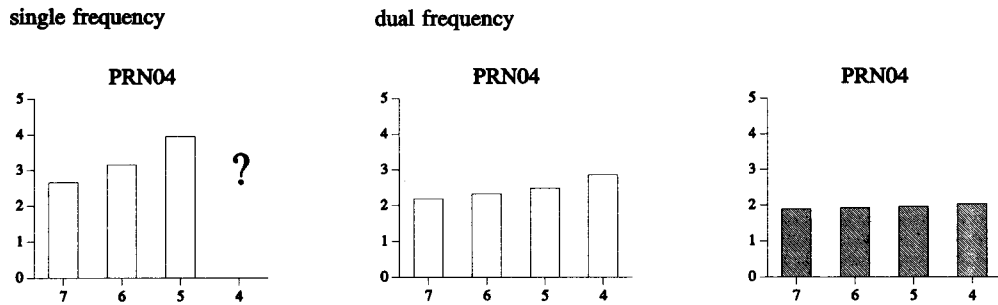


Figure 3.6: Internal reliability, Minimal Detectable Bias for outlier in code observation in meter, versus number of satellites; for float solution at first epoch $k=1$ (single frequency left, dual frequency middle) and for fixed solution (at right; single = dual frequency).

- number of satellites

Using more satellites is beneficial for (internal) reliability. The MDBs code and MDBs phase get smaller. With $m=4$ satellites, single frequency, there is no redundancy at the first epoch $k=1$. The MDB code is also infinite, figure 3.6. The MDB phase values remain large (both float and fixed) at later epochs, figure 3.7; for a kinematic receiver 3 new coordinate unknowns are introduced epochwise. An MDB of 10 cycles prohibits handling cycle slips adequately; this value corresponds to the MDB code (~ 2 m).

With dual frequency data and $m=4$ satellites, the MDBs are equal on all channels; the receiver-satellite geometry has been set off side (this exactly holds for the MDB code of the float solution at $k=1$).

- float vs fixed

At epoch $k=31$ the differences between the float and fixed solution concerning the MDBs are rather marginal. Note that with only one epoch of data $k=1$ (float) the MDBs phase are infinite; a cycle slip can not be distinguished from its ambiguity value.

Further conclusions that can be drawn from table 3.2 concern how the internal reliability behaves as function of time. If the ambiguities are fixed, the MDBs are about equal for all epochs (and therefore given only for epoch $k=31$). For the MDBs phase, the instantaneous receiver satellite geometry is involved (and this does not change much). The MDBs code are equal on all channels (and epochs). In the fixed solution namely, the coordinates are determined very precisely. In terms of single differences, the code observations (per observation type) have to determine only one common unknown, the differential receiver clock error. They practically do not contribute to the coordinate estimates. The MDB value can easily be computed using an analytical formula

$$|\nabla| = \sqrt{\lambda_o} \sqrt{\frac{m}{m-1}} \sigma_{SD}$$

where λ_o is the non-centrality parameter and σ_{SD} the standard deviation of the single difference code observable. With less satellites m , this value increases (giving less reliability). The values for the different scenarios are 1.894 m (7 svcs), 1.920 m (6 svcs), 1.960 m (5 svcs) and 2.024 m (4 svcs), figure 3.6 at right.

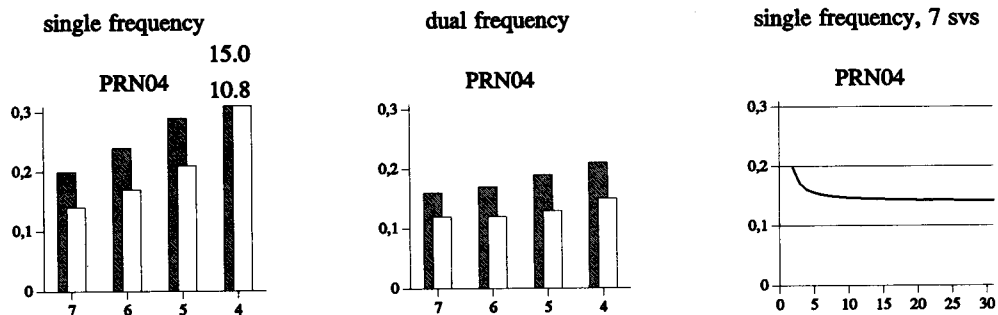


Figure 3.7: Internal reliability, Minimal Detectable Bias for (cycle) slip in phase observation in cycles, versus number of satellites for float solution; for epochs $k=2$ (hatched) and $k=31$ (white), single frequency (left) and dual frequency (middle) and (at right) as function of time for single frequency with 7 satellites.

The MDBs for outliers in code observations are typically at the 2 m level, thus quite large with a precise positioning application in mind. Propagation of a model error when left undetected, is described by external reliability. In section 5.1.2.6 it was concluded that, once the ambiguities are fixed, the bias in the (position) coordinates, caused by such an outlier, was absolutely not significant.

Note that between the MDBs code ($k=1$, float) and the MDBs phase (fixed), again the relation of 1/100 ($\sigma=30$ cm vs $\sigma=3$ mm) exists, with the MDBs phase expressed in meters (not in cycles).

At the first epoch $k=1$ of the float solution the instantaneous geometry is involved. The code observations (solely) determine the coordinate estimates and this is reflected in the MDBs. The MDBs improve as more epochs of data are used. With an increasing number of epochs the MDBs code converge to the above values (of the fixed solution) 1.894, 1.920, 1.960 and 2.024 m.

integer ambiguity estimation

For the various measurement scenarios a qualitative description of the integer ambiguity estimation problem will be given. It can be inferred a-priori whether successful ambiguity resolution will be likely or not.

In table 3.3 we consider the float experiments at epochs $k=1$ and $k=31$, for the first epoch see also figure 3.9. The standard deviation of double difference ambiguity 18-10 is given, together with the Ambiguity DOP, see [Teunissen, 1997c]. Below we will discuss the integer ambiguity estimation problem for the cases in table 3.3.

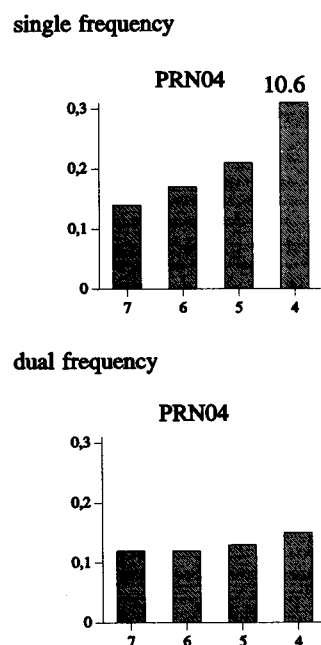


Figure 3.8: Internal reliability, Minimal Detectable Bias for (cycle) slip in phase observation in cycles (L1), versus number of satellites for fixed solution (given for epoch $k=31$), single frequency on top and dual frequency at bottom.

svs	float	dl/sg	n	σ_{18-10}		ADOP	
				k=1	k=31	k=1	k=31
7	fl	dl	12	1.86	0.33	0.07	0.01
7	fl	sg	6	2.63	0.47	0.26	0.05
6	fl	dl	10	1.87	0.33	0.09	0.02
6	fl	sg	5	2.65	0.47	0.42	0.07
5	fl	dl	8	1.97	0.35	0.14	0.02
5	fl	sg	4	2.79	0.50	0.86	0.16
4	fl	dl	6	2.23	0.40	0.25	0.04
4	fl	sg	3	3.15	0.57	2.81	0.50

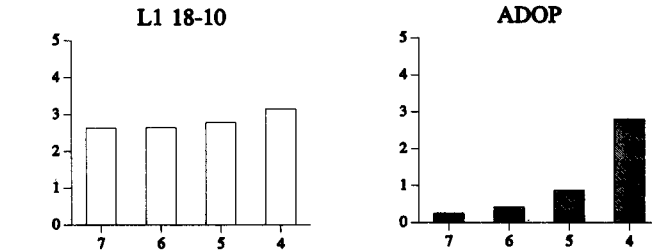
Table 3.3: Standard deviation of L1-ambiguity 18-10 and ADOP in [cyc]

- standard deviation of ambiguity

With dual frequency data there are twice as much ambiguities (with m satellites there are $2(m-1)$ vs $(m-1)$). From table 3.3 and figure 3.9 it can be seen that the precision for the dual frequency case is better than for the single frequency case; again the factor $\sqrt{2}$ shows up. For this short time span, the code observables (solely) have to (indirectly) determine the ambiguity estimators. With more satellites, there are also more ambiguities to estimate. The ambiguities however, become more precise.

Further conclusions that can be drawn from table 3.3 concern how the precision behaves as function of time. The standard deviation improves by approximately a factor \sqrt{k} . Practically a recursive adjustment is made upon the constant ambiguities with the code observables. The change in receiver-satellite geometry over these 30 seconds is still too small to have the phase observables contribute significantly in this.

single frequency



dual frequency

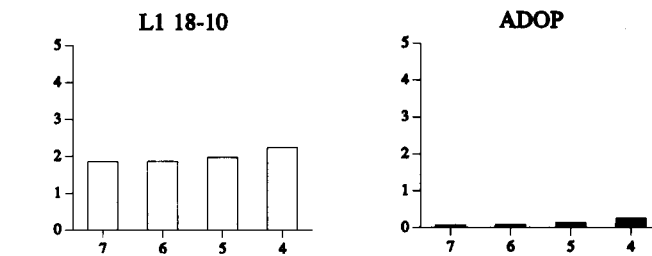


Figure 3.9: Precision of ambiguity as function of number of satellites: standard deviation of double difference ambiguity 18-10 (left) and ADOP (right), both in cycles, at epoch $k=1$ (float solution), single frequency (bottom) and dual frequency (top).

- ADOP

The ADOP is (approximately) the average precision of the transformed (decorrelated) ambiguity. It is computed from the determinant of the variance covariance matrix of the ambiguities $|Q_x|$. Analytical expressions for this determinant are given in [Teunissen, 1997a]. When this measure is at the few tenths of a cycle level (or smaller), ambiguity resolution can be expected to be successful. This is the case for all dual frequency cases.

For the single frequency case with only 5 satellites, the ADOP is almost 1 cycle and with 4 satellites the ADOP is almost 3 cycles. Correct and reliable resolution of the ambiguities will be problematic. It should be noted that for the ADOP, to be a true predictive measure, a realistic, adequate mathematical modelling is a prerequisite.

It can be seen that the ADOPs improve as more epochs are taken into account (by approximately the factor \sqrt{k}). Note that the ADOPs are much smaller than the standard deviation of the (untransformed) ambiguity 18-10. The difference gets less as the redundancy decreases (less satellites and single instead of dual frequency data). For the scenario with single frequency and 4 satellites, thus only 3 ambiguities, they are about equal. In this case there is not much to decorrelate, see also [Teunissen et al, 1997].

- elongation

The elongation of the ambiguity search ellipsoid is given by the square root of the ratio of the largest and smallest eigenvalue of the ambiguity variance covariance matrix. A (hyper-) spheroid has elongation $e=1$.

In [ibid] it is explained that there are 3 long axes and that the remaining ones are very short. The dual frequency ellipsoid, $2(m-1)$ -dimensional, is slightly more elongated than the corresponding single frequency one, $(m-1)$ -dimensional. With single frequency and $m=4$ satellites, all three axes have about equal length (of a few cycles); there are no small axes.

svs	float	d1/sg	n	e
7	f1	d1	12	$2.2 \cdot 10^2$
7	f1	sg	6	$1.9 \cdot 10^2$
6	f1	d1	10	$2.2 \cdot 10^2$
6	f1	sg	5	$1.9 \cdot 10^2$
5	f1	d1	8	$1.9 \cdot 10^2$
5	f1	sg	4	$1.5 \cdot 10^2$
4	f1	d1	6	$2.1 \cdot 10^2$
4	f1	sg	3	2.0

Table 3.4: Elongation of ambiguity search ellipsoid at epoch $k=1$

The elongation in these experiments is generally on the order $e=10^2$ and is typically prescribed by the precision of the code data, $\sigma \approx 10^{-1}$ m vs $\sigma \approx 10^{-3}$ m for the phase data. The elongation does not change much over the 30 seconds time span (geometry change is very small). Incorporating more epochs gives mainly a scaling effect on the variance covariance matrix, see the decrease in standard deviation of the ambiguity in table 3.3.

5.3.2.3 Positioning

First we will concentrate on the positioning performance that can be achieved with the kinematic GPS surveying measurement technique under operational conditions. The next section gives results on estimating the integer ambiguities.

trajectory

The baseline 15 (reference station) to 39 (rover on the van) is used. The van starts at about 2 km from the reference and makes a two-way trip with the turning point at 12 km distance.

The single frequency (C1+L1) data of 7 satellites were used to compute the trajectory, consisting of 2421 positions (the rover was assumed to be in permanent motion). The ambiguities could be fixed

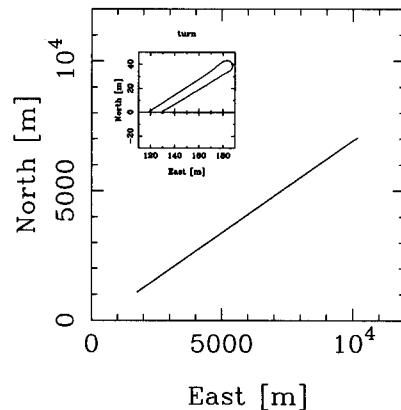


Figure 3.10: Trajectory of receiver 39: two-way trip from 2 km to over 12 km from the reference 15 at the origin

right away at the first epoch $k=1$. The trajectory in the local horizontal plane North-East (topocentric system at 15) is given in figure 3.10. The reference station 15 is at the origin (0,0). The return-trip along the dike with 3 static periods, boils down to a simple straight line. In the inset the turn at the far end is shown; the lower left corner of this plot corresponds to (10110, 6970).

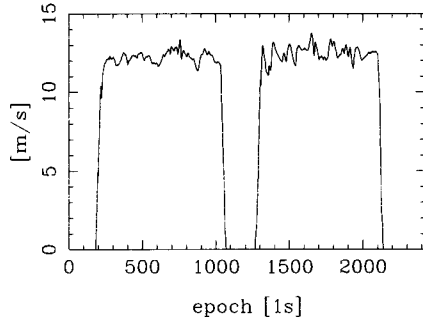


Figure 3.11: Velocity of van

The velocity is given in figure 3.11 and computed via the displacement in three dimensions over the 1 second intervals. There are three static periods, at the beginning, the end and halfway just before the turn. The van is driving at slightly over 40 km/h in 3rd gear.

height profiling

In figure 3.12 the ellipsoidal height of the rover-antenna is given, after differencing with the height of marker 15 (the reference station).

The vertical axis of figure 3.12 corresponds to only 60 cm. This difference in ellipsoidal heights is given for the full trajectory. The van drives to the far end, remains stationary from epoch $k=1075$ to $k=1258$, turns and uses the opposite lane of the same road for its return. The graph at left shows a symmetry in this static period; the same features of the road on the dike can be clearly identified in going and coming. The driving speed was kept as constant as possible, see figure 3.11.

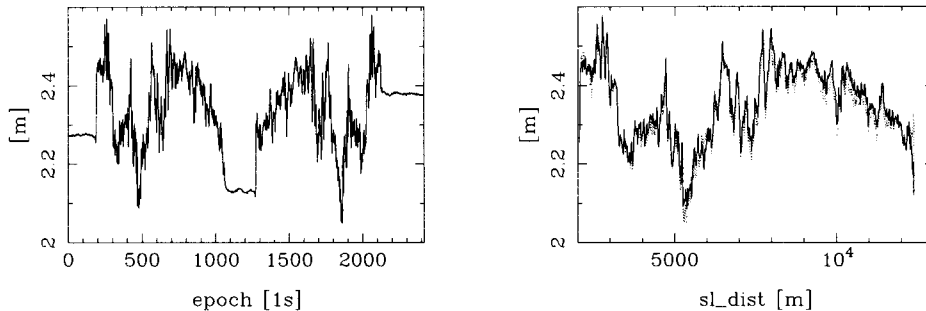


Figure 3.12: Ellipsoidal height difference versus time (left) and versus slope distance (right), going full, coming dotted

In the graph at right, the height is given as function of the slope distance from rover to reference. The slope distance ranges from about 2 km to over 12 km. Both ways of the return-trip are given in this graph and can be compared as the reference receiver and the trajectory are practically on one line (cf. figure 3.10). The agreement in height generally is on the 2-3 cm level, sometimes worse (up to 5 cm), sometimes better. Note that due to other traffic, the van sometimes had to take partly the emergency lane.

With figure 3.12 we would have obtained a kind of height profile of the Oostvaardersdijk. It shows the (ellipsoidal) height for the rover-antenna on the van (it is between 2.0 and 2.5 meters). This height has to be reduced to the road surface and vehicle suspension (and attitude) effects have to be taken into account in this. Also note that it is the height above the WGS84 ellipsoid, thus a geometric height, and not a levelled one (the geoid height has still to be taken into account for practical interpretation).

coordinate precision

To get an impression of the empirical precision of the coordinates, the estimates are given for the three static periods in figure 3.13. On the left are the scatters for the horizontal coordinates and on the right the vertical component. The vertical axis corresponds to 2 cm in all cases (the full number of meters of the horizontal coordinates has been chopped off for these plots). The spread in horizontal position is at the level 5-10 mm (and note that the antenna was on the van with the engine still running, crew inside and cars passing by; the van may move a little). The height is given as function of time. The spread is slightly larger than for the horizontal coordinates. Unmodelled effects, like multipath (the roof of the van is not a benign environment for a GPS antenna) and differential atmospheric delays could be present.

The formal precision is given in terms of standard deviation North, East and Height. It does not change dramatically over this 40 minutes span.

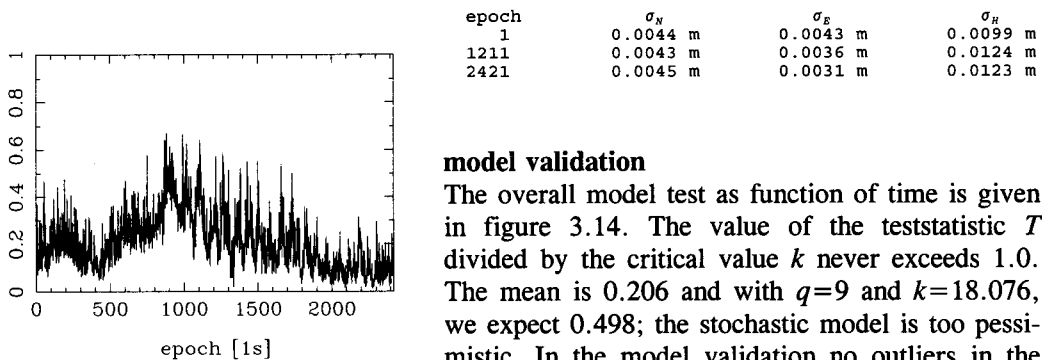


Figure 3.14: Overall model test T/k , single frequency code&phase (fixed)

model validation

The overall model test as function of time is given in figure 3.14. The value of the teststatistic T divided by the critical value k never exceeds 1.0. The mean is 0.206 and with $q=9$ and $k=18.076$, we expect 0.498; the stochastic model is too pessimistic. In the model validation no outliers in the C1-code nor cycle slips in the L1-phase data were encountered.

The behaviour of the test can not be really matched with the 3 static and 2 kinematic periods. A dependence of the noise of the (phase) observables on the receiver dynamics does not show up in this graph. The overall model teststatistics values do make us suspect time correlation in the data. This again may be due to unmodelled effects like multipath and differential atmospheric delays. A clear relation of the overall model test with baseline length is however not present.

code only

In the above estimation, the ambiguities were fixed right away at the first epoch $k=1$. The C1-code observations were actually not used for positioning (due to the difference in weighting). The trajectory is reprocessed with only the C1-code observations, to get an indication of the positioning capability with single frequency code. The C1+L1 ambiguity fixed solution is thereby treated as a deterministic reference; it can be considered as truth at the cm-level (there may be differential ionospheric effects). The coordinate estimates obtained are differenced with C1+L1 ambiguity fixed solution, see figure 3.15.

Especially in the plot for the North coordinate, one might distinguish some multipath effects (possibly from the roof of the van) with a period of about 1 minute. The Height is more noisy than the horizontal coordinates.

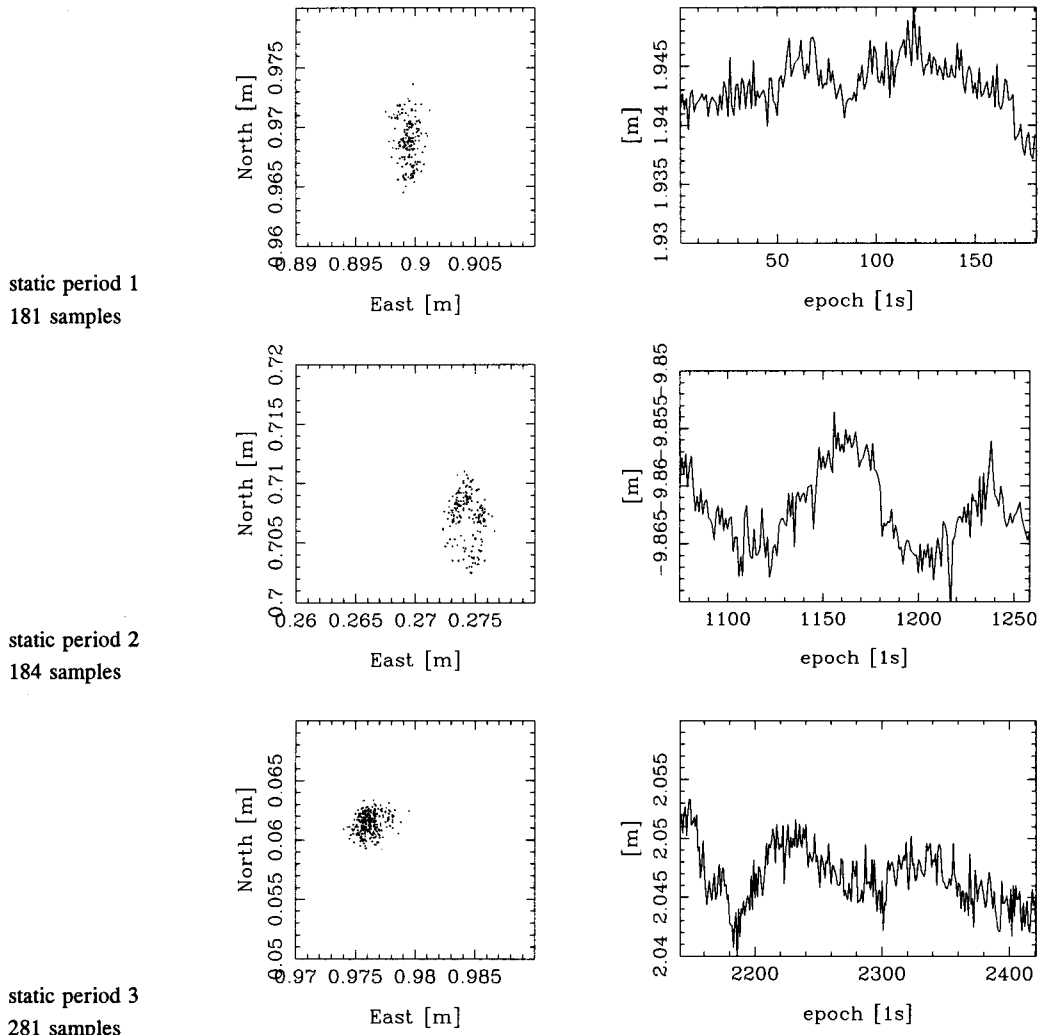


Figure 3.13: Position coordinates for three static periods

Per coordinate difference North, East and Height, the 2421 estimates are samples of random variables with zero mean. The random variable is assumed to be independent in time. In table 3.5 we give, per coordinate, the mean and empirical standard deviation. The deviation from zero is quite large for the Height-component. The empirical standard deviations are smaller than the formal ones. The stochastic model is too pessimistic.

	North	East	Height
mean	-0.060 m	0.039 m	-0.353 m
st.dev	0.254 m	0.178 m	0.698 m
formal standard deviation			
1	0.438 m	0.428 m	0.991 m
1211	0.431 m	0.356 m	1.241 m
2421	0.454 m	0.308 m	1.226 m

Table 3.5: Formal and empirical precision for kinematic, single frequency code solution

The values of the overall model teststatistic T , divided by the critical value k , are given in figure 3.16. There are no rejections at all. The mean is 0.062 and the expected value is 0.237 ($q=3$, $k=12.634$). There seems to be no difference between stationary and kinematic periods.

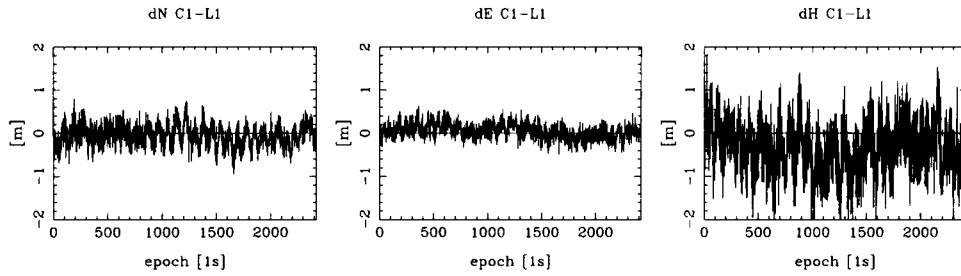


Figure 3.15: Coordinate estimates North, East and Height from code only solution

5.2.3.4 Ambiguity resolution

The integer ambiguities need to be correctly estimated and consequently fixed, in order to obtain positioning results with highest precision. This section should answer the question: how well can the integer ambiguities be estimated?

The full session is considered (2421 epochs) and 40 experiments of half a minute, spaced by another half minute are defined, they are numbered 1 through 40. The ambiguities will be resolved for each of these 40 experiments individually; as if each time a loss of lock (but not a physical one) has occurred. Only 5 satellites are used; PRNs 04, 10, 16, 27 and 18. The 5 satellites were chosen such, to have a not too bad configuration. The van is driven from about 2 km to over 12 km from the reference.

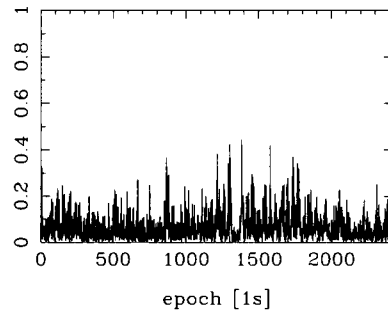


Figure 3.16: Overall model test T/k , kinematic, code-only

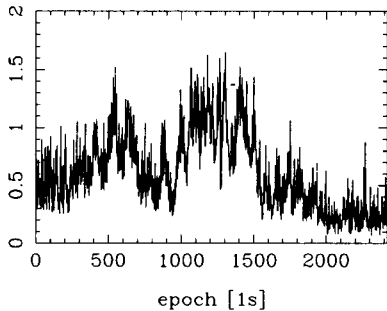


Figure 3.17: Overall model test T/k , dual frequency code&phase data

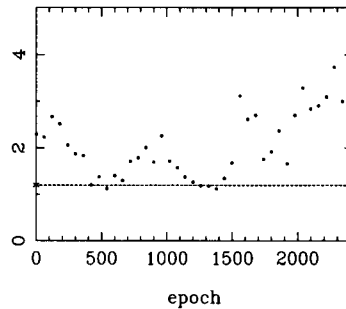


Figure 3.18: Ratio second best - best, σ_2/σ_1 , 40 experiments, threshold value 1.2

First the full trajectory of the kinematic receiver is recovered from dual frequency data (rover in permanent motion assumed). The value of the overall model teststatistic T , divided by the critical value k is given in figure 3.17. There are quite some rejections, but in general it is not severe (T/k is just slightly larger than 1.0). Identification usually points to the L2 phase observation of PRN27. The error is estimated to be 0.1 cycle or less. Adaptation was disabled; the data were used just as they came in. The mean of T/k is 0.596 and with $q=13$ and $k=21.725$ we expect 0.598.

Ambiguity resolution involves two stages: the estimation and the validation. The integer ambiguities are estimated with the LAMBDA method. Reference values for the integer ambiguities are available and the ambiguities do not change during the 40 minutes session; no cycle slips occur. Validation still is an open end at present, cf. section 1.7.3. In this experiment validation is therefore restricted to the so-called ratio-tests, as used in for example the Bernese software [Rothacher et al, 1996]. The acceptance test reads $\sigma_{fixed}/\sigma_{float} < 5.0$ and the discrimination test $\sigma_{fixed(2)}/\sigma_{fixed(1)} > 1.2$. If these two tests are passed, ambiguity resolution is declared to be reliable. We concentrate on the test for discriminability, see below. The acceptance test is passed in generally all cases.

■ ambiguity discrimination test

The ratio 'sigma fixed second best - sigma fixed best' is used here just to get a first (partial) impression of the reliability associated with the integer estimate for the vector of ambiguities. This ratio is commonly used to measure the discriminability between integer vectors. It is described in [Frei, 1991]. The theoretical justification for this measure is questionable.

The best candidate for the ambiguity vector, the integer least-squares estimate $\check{x}_I = x_I^1$ and the second best x_I^2 are compared. Their squared distances read, cf. equation (4:10) and appendix 1.A.7,

$$\chi^2(x_I^1) = (\hat{x}_I - x_I^1)^T Q_{\hat{x}_I}^{-1} (\hat{x}_I - x_I^1)$$

$$\chi^2(x_I^2) = (\hat{x}_I - x_I^2)^T Q_{\hat{x}_I}^{-1} (\hat{x}_I - x_I^2)$$

The ratio can be computed as

$$\frac{\check{\sigma}(x_I^2)}{\check{\sigma}(x_I^1)} = \frac{\sqrt{T_q + \chi^2(x_I^2)}}{\sqrt{T_q + \chi^2(x_I^1)}}$$

where T_q is the value of the overall model teststatistic of the float solution. Note that the degrees of freedom of the fixed solution is equal for both sigmas and therefore cancels in the ratio. Discriminability is decided to be sufficient if the ratio exceeds a certain threshold. Here, the value 1.2 was taken. ■

dual-frequency

With dual frequency data to 5 satellites a successrate of 100% is achieved. In all experiments, the integer ambiguities are correctly estimated right away at the first epoch. Validation may take a few more epochs in some cases (directly at epoch $k=1$, 90% is validated). Figure 3.18 gives the values for the discrimination test ratio $\sigma_{fixed(2)}/\sigma_{fixed(1)}$ for all 40 experiments (at epoch $k=1$); the dotted line gives the threshold value. There seems to be some relation with the overall model test in figure 3.17; if the overall model test is small, the ratio is large and vice versa.

single-frequency

Ambiguity resolution based on single frequency data is less successful. In table 3.6 we give the epoch at which the ambiguities are reliably fixed; it is indicated whether this fix

(integer vector) is correct or not (Y/N) and the discrimination teststatistic (σ_2/σ_1) is given for this epoch. Fixing is declared to be reliable, based on the two ratio tests. If the integer estimate is wrong, it is indicated by how many cycles (in absolute sense), for the original double difference ambiguities.

exp.	epoch	corr	σ_2/σ_1	4 ambiguities	epoch	corr	σ_2/σ_1	6 ambiguities
1	2	N	1.274	0 1 0 1	1	Y	2.176	
2	19	Y	1.302		2	Y	1.209	
3	1	Y	1.259		1	Y	1.497	
4	10	Y	1.253		1	Y	1.943	
5	6	N	1.241	2 1 1 1	1	Y	1.489	
6	6	N	1.228	0 0 1 1	1	Y	1.980	
7	15	N	1.208	1 1 1 2	1	Y	1.918	
8	2	N	1.205	1 1 1 2	1	Y	2.924	
9	18	N	1.277	0 1 1 1	1	Y	1.687	
10	>31			cnbrf	2	Y	1.438	
11	>31			cnbrf	1	Y	1.792	
12	1	N	1.260	0 2 1 1	1	Y	1.752	
13	1	Y	1.670		1	Y	1.535	
14	2	Y	1.301		1	Y	1.383	
15	1	N	1.219	0 3 1 1	>31			cnbrf
16	1	N	1.830	0 1 0 0	>31			cnbrf
17	13	Y	1.242		>31			cnbrf
18	1	N	2.328	3 2 2 4	>31			cnbrf
19	1	N	1.265	1 3 0 1	6	N	1.213	2 2 2 1 1 3
20	1	N	1.265	1 3 0 1	1	Y	1.360	
21	>31			cnbrf	1	Y	1.485	
22	8	N	1.227	1 1 4 3	9	Y	1.209	
23	1	N	1.612	0 1 2 1	1	Y	2.868	
24	30	N	1.223	0 1 0 0	1	Y	2.021	
25	1	N	1.388	2 2 3 3	2	Y	1.243	
26	1	N	3.356	3 1 1 3	1	Y	1.627	
27	5	N	1.235	1 1 3 2	1	Y	2.099	
28	3	Y	1.616		1	Y	1.457	
29	3	Y	1.470		1	Y	1.781	
30	5	N	1.379	2 1 1 2	1	Y	2.440	
31	1	Y	1.460		1	Y	2.969	
32	2	Y	1.526		1	Y	2.277	
33	1	N	1.233	1 1 1 1	1	Y	2.712	
34	1	N	1.230	2 1 2 2	1	Y	2.173	
35	4	N	1.230	1 1 2 1	1	Y	3.648	
36	5	Y	1.238		1	Y	3.494	
37	4	Y	1.396		1	Y	2.020	
38	7	Y	1.404		1	Y	2.343	
39	2	Y	1.781		1	Y	3.863	
40	9	Y	1.342		1	Y	2.181	
experiments	1- 3	are	static	4-18	kinematic	cnbrf	:	could not be reliably fixed
	19-21		static	22-36	kinematic			
	and	37-40	static					

Table 3.6: Ambiguity resolution with single frequency data; 5 satellites (left), 7 satellites (right)

For 22 experiments (=55%) the ambiguities are fixed, but not correctly. The overall impression is that reliably fixing with single frequency data of only 5 satellites is quite problematic over these baselines (2-12km). Though 15 out of 40 experiments (=38%) are correctly and reliably fixed.

In experiment 2 for instance, reliable fixing can finally take place at epoch $k=19$ (to the correct integer vector indeed). The integer vector is correctly estimated from epoch $k=15$ onwards. In the mean time the integer estimation result is swapping between this correct integer vector and a vector that deviates by 0 1 0 1 (in absolute sense) from the correct one. Discrimination is negative (values of 1.0-1.1) until epoch $k=19$.

For experiment 4 the behaviour of the integer estimation is given in figure 3.19 for the first ten epochs. The data are accumulated and at $k=10$, based on the float solution then available, reliable fixing seems possible. The integer estimates are correct from $k=7$

onwards and incidently on $k=5$. The vertical scales span 5 cycles; the spread in the ambiguity estimates is at the few cycles level, cf. figure 3.9.

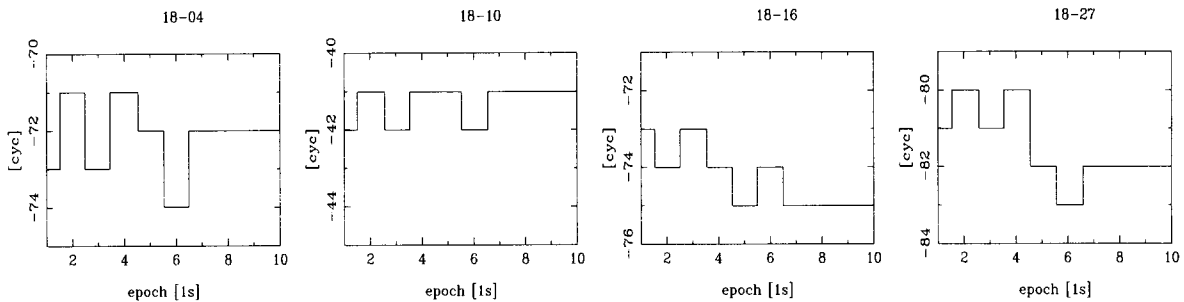


Figure 3.19: Integer estimation in experiment 4; the correct integer ambiguity values (last two digits only) are 18-04 -72 18-10 -41 18-16 -75 18-27 -82

Additionally ambiguity resolution was considered for single frequency data with 7 satellites. The results are given in table 3.6 as well. The two more satellites are very beneficial, cf. figure 3.9, in this single frequency case: 31 out of 40 experiments (=78%) could be correctly and reliably fixed directly at epoch $k=1$. Another 10% was fixed at a later epoch. One integer vector was validated, but was incorrect. The remaining four experiments could not be reliably fixed within the 30 seconds period.

5.3.2.5 Limitations of the model

The mathematical model derived in chapter 3 was said to hold for short GPS baselines. For instance differential atmospheric delays (troposphere and ionosphere) are assumed to be absent, thus zero. In this section we will explore experimentally the limitations of the functional part of the current mathematical model. We will encounter differential atmospheric delays and multipath and show their effect on the position estimates.

differential atmospheric delays

On longer baselines differential atmospheric delays must be accounted for. Below it will be shown that in this experiment the effect amounts to several centimeters over the static 12.7 km baseline.

A single frequency phase solution was computed for the baseline 15-28 (the two reference stations) with 7 satellites, 2421 epochs at 1 second. The integer ambiguities were constrained a-priori. Baseline coordinates for marker 28 were estimated on epoch-by-epoch basis (as if the receiver was in permanent motion). Reference coordinates for marker 28 were available and in figure 3.20, the estimated - reference coordinates are given, in local North, East and Height. The reference coordinates are believed to be good

	North	East	Height
mean	-0.0025 m	0.0052 m	-0.0042 m
st.dev	0.0082 m	0.0085 m	0.0322 m
formal standard deviation			
1	0.0044 m	0.0043 m	0.0099 m
2421	0.0045 m	0.0031 m	0.0123 m

Table 3.7: Empirical mean and standard deviation of coordinates, single frequency phase, 12.7 km baseline 15-28

at the 1 cm level. The estimated coordinates however, show a time-varying behaviour around these reference values; the variations amount to several centimeters. In table 3.7 the empirical mean and standard deviation are given for the coordinates.

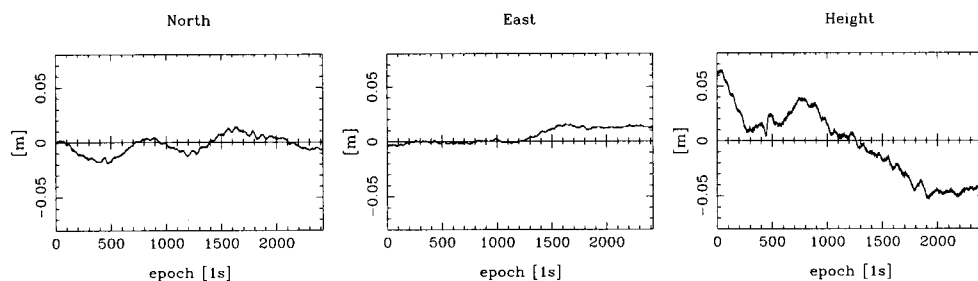


Figure 3.20: Estimated coordinates North, East and Height of marker 28

The deviations of the above coordinate differences from zero are formally significant. From a practical point of view, they are quite close to zero (only a few mm's). The empirical standard deviations are larger than formal ones. In figure 3.20 variations in the coordinate estimates can be clearly observed, especially in the Height, it varies from +6 cm to -4 cm. The cause of the effects probably is the differential atmospheric delay (ionospheric and tropospheric). In the current implementation no correction at all is applied for these delays. The effect on the coordinates is a few mm/km (ppm) in this experiment. Typically the Height is most affected. The variation is long term. The x-axis corresponds to over 2400 epochs at 1 second rate, or 40 minutes. Multipath is not the first suspect in this as it generally yields variations on much shorter term (tens of seconds or a few minutes).

During this experiment, the ionospheric delay (in absolute sense) was rather small and tropospheric conditions were not rare. The *differential* delays (ionospheric and/or tropospheric) turned out however, to be non-negligible (the difference in height between the two stations 15-28 of this baseline is marginal, a few decimeters only). The effect will be even larger when significant height-differences are present (e.g. with the kinematic receiver on an aircraft); the differential tropospheric delay will then play a (even more) prominent role.

The local overall model test, teststatistic value T divided by critical value k , is given in figure 3.21. The mean of T/k is 0.62; whereas with $q=3$ and $k=12.63$, 0.24 is expected. This may point to a discrepancy between data and model; the mathematical model may not be fully adequate for this experiment. Adaptation was disabled. There appears to be some correlation between the overall model test in figure 3.21 and the graph for the Height in figure 3.20; if the Height differs largely from zero, the value for the teststatistic is large.

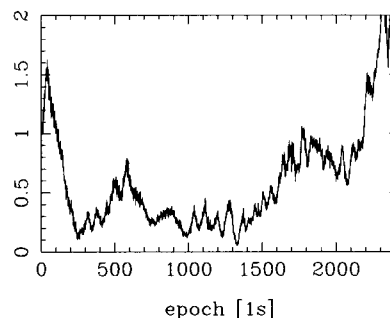


Figure 3.21: Local overall model test T/k , single frequency phase, baseline 15-28

Differential atmospheric delays are most likely the cause, beside possibly multipath. The effects amounts to several centimeters on this 12.7 km baseline. High precision applications require whether accounting for the differential tropospheric and ionospheric delays, or restricting the baseline length, when though using the simple mathematical model.

For a closer analysis on the mismodelling by the functional part of the model, the coordinates of the rover, point 28, were constrained to the reference values, and the (double difference) ambiguities to their integer values, see appendix A. Dual frequency

phase data were used. Per observation type (L1 and L2) error estimates were computed epochwise (locally) per channel. According to the alternative hypothesis, the unknowns are the (differential) receiver clock error and the model error. The observations are reduced for the known parameters. The observation equations in terms of single differences read

$$H_{a_i} : E\{\underline{P}_{12}^i\} = c\delta_{12}t + \nabla^i \quad i=1, \dots, m$$

$$H_{\bar{a}_i} : E\{\bar{\underline{P}}_{12}^i\} = c\bar{\delta}_{12}t + \bar{\nabla}^i$$

Unmodelled effects, represented by the model errors ∇ and $\bar{\nabla}$ are supposed to be the differential tropospheric T and ionospheric delays I , thus

$$\nabla^i = T^i - I^i$$

$$\bar{\nabla}^i = T^i - \frac{f_1^2}{f_2^2} I^i$$

Consequently double difference delays are computed from the error estimates according to the alternative hypotheses, by inverting the above relation. Two examples of double difference ionospheric delays are given in figure 3.22 and of tropospheric delays in figure 3.23. These atmospheric delays each clearly show a different behaviour, although the (magnitudes of the) delays are formally not significant; the formal precision reads $\sigma_T=0.018$ m and $\sigma_I=0.013$ m.

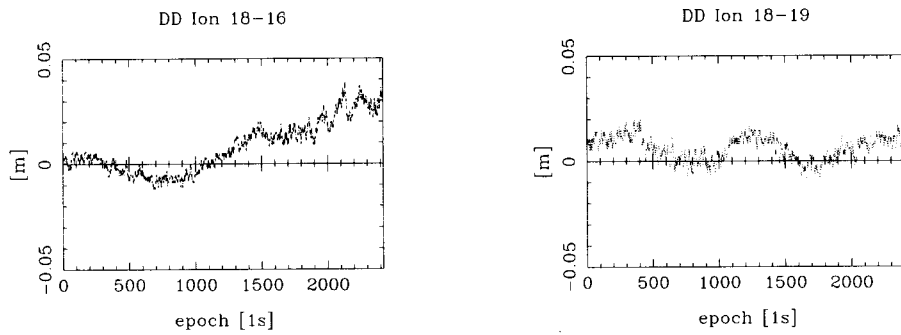


Figure 3.22: Double difference ionospheric delays

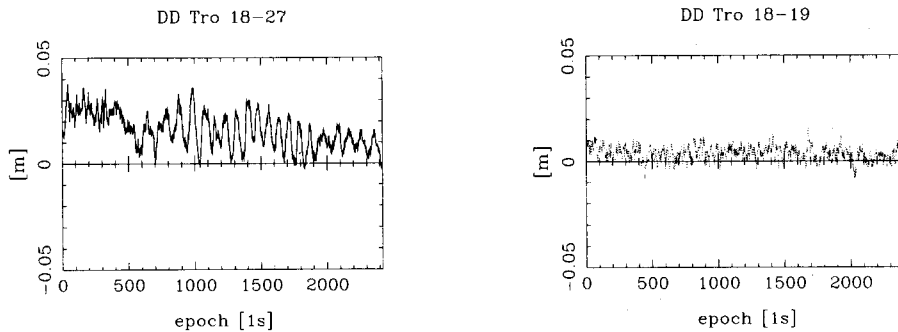


Figure 3.23: Double difference tropospheric delays

Satellite PRN 18 (high elevation) is taken the pivot for double differencing. Satellite PRN 16 sets (below 30° elevation) and the ionospheric delay increases up to 3 cm. Satellite PRN 19 is at high elevation and the ionospheric delay is small, between 0 and +1 cm; also the tropospheric delay is small and nicely constant. For satellite PRN 27 there clearly is multipath present, both on the computed tropospheric and ionospheric delay; the effect is several (2-3) centimeters.

float solution

As a side step the behaviour of the float solution is considered for this baseline 15-28. Single frequency code and phase data were used. New coordinate unknowns were introduced for each epoch (thus if receiver 28 was in permanent motion). The coordinate estimates were differenced with the reference values; they are given in figure 3.24, in the local North, East and Height system. The ambiguities are constants, but are not constrained to their integer values.

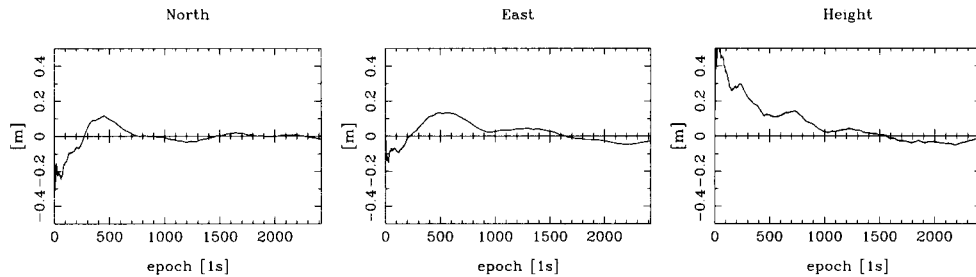


Figure 3.24: Coordinate estimates North, East and Height of float solution, C1+L1

It can be seen that as time passes, the float solution converges to the reference values (at least at the decimeter scale of figure 3.24), but it takes a long time.

The (formal) precision improves as time passes:

$$\begin{array}{l} \text{epoch } k=1 : \sigma_N = 0.438, \sigma_E = 0.429 \text{ and } \sigma_H = 0.991 \quad [\text{m}] \\ \text{epoch } k=2421 : \sigma_N = 0.005, \sigma_E = 0.004 \text{ and } \sigma_H = 0.013 \quad [\text{m}] \end{array}$$

The (local overall) model validation resulted in one rejection (at epoch $k=1579$).

multipath

Multipath could already be suspected in figure 3.23 of the static baseline. To experimentally show the effect of multipath, the short baseline 39-38 on the van is used. During a period of about 3 minutes (171 epochs at 1 second), prior to the actual processing session, the van was static. Multipath was expected to occur as the roof of the van is not a benign environment for a GPS antenna.

Single frequency code and phase data were used (6 satellites). New coordinate unknowns were introduced epochwise (as if receiver 38 was in permanent motion with respect to receiver 39). The ambiguities were (reliably) fixed at epoch $k=2$ (at epoch $k=2$, $\sigma_N=0.0051$, $\sigma_E=0.0030$ and $\sigma_H=0.0079$ m).

The coordinate estimates are given in figure 3.25, in the local North, East and Height system (at 39). The vertical scale represents 2 cm. In particular for the North and Height, a variation over 5 mm with a period of about 1 minute can be observed.

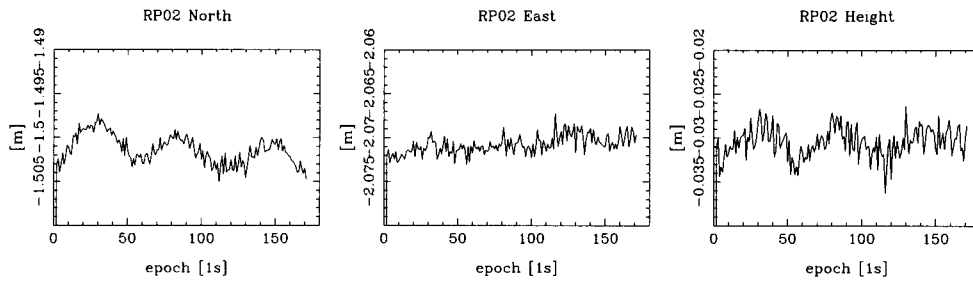
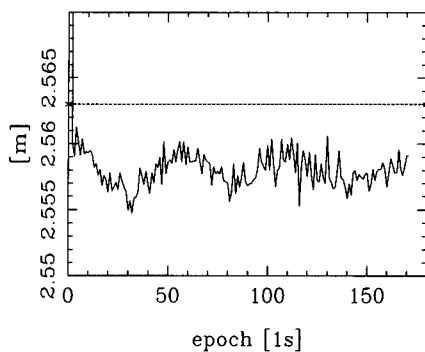


Figure 3.25: Coordinate estimates North, East and Height for 39-38

This baseline, rigidly connected to the van, must be quite insensitive to small motions of the van (crew, wind, traffic). On such a short baseline differential atmospheric delays can not play a role. What remains as the principal suspect, is multipath from the roof.

The model validation did not result in any rejection. The overall model test, teststatistic value T divided by critical value k , is given in figure 3.27. Value 0.43 was expected for T/k ; the mean was smaller, nl. 0.16.

Figure 3.26: Estimated length l , baseline 39-38 on van, single frequency data, reference length by tape 2.563 m

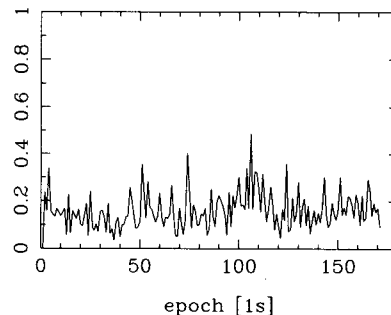
For figure 3.26 we consider one function of the three coordinate estimates: the baseline length. It is computed from

$$l = \sqrt{dN^2 + dE^2 + dH^2}$$

The vertical axis represents 2 cm. The formal precision is $\sigma_l = 0.0039$ m (at epoch $k=2$) and followed from applying the error propagation law on the coordinates variance covariance matrix using the linearized version of the above equation. Apart from the ~ 1 minute variation, the noise seems to be much smaller.

The variations observed in figure 3.25 are also present in figure 3.26, which practically rules out motions of the van (both antennas were rigidly mounted on a solid wooden bar). In a hostile environment, like the highly reflective roof surface, multipath seems to be clearly present and it currently yields a too large effect to be not taken into account in processing the data, see also [Heister et al, 1997].

In this experiment, the antennas were mounted some 15 centimeters above the roof of the van and ground planes were used. Physically seen the van, a large conducting (and reflecting) object, is in the near-field of the antenna(s). It may get electro-magnetically coupled and thereby affect the overall electro-magnetic properties, see [Elósegui et al, 1995]. The consequences on signal propagation/reception are hard to predict.

Figure 3.27: Overall model test T/k , baseline 39-38, single frequency data

The length of the baseline was also measured by tape and yields 2.563 m. This value is indicated in figure 3.26 by the dashed line. The discrepancy is at the few mm level (possibly a long term bias).

5.3.3 Summary

In this section we will first briefly review the findings of the kinematic GPS surveying experiment. Then we will give several recommendations for future developments on this measurement technique.

summary

In this experiment, the measurement set up for kinematic GPS surveying consisted of a reference station and a roving receiver on a moving van. The van was driven to over 12 kilometers from the reference.

The precision of the fixed solution is at the 1 cm level or better. The precision of the float solution (with 1 epoch of data) is 100 times poorer. The reliability of the measurement system is generally (more than) sufficient. The MDBs for outliers in the code are typically at the 2 meter level. They are quite large, but practically harmless to the precise coordinate estimators. MDBs for slips in the phase (after 31 epochs of data or with ambiguities fixed) are at the 2 cm level (or equivalently 0.1 cycle). Cycle slips are thus likely to be found. The above findings hold for an ordinary configuration with 6 or 7 satellites. It should also be mentioned that the quality of the dual frequency scenario is better than the corresponding single frequency one.

The spread in position is typically at the 1 cm level. With dual frequency data to only 5 satellites, the integer ambiguities could be instantaneously estimated correctly in all cases. With single frequency data this was problematic; more satellite redundancy is then needed.

From a technical point of view, surveying with kinematic GPS is feasible. Once the carrier phase ambiguities are fixed, the precision is at the millimeter level, even for very short observation time spans. The overall conclusion reads thus that the measurement technique can be successfully employed in practice for (high) production surveying. Kinematic GPS surveying has the potential for very fast and efficient surveying. One should however be aware of the limitations of current implementations. They are summarized below.

recommendations

The mathematical model, functional and stochastic part, was completely specified in chapter 3: $E\{\mathbf{y}\} = A\mathbf{x}$; $D\{\mathbf{y}\} = Q_y$. The results of this section indicate that extensions may be needed. The functional model may become $E\{\mathbf{y}\} = A\mathbf{x} + A_f\mathbf{x}_f$; additional unknown parameters x_f could be needed to cover e.g. the differential atmospheric delays. These delays were found to be currently the main error source and the situation will deteriorate when the baseline length is extended from 10 kilometer up to for instance 100 km. If they are not taken into account, they will bias the coordinate estimates, usually the vertical component more than the horizontal ones. The results really urge for the development of a method to deal with the differential atmospheric delays in a satisfying way.

For the highest precision applications, multipath reduction or prevention is required, probably on the hardware side, as modelling for the data processing is thought to be very difficult, if not impossible. Currently the effect of phase multipath was found to be several millimeters and it may reach up to the centimeter level and, as it is currently not taken into account, it will bias the (coordinate) estimates. It is generally expected that multipath at a site to be surveyed precisely, will average out to some extent, with several (e.g. 5-15) minutes of data. Occupying the site (stationary) for such a period will more or less eliminate the bias in the coordinates. For the time being this may be a practical solution; one is after isolating the direct-path signal, see the discussion in [Weill, 1997]. Multipath may be further reduced in future by improvements in antenna design, receiver hard- and software. The current state of the art on multipath reduction or its mitigation is discussed in [ibid] and [Garin et al, 1997].

Other effects, see table 4.4 in chapter 3, like the satellite orbit x^s and the coordinates of the reference receiver x_r are expected to play not a role. When Selective Availability (SA) is turned to zero, see e.g. [Sandlin et al, 1995], these effects will be reduced even further.

The last recommendation, a more fundamental and theoretical one, is that the probability density of the integer estimator needs to be investigated. This item is closely related to the statistical validation of the integer ambiguities, that is to be carried out prior to really fixing the ambiguities to the integer estimates. Currently only a preliminary ad-hoc validation was carried out.

Appendix 5.A Error estimation for a known baseline

A-priori introduction of geometric information in the mathematical model for data processing yields a very powerful tool for analysing the data. In particular data from a zero baseline (two receivers, one antenna) are very well suited for this kind of analysis, the baseline coordinates are deterministically known to be (0,0,0), as $x_1 = x_2$, or $x_2 - x_1 = 0$ (physically).

In this appendix the mathematical model used for the analysis will be discussed. As an example, we give the treatment of the L1-phase observations, denoted by P_r^s . Then it is shown that the analysis, per observation type, relies on the local error estimates.

mathematical model

We start from the mathematical model for one epoch of data, in terms of single differences, see equation (5.5) of chapter 3. When both receivers 1 and 2 observe m satellites, there are m single differences.

In (A.1) $P_{12}^s = P_2^s - P_1^s$ (in [m]) is the single difference observation for receivers 1 and 2 to satellite s . $c\Delta\delta_2 t$ is the differential receiver clock error; actually $c(\Delta\delta_2 t - \Delta\delta_1 t)$ is estimated. The satellite clock error is absent. A_{12}^s is the single difference ambiguity for satellite s , expressed in meters. The differential atmospheric delays (ionosphere I_{12}^s and troposphere T_{12}^s) are assumed to be zero. Multipath is not modelled.

$$(A.1) \quad E\left\{\begin{pmatrix} \Delta P_{12}^1 \\ \Delta P_{12}^2 \\ \vdots \\ \Delta P_{12}^m \end{pmatrix}\right\} = \begin{pmatrix} (-e_2^1)^T & 1 & 1 & & \\ (-e_2^2)^T & 1 & & 1 & \\ \cdot & \cdot & \cdot & \cdot & \\ \cdot & \cdot & \cdot & \cdot & \\ (-e_2^m)^T & 1 & & & 1 \end{pmatrix} \begin{pmatrix} \Delta x_2 \\ c\Delta\delta_2 t \\ A_{12}^1 \\ A_{12}^2 \\ \cdot \\ \cdot \\ A_{12}^m \end{pmatrix}; \quad D\left\{\begin{pmatrix} \Delta P_{12}^1 \\ \Delta P_{12}^2 \\ \vdots \\ \Delta P_{12}^m \end{pmatrix}\right\} = 2\sigma_P^2 \begin{pmatrix} 1 & & & & \\ & 1 & & & \\ & & \cdot & & \\ & & & \cdot & \\ & & & & 1 \end{pmatrix}$$

The variance covariance matrix for the undifferenced observables is taken a scaled unit matrix (equal standard deviation for all satellites). It is assumed that both receivers behave identically (but independently), i.e. $\sigma_{P_1^s} = \sigma_{P_2^s}$ and thereby $\sigma_{P_{12}^s} = \sqrt{2}\sigma_P$.

The design matrix of the above model has a rankdeficiency of 1 in the last $(m+1)$ columns; the receiver clock error interferes with the m single difference ambiguities. We will bring ambiguity A_{12}^1 into the clock error $c\Delta\delta_2 t$. The other $(m-1)$ single difference ambiguities become differences with the first ambiguity A_{12}^1 , and are actually double difference ambiguities, with pivot satellite 1. The transformation reads:

$$\begin{pmatrix} c\Delta\delta_2 t + A_{12}^1 \\ A_{12}^1 \\ A_{12}^2 \\ \cdot \\ \cdot \\ A_{12}^{1m} \end{pmatrix} = \begin{pmatrix} 1 & 1 & 0 & \cdot & \cdot & 0 \\ 0 & 1 & 0 & \cdot & \cdot & 0 \\ 0 & -1 & 1 & \cdot & \cdot & 0 \\ \cdot & \cdot & \cdot & \cdot & \cdot & \cdot \\ \cdot & \cdot & \cdot & \cdot & \cdot & \cdot \\ 0 & -1 & 0 & \cdot & \cdot & 1 \end{pmatrix} \begin{pmatrix} c\Delta\delta_2 t \\ A_{12}^1 \\ A_{12}^2 \\ \cdot \\ \cdot \\ A_{12}^m \end{pmatrix}$$

The inverse of this $(m+1) \times (m+1)$ transformation of unknowns, applied to the model of observation equations yields

$$(A.2) \quad E\left\{\begin{pmatrix} \Delta P_{12}^1 \\ \Delta P_{12}^2 \\ \vdots \\ \Delta P_{12}^m \end{pmatrix}\right\} = \begin{pmatrix} (-e_2^1)^T & 1 & 0 & & \\ (-e_2^2)^T & 1 & 1 & & \\ \cdot & \cdot & \cdot & \cdot & \\ \cdot & \cdot & \cdot & \cdot & \\ (-e_2^m)^T & 1 & & & 1 \end{pmatrix} \begin{pmatrix} \Delta x_2 \\ c\Delta\delta_2 t + A_{12}^1 \\ A_{12}^2 \\ \cdot \\ \cdot \\ A_{12}^{1m} \end{pmatrix}$$

The single difference ambiguity A_{12}^1 , as a separate unknown, has been left out. There are m single difference observations and $3+1+(m-1)$ unknown parameters. With only one epoch of data, it is not possible to estimate the full vector of unknown parameters.

In this analysis, the integer (double differenced) ambiguity values are known a-priori and used as such (i.e. constrained). The phase observations have actually become very precise code observations. The $(m-1)$ double difference ambiguities are thus initially constrained

to their reference values (integers; which can be assumed to be correct). They are brought to the left hand side. The variance covariance matrix is still left unchanged.

$$(A.3) \quad E\left\{ \begin{pmatrix} \Delta P_{12}^1 \\ \Delta P_{12}^2 - A_{12}^{12} \\ \vdots \\ \Delta P_{12}^m - A_{12}^{1m} \end{pmatrix} \right\} = \begin{pmatrix} (-e_2^1)^T & 1 \\ (-e_2^2)^T & 1 \\ \vdots & \vdots \\ (-e_2^m)^T & 1 \end{pmatrix} \begin{pmatrix} \Delta x_2 \\ c\Delta\delta_2 t + A_{12}^1 \end{pmatrix}$$

Single epoch positioning is possible now, when $m \geq 4$. With code data, no ambiguities are involved.

known baseline

When the coordinates of receiver 2 are (deterministically or very precisely) known: $\Delta x_2 = 0$ and can be left out from the model:

$$(A.4) \quad E\left\{ \begin{pmatrix} \Delta P_{12}^1 \\ \Delta P_{12}^2 - A_{12}^{12} \\ \vdots \\ \Delta P_{12}^m - A_{12}^{1m} \end{pmatrix} \right\} = \begin{pmatrix} 1 \\ 1 \\ \vdots \\ 1 \end{pmatrix} (c\Delta\delta_2 t + A_{12}^1)$$

When the single difference observations are corrected a-priori (and deterministically) for the known baseline coordinates and possibly for the known integer ambiguities, the resulting functional model is linear (A.5); the pivot single difference A_{12}^1 is not explicitly denoted.

$$(A.5) \quad E\left\{ \begin{pmatrix} P_{12}^1 \\ P_{12}^2 \\ \vdots \\ P_{12}^m \end{pmatrix} \right\} = \begin{pmatrix} 1 \\ 1 \\ \vdots \\ 1 \end{pmatrix} (c\delta_2 t)$$

The functional model comprises m corrected single difference observations in vector y , $m \times 1$ matrix A and only one unknown parameter in x (per epoch); the redundancy equals $m-1$. The variance covariance matrix (A.1) is still left unchanged.

error estimation

The data analysis relies on the error estimates. For each single difference observation individually (all channels/satellites and the whole series in time), the (local) outlier hypothesis is considered. For one epoch of data, for the L1-phase observations, the following set of m alternative hypotheses H_{a1} through H_{am} are considered, one at a time:

$$(A.6) \quad E \begin{pmatrix} P_{12}^1 \\ P_{12}^2 \\ \vdots \\ P_{12}^m \end{pmatrix} = \begin{pmatrix} 1 \\ 1 \\ \vdots \\ 1 \end{pmatrix} (c\delta_2 t) + \begin{pmatrix} 1 \\ 0 \\ \vdots \\ 0 \end{pmatrix} \nabla^1 + \begin{pmatrix} 0 \\ 1 \\ \vdots \\ 0 \end{pmatrix} \nabla^2 + \dots + \begin{pmatrix} 0 \\ 0 \\ \vdots \\ 1 \end{pmatrix} \nabla^m$$

Due to the simple structure of the design matrix, the error estimators can be easily expressed in terms of the (corrected) observables:

$$(A.7) \quad \begin{pmatrix} \hat{\nabla}^1 \\ \hat{\nabla}^2 \\ \vdots \\ \hat{\nabla}^m \end{pmatrix} = \begin{pmatrix} 1 & -\frac{1}{m-1} & \dots & -\frac{1}{m-1} \\ -\frac{1}{m-1} & 1 & \dots & -\frac{1}{m-1} \\ \vdots & \vdots & \ddots & \vdots \\ -\frac{1}{m-1} & -\frac{1}{m-1} & \dots & 1 \end{pmatrix} \begin{pmatrix} P_{12}^1 \\ P_{12}^2 \\ \vdots \\ P_{12}^m \end{pmatrix}$$

and their variance covariance matrix reads

$$(A.8) \quad D \begin{pmatrix} \hat{\nabla}^1 \\ \hat{\nabla}^2 \\ \vdots \\ \hat{\nabla}^m \end{pmatrix} = 2\sigma_p^2 \begin{pmatrix} \frac{m}{m-1} & -\frac{m}{(m-1)^2} & \dots & -\frac{m}{(m-1)^2} \\ -\frac{m}{(m-1)^2} & \frac{m}{m-1} & \dots & -\frac{m}{(m-1)^2} \\ \vdots & \vdots & \ddots & \vdots \\ -\frac{m}{(m-1)^2} & -\frac{m}{(m-1)^2} & \dots & \frac{m}{m-1} \end{pmatrix}$$

Note from (A.7) that the sum of the error estimates equals zero, that is $\sum_{i=1}^m \hat{\nabla}^i = 0$, or, the last estimator $\hat{\nabla}^m$ is a linear combination of the above $\hat{\nabla}^1$ through $\hat{\nabla}^{m-1}$, cf. also section 4.2.1 on separability. From (A.8) it can be seen that when m is large, the mutual correlation between the error estimators is small, $\rho_{\nabla^i \nabla^j} = -\frac{1}{m-1}$. There is no correlation in time, if the observables are also not time correlated.

Note also, that for model (A.5), there exists a simple relation between the vector of error estimators (A.7) and the m -vector of least-squares residuals (section 7.2 of chapter 1), namely $\hat{\underline{e}} = \frac{m-1}{m} \hat{\underline{\nabla}}$.

The error estimates, computed according to the outlier hypotheses, provide a powerful tool for analysis per observation type on channel (satellite) basis. Under the null hypothesis, the distribution of the estimator (mean and standard deviation) is known.

$$(A.9) \quad \hat{\nabla} \sim N(0, \sigma_p^2)$$

The error estimator has thus zero mean. Once a series of error estimates (samples) has been computed, we can confront it with these known (formal) parameters. Discrepancies between assumed model and actual data, if present, will show up; the mean primarily concerns the functional model, the standard deviation the stochastic model.

Appendix 5.B Elevation dependence in observation precision

In this appendix we will discuss the dependence of the observation precision on elevation. Starting from a scaled unit variance covariance matrix, equation (A.1) in appendix A (the example for one epoch of L1-phase observables), the elevation dependence is generally the first step to refine the stochastic model:

$$(B.1) \quad D\left\{\begin{pmatrix} \Delta P_{12}^1 \\ \Delta P_{12}^2 \\ \vdots \\ \Delta P_{12}^m \end{pmatrix}\right\} = 2 \begin{pmatrix} \sigma_{P^1}^2 & & & \\ & \sigma_{P^2}^2 & & \\ & & \ddots & \\ & & & \sigma_{P^m}^2 \end{pmatrix}$$

which is a diagonal matrix with varying entries.

observation noise

Noise in GPS code and phase observations may originate from various sources. They can lie in the whole trajectory from the generation of the signal in the satellite circuits, via antennas and propagation media, to the processing by the receiver circuitry. It starts with the satellite's transmission and antenna pattern. Then space loss is caused by the spreading of the signal in space; with GPS, the distance satellite-receiver is shortest when the satellite is in the zenith. The earth is surrounded by several layers (as shells) containing particles, that cause atmospheric loss. The longer the path through the atmosphere, the more the signal gets attenuated, resulting in a lower signal to noise ratio; this is the case for decreasing elevation. Additional foliage attenuation is possible. Finally, the receiver-antennas are usually designed to have low gain at low elevation, in order to avoid multipath to some extent, and again this results in a lower signal to noise ratio for the signal that enters the receiver. These items are dealt with in chapters 6, 3, 12, 13 and 8 of [Parkinson et al, 1996].

elevation dependence

From the above list, the receiver antenna gain is thought, under normal operating conditions, to be the dominant factor. Measurements taken under low elevation will be subject to larger noise, as compared with measurements taken at high elevation. Additionally at low elevations, multipath, a (functionally) unmodelled effect, is more likely. For this item on antenna gain, the discussion in [Elósegui et al, 1995] is summarized. Preferably the antenna should reject entirely any signal arriving from a negative elevation angle (as well as any signal with a left-handed circular polarization). On the other hand, it must receive signals arriving from any positive elevation angle. As a compromise the antenna gain has had to be gradually reduced towards low positive elevation angles, see also the amplitude patterns in [Schupler et al, 1994]. As a result the antenna gain pattern

is likely to translate into an elevation dependence for the standard deviation of the phase and code observable.

modelling

The elevation dependence is discussed in the context of surveying/geodesy, where the antenna's boresight axis always remains (more or less) directed to the local zenith (local level) and thereby (approximately) parallel to the Height/Up direction of the local topocentric system. The elevation ϵ is then the angle between the line of sight to the satellite and the local horizon (North-East).

An example for the standard deviation of the code observable $\sigma_p = f(\epsilon)$ is given in [Euler et al, 1991], see also [Jin, 1995]:

$$\sigma_p = a_o + a_1 e^{-\epsilon/\epsilon_o}$$

where

- σ_p : standard deviation of observable p
- ϵ : elevation angle under which observation is made [deg]
- ϵ_o : reference elevation angle [deg]
- a_o : (approx.) standard deviation [m] at $\epsilon=90$ deg
- a_1 : standard deviation [m] at $\epsilon=0$ deg equals a_o+a_1

As above, the standard deviation is usually taken a monotone decreasing function of the satellite elevation; in addition, also the relation with the signal strength (signal-to-noise ratio SNR) is used in [Gerdan, 1995] and [Gianniou, 1996]. The advantage of the latter is that the actual measurement situation (epoch and location) is taken into account, and the SNR values are available as the observations come out of the receiver. The value and interpretation of these ratios however, are in general not clear. The first approach concerns a *fixed* relation between standard deviation and satellite elevation (and thereby assumes azimuthal symmetry and that all satellites transmit equal power). It does not depend on the actual circumstances (atmosphere).

consequences

Switching from the simple scaled unit variance covariance matrix to a stochastic model that incorporates the elevation dependence will effect the quality, in terms of precision and reliability, of the measurement system. There can be two consequences. When only short observation time spans are used, as in kinematic GPS surveying, the elevation dependence has practically no time-varying effect as the elevations of the satellites do change only slowly. The only purpose of this modelling is then, to weight different satellites differently.

In general, at least when the overall level of precision is not changed, the effects are not dramatically. Low elevation satellites will get down-weighted, in favour of high elevation satellites. The Minimal Detectable Bias for an outlier in a range observation from a low elevation satellite will typically be larger than for a high elevation one. Because of the weighting, propagation of this large MDB into the estimators however, will be limited.

Concerning the precision of the coordinate estimators, it is to be expected that in general the difference in precision between Height on the one hand, and North and East on the

other, gets less pronounced by introducing the elevation dependence into the stochastic model. The following example should make this plausible.

■ As an example, we consider the optimal receiver-satellites geometry case. The configuration, with four satellites, consists of three at zero degree elevation (azimuths 0°, 120° and 240°) and one in the local zenith. The total spread in elevation angles is at maximum. For the standard stochastic model (all observables unit standard deviation) the variance covariance matrix of the coordinate estimators (North, East and Height) is given at left.

$$Q_{\hat{x}} = \frac{2}{3} \begin{pmatrix} 1 & & \\ & 1 & \\ & & 2 \end{pmatrix} \quad Q_{\hat{x}} = \frac{2}{3} \begin{pmatrix} 1 & & \\ & 1 & \\ & & 1 \end{pmatrix}$$

The matrix is diagonal and the precision (standard deviation) of the Height is factor $\sqrt{2}$ poorer than of the North and East.

In the elevation dependent model, the standard deviation of the zenith observable is set to $\sqrt{1/3} \approx 0.6$, the others remain unit. The resulting variance covariance matrix (at right) is a scaled unit matrix! The precision of the Height, w.r.t. the North and East, has improved. The correlation between the Height and the clock error is $\rho = \frac{\sqrt{2}}{2} \approx 0.71$. ■

Appendix 5.C Cross-correlation measurement technique

Originally the Turbo-Rogue came with the cross-correlation measurement capability to circumvent Anti-Spoofing, see also section 2 in chapter 3. Later models of Trimble employ it too and Ashtech phase data is likely to result also from cross-correlation.

In this appendix a mathematical description of the measurement technique is hypothesized. No proof is given for the statements, but the findings of section 2 on the zero baselines do not contradict them.

measurement technique

Usually the received CA-code is correlated with the receiver generated CA-code. The correlation yields a difference in time Δt_{C1} , which multiplied by the speed of light c , gives the pseudo-range (or the C1-code) observation p in meters.

For cross-correlation the receiver uses the incoming L1-signal *and* L2-signal, both containing the P-code (encrypted into Y-code; it is secret, but equal on both L1 and L2). The two codes are matched and this yields the differential time difference Δt_{P2-P1} . This difference can be multiplied by c and yields the differential pseudo-range observation q in meters. This observation q can be added directly to p to yield the reconstructed pseudo-range (or P2-code) observation on L2, \bar{p} .

Usually the phase of the incoming carrier, after removing the code modulation (by code-correlation), is compared with the receiver generated carrier. This yields the carrier phase observation, (after multiplication by λ_j) P on L1 [meters].

For cross-correlation the incoming L1 and L2 signal have been mixed, see also [Dieren-donck, 1994]. Two carriers, with frequency f_1 and f_2 , have been mathematically multiplied. This yields a low frequency ($\omega_2 - \omega_1$) carrier which is used for further processing. It has frequency $f_1 - f_2 = 347.82$ MHz. The phase of this signal is measured (with respect to the receiver oscillator's), $\phi_{2-1} = \phi_2 - \phi_1$, and it is the differential phase observation (in cycles). The reconstruction now takes place by a *direct* addition in terms of *cycles* $\phi_2 = \phi_1 + (\phi_2 - \phi_1)$ and multiplied by the L2-wavelength λ_2 , this yields the observation L2 P in meters.

stochastic model

For a cross-correlation receiver one should account for the statistical correlation between the dual frequency code and phase observables. The two (direct) observables are p and q :

$$D\left\{\begin{pmatrix} p \\ q \end{pmatrix}\right\} = \begin{pmatrix} \sigma_p^2 & \\ & \sigma_q^2 \end{pmatrix}$$

where p is the code observable on L1 (C1), and q the cross-correlation observable (Y2-Y1). The observations are expressed in meters; both result from observing a time difference (multiplied by c , the speed of light). It is assumed that code correlation and cross correlation yield uncorrelated observables. The code observation on L2, usually denoted by P2 (or C2), is reconstructed (in meters) as $p + q$, thus $P2 = C1 + (Y2 - Y1)$. The transformation of observables thus reads

$$\begin{pmatrix} p \\ \bar{p} \end{pmatrix} = \begin{pmatrix} 1 & 0 \\ 1 & 1 \end{pmatrix} \begin{pmatrix} p \\ q \end{pmatrix}$$

where \bar{p} denotes the (reconstructed) code observable on the second frequency. The corresponding stochastic model becomes

$$(C.1) \quad D\left\{\begin{pmatrix} p \\ \bar{p} \end{pmatrix}\right\} = \begin{pmatrix} \sigma_p^2 & \sigma_p^2 \\ \sigma_p^2 & \sigma_p^2 + \sigma_q^2 \end{pmatrix} = \begin{pmatrix} \sigma_p^2 & \sigma_p^2 \\ \sigma_p^2 & \sigma_{\bar{p}}^2 \end{pmatrix}$$

where the variance of \bar{p} shows up also as the two off-diagonal elements. $\sigma_{\bar{p}}^2$ now denotes the variance of the code observable on L2.

The two (direct) phase observables are P and Q :

$$D\left\{\begin{pmatrix} P \\ Q \end{pmatrix}\right\} = \begin{pmatrix} \sigma_P^2 & \\ & \sigma_Q^2 \end{pmatrix}$$

where P is the phase observable on L1, and Q the cross-correlation observable (L2-L1). The observations are expressed in meters. It is assumed that phase comparison and cross correlation yield uncorrelated observables. The phase observation on L2, is reconstructed

(in cycles) as $P/\lambda_1 + Q/\lambda_2$, thus $L2=L1+(L2-L1)$. The transformation of observables thus reads

$$\begin{pmatrix} P \\ \bar{P} \end{pmatrix} = \begin{pmatrix} 1 & 0 \\ \frac{\lambda_2}{\lambda_1} & 1 \end{pmatrix} \begin{pmatrix} P \\ Q \end{pmatrix}$$

where \bar{P} denotes the (reconstructed) phase observable on the second frequency. The corresponding stochastic model becomes

$$(C.2) \quad D\left\{\begin{pmatrix} P \\ \bar{P} \end{pmatrix}\right\} = \begin{pmatrix} \sigma_P^2 & \frac{\lambda_2}{\lambda_1} \sigma_P^2 \\ \frac{\lambda_2}{\lambda_1} \sigma_P^2 & (\frac{\lambda_2}{\lambda_1})^2 \sigma_P^2 + \sigma_Q^2 \end{pmatrix} = \begin{pmatrix} \sigma_P^2 & \frac{\lambda_2}{\lambda_1} \sigma_P^2 \\ \frac{\lambda_2}{\lambda_1} \sigma_P^2 & \sigma_P^2 \end{pmatrix}$$

where the variance of \bar{P} shows up also in the two off-diagonal elements. $\sigma_{\bar{P}}^2$ now denotes the variance of the phase observable on L2. The covariance $\sigma_{P\bar{P}}$ is a consequence of measuring the L1-phase and the L1-L2 (actually the wide lane) phase (instead of the L2-phase itself).

consequences

It has been shown that for a cross-correlating GPS receiver, the observables (dual frequency phase and code) do have a *block* diagonal matrix, instead of the traditional diagonal one. In the data processing, for both estimation and quality control, the correct stochastic model should be used. Below we will briefly indicate a consequence of using the cross-correlation stochastic model over the current simple model.

The (linear) model of observation equations (in terms of one double difference, cf. equations (5.7) in section 3.5 and (6.2) in 3.6) for a short baseline, can be reformulated by using a square and full rank transformation, into

$$(C.3) \quad E\left\{\begin{pmatrix} p \\ q \\ \bar{P} \\ Q \end{pmatrix}\right\} = \begin{pmatrix} 1 & 0 & 0 \\ 0 & 0 & 0 \\ 1 & 1 & 0 \\ \frac{\lambda_1 - \lambda_2}{\lambda_1} & -\frac{\lambda_2}{\lambda_1} & 1 \end{pmatrix} \begin{pmatrix} \rho \\ A \\ A \end{pmatrix} ; \quad D\left\{\begin{pmatrix} p \\ q \\ \bar{P} \\ Q \end{pmatrix}\right\} = \begin{pmatrix} \sigma_p^2 & & & \\ & \sigma_q^2 & & \\ & & \sigma_{\bar{P}}^2 & \\ & & & \sigma_Q^2 \end{pmatrix}$$

The cross-correlation reconstruction has been undone in (C.3) and the variance covariance matrix is diagonal. The cross-correlation code observable q has expectation equal zero; it is not related at all to the geometry contained in the range ρ . Hence the severe consequence is, that the cross-correlated code observable, P2-P1, is set completely aside in the estimation; it does not contribute to the estimators (for e.g. the baseline coordinates). The cross-correlated phase observable \bar{Q} does contribute by the grace of the wavelengths being not equal, $\lambda_2 \neq \lambda_1$.

References

- [Beckers, 1996] Beckers, G.W.J. (1996). The skyplots, figures 1.1, 1.9, 1.10, 2.1, 2.16 and 3.2 are created with SKYPLOT. Delft Geodetic Computing Centre, Delft University of Technology.
- [Chatfield, 1989] Chatfield, C. (1989). The analysis of time series - an introduction. Fourth edition. Chapman & Hall. London.
- [Dierendonck, 1994] Dierendonck, A.J. van (1994). Understanding GPS receiver terminology: a tutorial on what those words mean. Proceedings of KIS94. Banff, Canada. Aug. 30 - Sept. 2. pp. 15-24.
- [Eissfeller, 1997] Eissfeller, B. (1997). A dynamic state space error model for GPS receivers. Proceedings of KIS97. Banff, Canada. June 3-6. pp. 245-255.
- [Elósegui et al, 1995] Elósegui, P., J.L. Davis, R.T.K. Jaldehay, J.M. Johansson, A.E. Niell and I.I. Shapiro (1995). Geodesy using the Global Positioning System: the effects of signal scattering on estimates of site position. Journal of Geophysical Research. Vol. 100. No. B7. pp. 9921-9934.
- [Euler et al, 1991] Euler, H-J. and C.C. Goad (1991). On optimal filtering of GPS dual frequency observations without using orbit information. Bulletin Géodésique. Vol. 65. pp. 130-143.
- [Euler, 1997] Euler, H-J. (1997). Personal communication. Leica AG Heerbrugg. June.
- [Frei, 1991] Frei, E. (1991). Rapid differential positioning with the Global Positioning System. Geodätisch-geophysikalische Arbeiten in der Schweiz. Band 44. Berne.
- [Garin et al, 1997] Garin, L. and J-M. Rousseau (1997). Enhanced strobe correlator multipath rejection for code and carrier. Proceedings of ION GPS-97. Kansas City, USA. September 16-19. pp. 559-568.
- [Gianniou, 1996] Gianniou, M. (1996). Genauigkeitssteigerung bei kurzzeit-statischen und kinematischen Satellitenmessungen bis hin zur Echtzeitanwendung. Ph-D thesis. Deutsche Geodätische Kommission. Reihe C. Nr. 458. München.
- [Gerdan, 1995] Gerdan, G.P. (1995). A comparison of four methods of weighting double difference pseudorange measurements. Trans Tasman Surveyor. Vol. 1, No. 1. December. pp. 60-66.
- [Heister et al, 1997] Heister, H., R. Hollmann and M. Lang (1997). Multipath-Einfluß bei GPS-Phasenmessungen: Auswirkungen und Konsequenzen für praktische Messungen. AVN No. 5. pp. 166-177.
- [Jin, 1995] Jin, X.X. (1995). A recursive procedure for computation and quality control of GPS differential corrections. LGR series No. 8. Delft Geodetic Computing Centre. Delft University of Technology.
- [Kuang et al, 1996] Kuang, D., B.E. Schutz and M.M. Watkins (1996). On the structure of geometric positioning information in GPS measurements. Journal of Geodesy. Vol. 71. pp. 35-43.
- [Langley, 1997] Langley, R.B. (1997). GPS receiver system noise. GPS World. Innovation. June. pp. 40-45.
- [Nolan et al, 1992] Nolan, J., S. Gourevitch and J. Ladd (1992). Geodetic processing using full dual band observables. Proceedings of ION GPS-92. Albuquerque, USA. September 16-18. pp. 1033-1041.
- [Parkinson et al, 1996] Parkinson, B.W. and J.J. Spilker (1996). Global Positioning System: theory and applications. Progress in Astronautics and Aeronautics. Vols. 163 and 164. AIAA, Washington.
- [Roberts et al, 1997] Roberts, W., M. Rayson and P. Cross (1997). Verification of the UKOOA differential GPS guidelines. The Hydrographic Journal. No. 85, July. pp. 17-21.

- [Rothacher et al, 1996] Rothacher, M. and L. Mervart (Eds) (1996). Bernese GPS software version 4.0. Astronomical Institute, University of Berne. September.
- [Sandholzer, 1992] Sandholzer, J. (1992). Optional timemark output and clock steering - accuracy of the timemark. Wild GPS system 200. Leica AG Heerbrugg. August. 4 pp.
- [Sandlin et al, 1995] Sandlin, A., K. McDonald and A. Donahue (1995). Selective Availability: to be or not to be? GPS World. September. pp. 44-51.
- [Schupler et al, 1994] Schupler, B.R., R.L. Allshouse and T.A. Clark (1994). Signal characteristics of GPS user antennas. Navigation. Vol. 41. No. 3. pp. 277-295.
- [Teunissen, 1990] Teunissen, P.J.G. (1990). GPS op afstand bekeken. Een halve eeuw in de goede richting. Lustrumboek Snellius 1985-1990. pp. 215-233. Technische Universiteit Delft.
- [Teunissen, 1993] Teunissen, P.J.G. (1993). Least-squares estimation of the integer GPS ambiguities. Invited lecture. Section IV Theory and Methodology. IAG General Meeting. Beijing, China. August. (16 p.).
- [Teunissen et al, 1994] Teunissen, P.J.G., P.J. de Jonge and C.C.J.M. Tiberius (1994). On the spectrum of the GPS DD phase ambiguities. Proceedings of ION GPS-94. Salt Lake City, USA. September 20-23. pp. 115-124.
- [Teunissen, 1995] Teunissen, P.J.G. (1995) The least-squares ambiguity decorrelation adjustment: a method for fast GPS integer ambiguity estimation. Journal of Geodesy. Vol.70, No. 1/2, pp. 65-82.
- [Teunissen et al, 1996] Teunissen, P.J.G., P.J. de Jonge and C.C.J.M. Tiberius (1996). The volume of the GPS ambiguity search space and its relevance for integer ambiguity resolution. Proceedings of ION GPS-96. Kansas City, USA. September 17-20. pp. 889-898.
- [Teunissen, 1997a] Teunissen, P.J.G. (1997). Closed form expressions for the volume of the GPS ambiguity search spaces. Artificial Satellites, Journal of Planetary Geodesy. Vol. 32, No. 1. pp. 5-20.
- [Teunissen, 1997b] Teunissen, P.J.G. (1997). A canonical theory for short GPS baselines, part I: the baseline precision. Journal of Geodesy. Vol. 71, No. 6, pp. 320-336.
- [Teunissen, 1997c] Teunissen, P.J.G. (1997). A canonical theory for short GPS baselines, part IV: precision versus reliability. Journal of Geodesy. Vol. 71, No. 9. pp. 513-525.
- [Teunissen et al, 1997] Teunissen, P.J.G., P.J. de Jonge and C.C.J.M. Tiberius (1997). The least-squares ambiguity decorrelation adjustment: its performance on short baselines and short observation spans. Journal of Geodesy. Vol. 71. No. 10. pp. 589-602.
- [UNAVCO, 1995] C. Rocken, C. Meertens, B. Stephens, J. Braun, T. VanHove, S. Perry, O. Ruud, M. McCallum and J. Richardson (1995). UNAVCO Academic Research Infrastructure (ARI) receiver and antenna test report. Boulder, Colorado. Internet URL <http://www.unavco.ucar.edu/>
The data - the 1995 ARI Receiver Test - are available on-line through Internet.
- [Weill, 1997] Weill, L.R. (1997). Conquering multipath: the GPS accuracy battle. GPS World. Innovation. April. pp. 59-66.

6. Conclusions and recommendations

The research underlying this thesis was initiated by the question: 'Can the kinematic GPS measurement technique be used for surveying, and if so, how good is it, or in other words, what is the quality of the coordinate estimators?'. Directly related is the question: 'What shortcomings in modelling and/or processing do show up, when highest demands are put on the quality?'. The answer to the first question is positive, as already evidenced in practice. The second and third item have been extensively dealt with.

6.1 Summary

In the theoretical part of this thesis 'Recursive data processing for kinematic GPS surveying', a procedure for processing the GPS data was developed. The theory on mathematical geodesy, recursive data processing and mathematical modelling for (kinematic) GPS surveying were dealt with, the chapters 1 through 3.

measurement set up

The measurement set up of kinematic GPS surveying involves the use of two receivers (relative positioning). The reference receiver is stationary, the other - the roving receiver - can be either in motion or stationary. The distance between the receivers lies in the order of a few kilometers with an upper limit of typically ten kilometer. Both receivers simultaneously make observations to the same set of satellites. When the data of the reference receiver is then transferred to the roving receiver by means of a telemetry link, data processing can take place in real time at the site of the roving receiver. Kinematic GPS surveying as a measurement technique and the variations therein, together with the applications, have been briefly discussed in section 3.1. The adjective 'kinematic' refers to the motion of the receiver during the survey and thereby to increased surveying productivity.

mathematical model

The mathematical model - functional model and stochastic model - for the GPS phase and code observable has been discussed in section 3.4. The restriction of the baseline-length to ten kilometer is caused mainly by the assumption of equal atmospheric delays at both receiver sites. For the implementation, an equivalent formulation of the model of observation equations in terms of double differences is given (section 3.5). The unknown parameters are baseline coordinates and double difference ambiguities.

recursive data processing

The data processing in kinematic GPS surveying will be recursive. The incoming data are treated in a sequential manner. At every epoch, based on the data and previous estimation results, new estimation results are computed according to a certain scheme. In chapter 2

the Square Root Information Filter (SRIF) implementation has been proposed. Validation of the mathematical model is carried out with the Detection, Identification and Adaptation (DIA) procedure; it has been reviewed in appendix B of chapter 2. This testing procedure is integrated in the recursion. The full data processing is recursive and can therefore be carried out in (near) real time, parallel to the gathering of the data. Quality control can be performed already in the field and positioning results are directly available. When quality turns out to be insufficient, corrective actions can be taken immediately. A re-survey, caused by insufficient quality, can then be avoided. The quality of the positioning results is controlled in the field. The principles and concepts of estimation and testing have been given in chapter 1. The integer double difference ambiguities are handled by the Least-squares AMBiguity Decorrelation Adjustment (LAMBDA)-method, section 1.4.

process

The purpose of kinematic GPS surveying is to provide - in an efficient way - high quality geometric information on a local scale. As a result of the recursive processing of GPS code and phase data, estimates are available for the unknown parameters of which the geometric unknowns - the baseline coordinates - are of primary interest. The process is summarized in the concise flow diagram of figure 1.1. This diagram is run through every epoch. The quality of the (coordinate) estimators comprises precision and reliability. Measures of precision and reliability have been given in chapter 4. This chapter also dealt with several implementation, computational and practical aspects of the data processing.

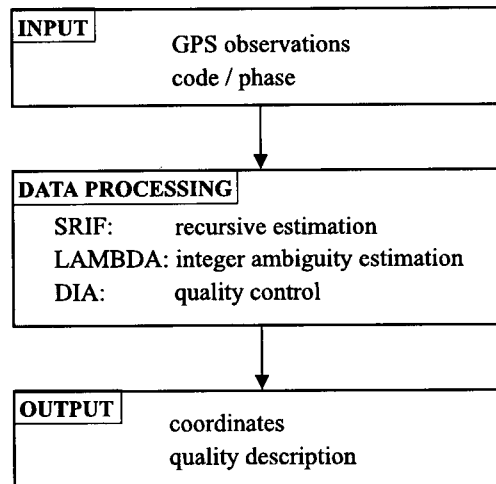


Figure 1.1: Flow diagram for GPS data processing

The experimental part, chapter 5, consisted of the data processing results and the analysis for three GPS measurement campaigns.

Ypenburg 94

The first campaign Ypenburg 94 - a representative case (configuration) from practice - was used primarily to analyse the quality of the coordinate estimators. The analysis was actually a designing process. Quality was described in terms of precision and reliability. For the set up of kinematic surveying (relative positioning), various measurement scenarios were analysed: code only, code and phase, single and dual frequency and with the carrier phase ambiguities float and fixed.

UNAVCO 95

The UNAVCO 95 campaign was used to analyse the stochastic model. The importance of an adequate stochastic model is evidenced by the fact that beside precision and reliability, also the estimation results themselves do depend on this model. The analysis revealed that the stochastic model currently in use, is definitely in-adequate and need to be refined. The data of four geodetic GPS receivers were extensively analysed; all four observation types were considered, dual frequency code and phase (under Anti-Spoofing). The results showed elevation dependence for the measurement precision of the observables, cross-

correlation between frequencies (as a consequence of the measurement technique under Anti-Spoofing for some receivers) and also mutual correlation between satellites. The functional model was found to be adequate for the data of the zero baselines. Clearly the stochastic model must be further tuned and this research is thought to give a first idea of what an adequate stochastic model should comprise.

Flevo 96

The Flevo 96 campaign was used to show the kinematic GPS surveying technique at work in practice. After a design analysis of quality, the positioning performance was shown, together with the capability of resolving the ambiguities. The precision of the coordinate estimators is at the 5-10 mm level, once the ambiguities are resolved. The ambiguities were demonstrated to be correctly estimated based on data from a very short time span only, by the computational efficiency of the LAMBDA method and its strict application of the least-squares estimation criterion to these parameters. Resolution can be realized instantaneously at a high successrate when dual frequency code and phase data are available. With single frequency data, sufficient satellite redundancy is indispensable for this. The capability of spotting errors in the observations, e.g. cycle slips in the phase, was shown. Reliability, the resistance of the data processing against the errors, was good. The limitations of the mathematical model for GPS surveying were shown concerning the functional model. Differential atmospheric delays were neglected (assumed to be zero in the model), but may play a role, especially for longer baselines (longer than several kilometers). Multipath may still be a matter of concern for the highest precision applications at any baseline length.

6.2 Conclusions

The developed prototype implementation of the data processing worked satisfactorily. The implementation features the recursive estimation with the Square Root Information Filter (SRIF), the Detection, Identification and Adaptation (DIA) - procedure for quality control and the integrated LAMBDA method for integer estimation of the ambiguities.

The kinematic GPS surveying measurement technique, combined with the developed implementation of the data processing, provides relative positions with mm-cm precision, in principle instantaneously, thus based on one epoch of data only. As the data processing is recursive, results can be made available in (near) real time in the field, while the survey is run.

Answering the research question, the conclusion reads that, the kinematic GPS measurement technique, from a technical point of view, is very well suited for use in surveying. It has the potential of providing geometric information in a fast, easy and efficient way, thereby enabling a high productivity. The quality of the geometric information obtained with kinematic GPS surveying, has been described in chapter 5 for various measurement set ups, configurations and scenarios.

6.3 Recommendations

Recommendations for direct further research concern refinements of the current mathematical model for GPS surveying, or positioning in general. The complete neglect of differential atmospheric delays in the functional model for instance, limits the inter

receiver distance (the baseline length) to roughly 10 kilometers (sometimes less, sometimes more). Research should be made to finally arrive at a uniform model, adequate for the whole range of baseline lengths, starting from zero. One may think of a stochastic modelling of the (differential) delay parameters and using data from a GPS reference network.

Refinements to the stochastic model have been indicated. Models currently in use are in general quite simple and seem to give not a proper description of the GPS code and phase observation noise. The stochastic model will to a certain degree also depend on circumstances outside the receiver, and therefore a regular calibration, also in the field, is recommended for the highest precision applications.

Further, less urgent, but more fundamental recommendations concern the stochasticity of quantities, currently assumed deterministic. There are the probability density of the integer estimator, as mentioned in section 6 of chapter 1 (with a direct impact on the validation in the ambiguity resolution process) and the stochasticity of satellite position and reference receiver position, as mentioned in section 3 of chapter 3, or more generally, the connection of the new measured geometric information to the existing geodetic infrastructure.